THERMAL TRANSITIONS IN LAYER-BY-LAYER ASSEMBLIES

A Dissertation

by

CHOONGHYUN SUNG

Submitted to the Office of Graduate and Professional Studies of
Texas A&M University
in partial fulfillment of the requirements for the degree of

DOCTOR OF PHILOSOPHY

Chair of Committee,	Jodie Lutkenhaus
Committee Members,	Mustafa Akbulut
	Michael V. Pishko
	Nicole Zacharia
Head of Department,	N. Nazmul Karim

December 2014

Major Subject: Chemical Engineering

ABSTRACT

Thermal transitions in layer-by-layer (LbL) assemblies were investigated under dry and hydrated conditions. In the dry state, the effects of film thickness and the film deposition method on the glass transition temperature (T_g) were studied. In aqueous conditions, the thermal behavior of microtubes and ultrathin films were studied.

The effect of film thickness on the T_g for poly(ethylene oxide)/poly(acrylic acid) (PEO/PAA) and PEO/poly(methacrylic acid) (PMAA) hydrogen-bonded LbL assemblies was investigated in the dry state. The T_g of PEO/PAA LbL films increased by 9 ℃ as the thickness decreased from 150 nm to 30 nm. In contrast, the T_g of thermally crosslinked PEO/PMAA LbL films was not influenced by film thickness

The thermal properties of dry PEO/PAA and PEO/PMAA LbL assemblies prepared using dip- and spray-assisted methods were compared. For both LbL assemblies, T_g's were similar regardless of deposition method. However, the breadth of glass transition was larger for the spray-assisted films. While PEO/PAA LbL assemblies showed smooth surface morphologies regardless of the deposition method, PEO/PMAA LbL assemblies showed different surface morphologies depending on the deposition method

The temperature-triggered transformation of LbL microtubes consisting of poly(allylamine hydrochloride) (PAH) and poly(acrylic acid) (PAA) was studied in aqueous media. LbL microtubes were assembled from sacrificial porous membranes.

Released microtubes became spherical and ellipsoidal upon high temperature incubation. In comparison, unreleased microtubes exhibited periodic perforations.

The thermal transition of LbL assemblies of poly(diallyldimethylammonium chloride) (PDAC) and poly(styrene sulfonate) (PSS) was probed using electrochemical impedance spectroscopy (EIS). Two thermal transition temperatures were obtained from the plot of film resistance ($T_{tr,Rf}$) and the charge transfer resistance ($T_{tr,Rct}$) as a function of temperature. Below 20 layers, PSS-capped LbL films showed higher $T_{tr,Rct}$ values compared to PDAC-capped films. In contrast, $T_{tr,Rf}$ was largely uninfluenced by assembly parameters.

In conclusion, thermal transitions in dry LbL assemblies were influenced by the film thickness and film deposition method. Thermal behavior of LbL microtubes were linked to the thermal transitions in hydrated state. EIS study on thermal transitions provided unique information on the structure of LbL assemblies.

나의 주인되신 하나님,

사랑하는 아내 한숙,

자랑스런 아들 치윤, 그리고

항상 격려 해주시는 부모님께

To my Lord God,

my beloved wife, Han Suk,

my proud son, Chiyoon, and

the unconditional supporter, my parent

ACKNOWLEDGEMENTS

I thank my advisor, Jodie L. Lutkenhaus, for sincere encouragement and excellent guidance throughout my research. It was great luck for me to conduct the research under her guidance. She taught me patience, sincerity, insights, cooperation, and creativity to become an independent researcher.

I also would like to thank my committee members, Dr. Zacharia, Dr. Akbulut, and Dr. Pishko for their guidance throughout the course of this research. I especially thank Dr. Zacharia, who taught me in polymer courses and generously shared her equipment.

I thank my group members, Ajay Vidyasagar, Ju-Won Jeon, Lin Shao, Daryia Leid, Joe Puhr, Sera Kwon, Hyosung An, Yanpu Zhang, Josh O'Neal, Jared Mike, and Lu Zhang. I also would like to thank my undergraduate students, Katelin Hearn, Ben Swerdlow, and Yixin Ye.

The biggest thanks go to my family. I thank my wife, Han Suk, who first proposed that I pursue Ph.D. in the U.S. and who has been praying for me the whole time. She has been an excellent wife, mother, and researcher. I also thank my little son, Chiyoon, who loves me so much even though I could not spend much time with him. Finally, I thank my parents for their love and prayers.

Lastly, I thank God for giving me wisdom and insight, self-control, and letting me get through the hard times. I confess that God began and finished everything.

NOMENCLATURE

LbL	Layer-by-layer
PEO	Poly(ethylene oxide)
PAA	Poly(acrylic acid)
PMAA	Poly(methacrylic acid)
PDAC	Poly(diallyldimethylamonium chloride)
PSS	Poly(styrene sulfonate)
PAH	Poly(allylamine hydrochloride)
DSC	Differential scanning calorimetry
QCM-D	Quartz crystal microbalance with dissipation
EIS	Electrochemical impedance spectroscopy
R_s	Solution resistance
R_f	Film resistance
R_{ct}	Charge transfer resistance
CPE	Constant phase element
C_{dl}	Double layer capacitance
Z_w	Warburg impedance
T_g	Glass transition temperature
T_m	Melting temperature
$T_{tr,Rf}$	Thermal transition temperature obtained from R_f
$T_{tr,Rct}$	Thermal transition temperature obtained from R_{ct}

TABLE OF CONTENTS

Page

ABSTRACT……. ii

DEDICATION……. iv

ACKNOWLEDGEMENTS……. v

NOMENCLATURE……. vi

TABLE OF CONTENTS……. vii

LIST OF FIGURES……. x

LIST OF TABLES……. xv

CHAPTER I INTRODUCTION……. 1

1.1 Introductory Remarks……. 1
1.2 General Introduction……. 1
1.2.1 Layer-by-layer (LbL) Assembly Technique……. 1
1.2.2 Film Growth and Internal Structure of LbL Assemblies……. 5
1.2.3 Advances in Assembly Technique……. 9
1.2.4 Template-Assisted Fabrication of LbL Microtubes……. 11
1.3 Thermal Transitions in LbL Assemblies……. 14
1.4 Thesis Overview……. 17

CHAPTER II EFFECT OF THICKNESS ON THE THERMAL PROPERTIES OF HYDROGEN-BONDED LBL ASSEMBLIES……. 21

2.1 Introduction……. 21
2.2 Experimental Section……. 26
2.2.1 Materials……. 26
2.2.2 Layer-by-Layer Film Assembly……. 26
2.2.3 Modulated Differential Scanning Calorimetry (Modulated DSC)……. 27
2.2.4 Ellipsometry……. 28
2.2.5 Quartz Crystal Microbalance with Dissipation……. 29
2.3 Results……. 30
2.3.1 PEO, PAA, and PMAA Homopolymers……. 30
2.3.2 PEO/PAA and PEO/PMAA LbL Assemblies……. 36
2.4 Discussion……. 50
2.5 Conclusion……. 55

CHAPTER III A COMPARISON OF THERMAL TRANSITIONS IN DIP- AND SPRAY-ASSISTED LAYER-BY-LAYER ASSEMBLIES…….. 57

3.1 Introduction…… 57
3.2 Experimental Section……..……. 59
3.2.1 Materials…… 59
3.2.2 Substrate Preparation…… 59
3.2.3 Dip-Assisted LbL Assembly……. 60
3.2.4 Spray-Assisted LbL Assembly……. 60
3.2.5 Profilometry…….. 61
3.2.6 Atomic Force Microscopy (AFM)…… 61
3.2.7 Ellipsometry……. 61
3.2.8 Modulated Differential Scaning Calorimetry (Modulated DSC)……. 62
3.3 Results and Discussion……...……. 63
3.3.1 LbL Film Growth…….. 63
3.3.2 Surface Morphologies of LbL Assemblies…… 66
3.3.3 Thermal Properties of LbL Assemblies…… 72
3.4 Conclusion…….. 81

CHAPTER IV TEMPERATURE-TRIGGERED SHAPE-TRANSFORMATIONS IN LAYER-BY-LAYER MICROTUBES……. 82

4.1 Introduction…… 82
4.2 Experimental Section……. 84
4.2.1 Materials…… 84
4.2.2 Preparation of FITC-Labeled PAH (FITC-PAH)……. 84
4.2.3 LbL Microtube Preparation…….. 85
4.2.4 High Temperature Incubation……... 86
4.2.5 Electron Microscopy……. 86
4.2.6 Modulated Differential Scaning Calorimetry (Modulated DSC)…….. 86
4.2.7 Confocal Laser Scanning Microscopy (CLSM)…… 87
4.3 Results and Discussion……... 87
4.3.1 Route A. Incubation of Released LbL Microtube……... 88
4.3.2 Route B. Incubation of Unreleased LbL Microtubes…… 97
4.4 Conclusion……. 102

CHAPTER V THERMAL TRANSITIONS IN HYDRATED LAYER-BY-LAYER ASSEMBLIES OBSERVED USING ELECTROCHEMICAL IMPEDANCE SPECTROSCOPY……..……. 104

5.1 Introduction…… 104
5.2 Experimental Section……. 108
5.2.1 Material……. 108
5.2.2 Preparation of Layer-by-Layer Assemblies…….. 108

5.2.3 Electrochemical Characterization……. 109
5.2.4 UV-Vis Spectroscopy……... 109
5.2.5 Surface Morphology and Film Thickness……. 110
5.3 Results and Discussion……... 110
5.3.1 Nyquist Plots and Electric Circuit Modeling…… 110
5.3.2 Thermal Transition from Circuit Elements……... 115
5.3.3 Factors Influencing the Thermal Transition Temperature…… 125
5.4 Conclusion…….. 135

CHAPTER VI SUMMARY AND FUTURE WORK…..……... 138

6.1 Summary…… 138
6.2 Future work…… 141

REFERENCES…… 144

.

LIST OF FIGURES

FIGURE Page

1.1 Schematic picture of layer-by-layer assembly……..……... 2

1.2 Growth behavior of PAH/PAA multilayer as a function of pH region……. 3

1.3 Molecular image of exponential growth mechanism……. 6

1.4 Schematic of a polyelectrolyte multilayer composed of 10 layers……. 8

1.5 Schematic illustration of nano- and microtube production……. 12

2.1 Modulated DSC thermograms of (a) PEO (2^{nd} heating cycle), (b) PAA (2^{nd} heating cycle), (c) PMAA (1^{st} heating cycle), and (d) PMAA (2^{nd} heating cycle)……..…… 31

2.2 Thickness vs. temperature data for (a) PEO, (b) PAA, and (c) PMAA…..... 34

2.3 Dry PEO/PAA and PEO/PMAA LbL assembly thickness as a function of the number of layer pairs as measured by profilometry…….…….. 37

2.4 LbL buildup as measured by QCM-D for (a) PEO/PAA and (b) PEO/PMAA LbL assemblies……... 37

2.5 Hydrated film thickness and composition as a function of layer number for (a) PEO/PAA and (b) PEO/PMAA LbL assemblies calculated from QCM-D data using a Voigt viscoelastic model…… 38

2.6 Modulated DSC thermograms of (a) $(PEO/PAA)_{30}$, (b) $(PEO/PMAA)_{30}$, and (c) $(PEO/PMAA)_{10}$ LbL assemblies, second heating scan……..……. 40

2.7 ATR/FT-IR spectra of PEO/PMAA LbL assemblies of (a) before heat treatment and (b) after heat treatment at 250℃, 5min……... 41

2.8 Effect of thickness on the T_g of (a) PEO/PAA and (b) PEO/PMAA LbL ssemblies…….……... 43

2.9 Effect of thickness on the (a) glass transition temperature range (ΔT) and (b) heat capacity change (ΔC_p) of PEO/PAA and PEO/PMAA LbL assemblies measured using modulated DSC……..…… 44

2.10 The onset and end temperatures for the glass transition of (a) PEO/PAA and

(b) PEO/PMAA LbL assembly measured using modulated DSC……. 45

2.11 Thickness vs. temperature data for (a) $(PEO/PAA)_7$ and (b) $(PEO/PMAA)_6$ LbL assemblies on silicon measured using ellipsometry…….. 46

2.12 Refractive index vs. temperature for (a) $(PEO/PAA)_7$ and (b) $(PEO/PMAA)_6$ LbL assemblies measured using ellipsometry…… 47

2.13 Effect of dry film thickness on the T_g of (a) PEO/PAA and (b) PEO/PMAA LbL assemblies identified using temperature-controlled ellipsometry…….. 48

2.14 Thickness as a function of temperature for a $(PEO/PMAA)_6$ LbL assembly showing the PEO melting region measured using ellipsometry……. 49

2.15 Thermal expansion coefficients (α) of (a) PEO/PAA and (b) PEO/PMAA LbL assemblies of varying film thicknesses…….. 50

3.1 Dry film thickness of LbL assemblies of (a) PEO/PAA, (b) PEO/PMAA as a function of the number of layer pairs measured using profilometry, and (c) layer pair thickness obtained from (a,b)……. 64

3.2 AFM images (135 µm × 135 µm) of (a, b) PEO/PAA LbL assemblies and (c, d) PEO/PMAA LbL assemblies prepared at assembly pH 2.0, and (e) root-mean-square roughness of various ~5 µm thick LbL assemblies measured using AFM……..… 67

3.3 Optical images of (a, b) PEO/PAA LbL assemblies and (c, d) PEO/PMAA LbL assemblies prepared at assembly pH 2.0…… 68

3.4 AFM images (5 µm × 5 µm) of (a, b) PEO/PAA LbL assemblies and (c, d) PEO/PMAA LbL assemblies prepared at assembly pH 2.0, and (e) root-mean-square roughness of ~ 5 µm thick LbL films measured using AFM ……..... 69

3.5 Optical microscope image of a PEO/PMAA spray-assisted LbL film using 30 sec of spraying…… 71

3.6 Modulated DSC thermograms of (a) PEO/PAA (2^{nd} heating cycle), (b) PEO/PMAA (1^{st} cooling cycle), and (c) PEO/PMAA (2^{nd} heating cycle) spray-assisted LbL assemblies……... 73

3.7 Modulated DSC thermogram of PEO/PMAA spray-assisted LbL assemblies (2^{nd} heating cycle)……... 74

3.8 Glass transition temperature of (a) PEO/PAA LbL assemblies, (b) PEO/PMAA LbL assemblies prepared by dipping and spraying, as well as the transition's temperature range, ΔT……...…….. 77

3.9 Volume percent PAA within dip- and spray-assisted PEO/PAA LbL films as determined using ellipsometry……... 78

3.10 Percent PMAA by volume in dip-assisted PEO/PMAA LbL assemblies as calculated using ellipsometry…… 79

3.11 Enthalpy of melting of PEO/PMAA LbL assemblies taken from the second Modulated DSC heating scan…… 80

4.1 A schematic illustration of the two routes…… 88

4.2 (a) SEM and (b) TEM images of microtubes released from the sacrificial membrane using dichloromethane, (c) SEM image of the microtubes after dialysis in water, and (d) CLSM image of microtubes in water at room temperature……. 89

4.3 TEM images of $(PAH/PAA)_{10}$ microtubes incubated at (a) 25, (b) 85, and (c) 95℃…… 90

4.4 SEM images of the microtubes incubated at (a) 70, (b) 95, and (c) 121 ℃. CLSM image of the microtubes in water after incubated at 121 ℃……. 91

4.5 TEM images of $(PAH/PAA)_{10}$ microtubes incubated at (a) 85, and (c) 95℃…….. 91

4.6 SEM images of $(PAH/PAA)_{10}$ microtubes incubated at 70℃ for (a) 15 min, (b) 30 min, (c) 2 hr, and (d) 5 hr…… 92

4.7 Length and outer diameter of $(PAH/PAA)_{10}$ microtubes as a function of (a) incubation temperature and (b) incubation time at 70 ℃……. 93

4.8 Confocal microscopy images of $(PAH/PAA)_{10}PAH$ microtubes in water (a) after dialysis and after incubation at (c) 40 and (d) 95 ℃……. 95

4.9 SEM images of $(PAH/PAA)_{10}PAH$ microtubes (a) after dialysis, and after incubation at (b) 40, (c) 55, (d) 70, (e) 95, and (f) 121 ℃…… 96

4.10 Microtube volume as a function of incubation temperature calculated from SEM images…….. 97

4.11 SEM images of microtubes that had been incubated in water at temperatures of (a) 40, (b) 75, (c) 85 ℃ during which the microtubes were confined to the template, and (d) TEM image of microtubes incubated at 85℃…… 98

4.12 Modulated DSC thermogram of a hydrated $(PAH/PAA)_{100}$ freestanding film.. 99

5.1 Nyquist plots of electrochemical impedance spectra taken at different temperatures for an ITO electrode modified with (a) $(PDAC/PSS)_{11}$ assembled at 0.5 M NaCl (~100 nm) and (b) $(PDAC/PSS)_7$ (~125nm) assembled at 1.0 M NaCl, as well as (c) an unmodified ITO electrode……. 111

5.2 Bode plots for the ITO electrode modified with (a) $(PDAC/PSS)_{11}$ LbL film assembled at 0.5M NaCl, (b) $(PDAC/PSS)_7$ LbL film assembled at 1.0M NaCl, and for (c) bare ITO electrode……. 112

5.3 Modified Randles equivalent circuit used to model electrochemical impedance spectra……..…….. 114

5.4 Nyquist plots taken at (a) 35 and (b) 75 ℃ for ITO electrodes modified with $(PDAC/PSS)_{11}$ LbL films assembled at 0.5 M NaCl…….. 114

5.5 Film resistance (R_f) as a function of temperature for (a) $(PDAC/PSS)_{11}$ LbL film assembled at 0.5 M NaCl (~100 nm) and (b) $(PDAC/PSS)_9$ LbL film assembled at 1.0 M NaCl (~225 nm)…….……. 116

5.6 Charge transfer resistance (R_{ct}) as a function of temperature for (a) $(PDAC/PSS)_{11}$ LbL films assembled at 0.5 M (~100 nm) and (b) $(PDAC/PSS)_7$ assembled at 1.0 M NaCl (~125 nm)……..…… 120

5.7 CPE-P as a function of temperature for $(PDAC/PSS)_{11}$ LbL film assembled at 0.5 M NaCl and $(PDAC/PSS)_7$ LbL film assembled at 1.0 M NaCl……. 122

5.8 C_{dl} as a function of temperature for $(PDAC/PSS)_{11}$ LbL films assembled at 0.5 M NaCl and $(PDAC/PSS)_7$ LbL film assembled at 1.0 M NaCl……. 123

5.9 Diffusion coefficient of the redox probe as a function of temperature for $(PDAC/PSS)_7$ LbL films assembled at 1.0 M NaCl……... 124

5.10 The transition temperature ($T_{tr,Rf}$) obtained from plots of R_f vs. temperature, and (b) the transition temperature ($T_{tr,Rct}$) obtained from plots of R_{ct} vs. temperature as a function of film thickness and salt concentration for PSS-terminated LbL films……. 126

5.11 (a) The transition temperature ($T_{tr,Rf}$) obtained from plots of Rf vs. temperature, and (b) the transition temperature ($T_{tr,Rct}$) obtained from the plots of Rct vs. temperature as a function of film thickness and outermost layer for LbL films assembled at 0.5 M NaCl concentration……. 128

5.12 Dry PDAC/PSS LbL film thickness vs. number of layers……. 129

5.13 R_f and R_{ct} as a function of layers for LbL films assembled at 0.5 M NaCl, evaluated at 25 ℃…….. 131

5.14 UV spectra of PDAC/PSS-coated quartz slides taken after annealing in the supporting electrolyte as a function of temperature……... 132

5.15 The relative amount of PSS in a PDAC/PSS LbL film after annealing in 0.5 M NaCl supporting electrolyte at varying temperatures for 30 min…….. 133

5.16 The relative dry LbL film thickness after annealing in the 0.5 M NaCl supporting electrolyte at varying temperatures for 30 min…… 134

5.17 AFM topographic images of $(PDAC/PSS)_{11}$ LbL films assembled at 0.5 M NaCl (a) as-made, (b) after EIS measurement, and after annealing in supporting electrolyte (c) at 25 ℃ for 7 hours, and (d) at 80 ℃ for 30 min….. 135

LIST OF TABLES

TABLE Page

2.1 Thermal transitions of homopolymers and LbL assemblies measured using modulated DSC and ellipsometry……. 33

4.1 Thermal properties of freestanding PAH/PAA films obtained from the modulated DSC thermogram shown in Figure 4.12…….. 99

CHAPTER I

INTRODUCTION

1.1 Introductory Remarks

The layer-by-layer (LbL) assembly technique is a simple technique to build polyelectrolyte multilayers. It is easy to control the thickness and adjust the properties of LbL assemblies using assembly conditions and film compositions. Film growth and internal structure of LbL assemblies have been extensively studied. LbL assemblies have found a variety of applications in the areas of energy, optics, and health.

This chapter serves to provide background on LbL assemblies to better understand this thesis. The first part covers the general introduction to LbL assemblies. In the second part, current studies on the thermal properties of LbL assemblies are presented. Finally, the outline and scope of this thesis are provided.

1.2 General Introduction

1.2.1 Layer-by-layer (LbL) Assembly Technique

The LbL assembly technique has attracted great attention since the first demonstration by Iler[1] and later Decher.[2] LbL assemblies are built up by the sequential deposition of oppositely charged polyelectrolytes. The main driving force for assembly is the increase of entropy due to the release of water and counter-ions upon the association of polycations and polyanions.[3] Typically, a given substrate is alternately immersed into oppositely charged polyelectrolyte solutions with rinsing steps in between

to remove weakly bound polymers as shown in Figure 1.1.[2] The LbL assembly technique has several advantages. Film thickness is easy to control by the number of deposition cycles. It allows the coating of almost any object of any shape. The structure and properties of LbL assemblies can be controlled using material chemistry and assembly conditions. LbL assemblies have been extensively explored for application in the areas of drug delivery, optics, energy, separation, etc.

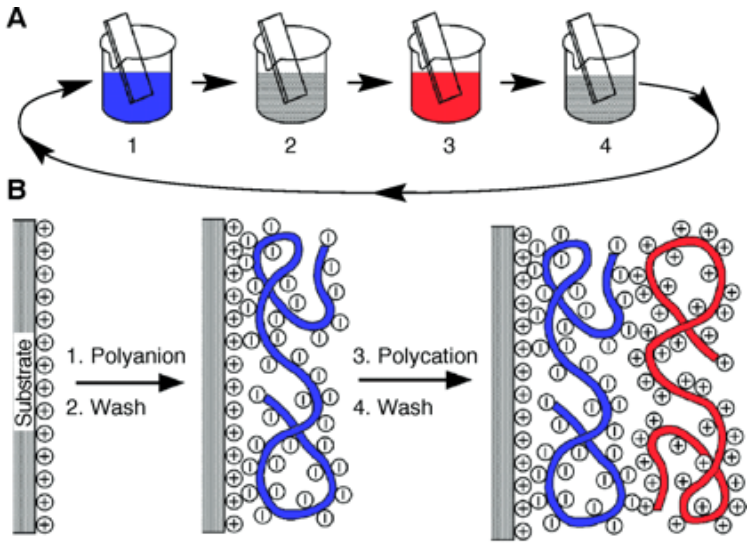

Figure 1.1 Schematic picture of layer-by-layer assembly. Reprinted with permission from ref 2. Copyright (1997) The American Association for the Advancement of Science.

Charge density of polyelectrolytes is an important parameter for the buildup of LbL assemblies. For LbL assemblies of weak polyelectrolytes, the charge density can be controlled by adjusting the assembly pH, and the architecture of LbL films can be

altered. At pH-values below pK_a, negatively charged polyelectrolytes take a less extended chain conformation due to the low degree of ionization. Above the pK_a, negatively charged polyelectrolytes exhibit a more extended chain conformation due to electrostatic repulsion driven by the high degree of ionization. Figure 1.2 shows the effect of assembly pH on the thickness of polyallylamine hydrochloride (PAH)/polyacrylic acid (PAA) multilayer.[4] In region III, where both PAH and PAA are

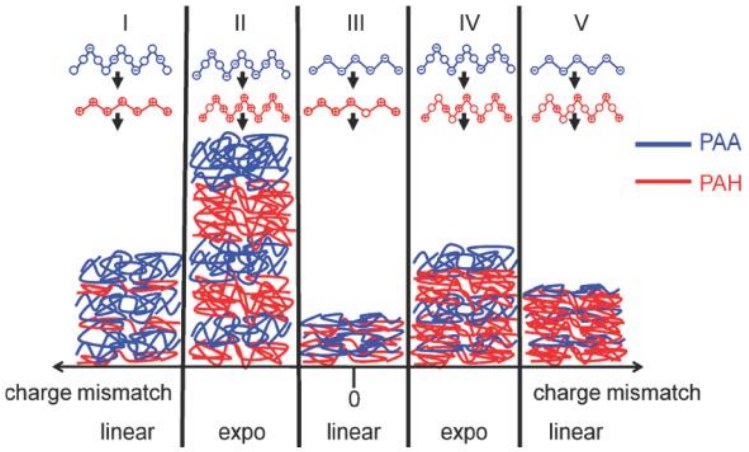

Figure 1.2 Growth behavior of PAH/PAA multilayer as a function of pH region (Region I : pH 3~4.5, II : pH 4.5~6, III : pH 6~8, IV : pH 8~10, V : pH 10~12). Reprinted with permission from ref 4. Copyright (2010) American Chemical Society.

fully charged, the thickness of each layer is small. When there is charge mismatch (region I and V), clear asymmetry in the individual thickness is observed. In region I (or V), the thickness of PAA (or PAH) is relatively thicker than PAH (or PAA) due to low charge density, respectively. In region II, where PAH is fully charged and PAA is

partially charged, a thick multilayer is observed. A thick multilayer is also observed in region IV where PAA is fully charged and PAH is partially charged.

Ionic strength also influences the structure of LbL assemblies. The LbL film thickness generally increases as the salt concentration increases. Added salt screens the electrostatic charges on the polyelectrolyte chains, and polyelectrolytes take a more coiled conformation. As a results, the thickness of the LbL assemblies increases. At a higher salt concentration, a decrease in film thickness was observed in some systems.[5, 6] For instance, the thickness of poly(diallyldimethyl ammonium chloride (PDAC)/PAA LbL assemblies decreased above the NaCl concentration of 0.3M when the film was grown at pH 11.[6] This is because added salt screens the attraction between the polyelectrolytes. Dissolution of preformed multilayers of PDAC/PAA was observed when the assembly salt concentration was above 0.6M.[6]

In addition to electrostatic interactions, hydrogen bonding has been used for LbL assemblies. Hydrogen bonding LbL assembly is based on hydrogen bonding between hydrogen bond acceptors and hydrogen bond donors. For example, oxygen atoms on the backbone of polyethylene oxide (PEO) act as acceptors, and the carboxylic acid groups of PAA act as donors. Hydrogen-bonding LbL assembly was first demonstrated by Stockton and Rubner.[7] The studies explored LbL assembly of polyaniline with various water-soluble polymers such as such as poly(vinyl-pyrrolidone) (PVPON), poly(vinyl alcohol) (PVA), polyacryl-amide (PAAm), and PEO. Hydrogen-bonded LbL assemblies have been extensively studied as pH-sensitive release systems since the pioneering work by Granick and Sukhishvili.[8] The authors demonstrated the disintegration of hydrogen -

bonded multilayers above a critical pH. Neutral polymers such as PEO and PVPON were used as hydrogen bond acceptors. Polyacids such as PAA and poly(methacrylic acid) (PMAA) were used as hydrogen bond donors. Hydrogen bonds are stable when the ionization of polyacids is fully suppressed. However, above the critical pH, the ionization of the acid groups destabilizes the hydrogen bonding, and the multilayer disintegrates. The critical pH was 3.5 and 4.6 for PEO/PAA and PEO/PMAA LbL assemblies, respectively. Recently, Erel-Unel et al. demonstrated that the critical pH of hydrogen-bonded multilayers can be tuned from 3.5 to 9.5 using neutral polymers and polyacids of high and low pH stability.[9]

1.2.2 Film Growth and Internal Structure of LbL Assemblies

Most multilayers grow linearly as the number of deposition cycle increases. In general, the thickness of linearly growing film is smaller than that of exponentially growing films. Linear growth is due to charge overcompensation. Castelnovo et al. explained the linear growth assuming that polyelectrolytes in the solution complexes only with the oppositely charged polyelectrolytes on the film surface.[10] Shafir et al. emphasized the importance of the strong short range interactions between oppositely charge polyelectrolytes for the linear growth.[11] In some cases, the initial growth can be not linear. The surface charge of the substrate is an important parameter that determines the properties of the first few layers.[2] After several layers, a linear growth regime starts.

Exponential (or non-linear) growth was first observed in LbL assemblies of poly(L-lysine) (PLL) and sodium alginate.[12] Picart et al. published seminal work on the exponential growth mechanism of PLL/hyaluronic acid (HA) multilayer.[13] One single

PLL layer was fluorescein-labeled, and one or two HA layers were labeled with Texas red. These labeled layers were monitored using confocal laser scanning microscopy during the film growth. HA stayed in the same position as a well-defined layer, but PLL inter-diffused over the whole film. Based on the observation, a theoretical model was proposed (Figure 1.3).[14] In a given multilayer with a polyanion (HA) as the outermost layer (Figure 1.3a), polycations (PLL) diffuse through the film during adsorption. Some fraction of polycations (PLL) form a complex in the surface and other "free" chains distribute in the film (Figure 1.3b and c). When polyanion (HA) is adsorbed on the surface again, free polycation (PLL) diffuses up to surface to form a complex (Figure 2.3d and e). Because the concentration of the free polycation (PLL) in the film is

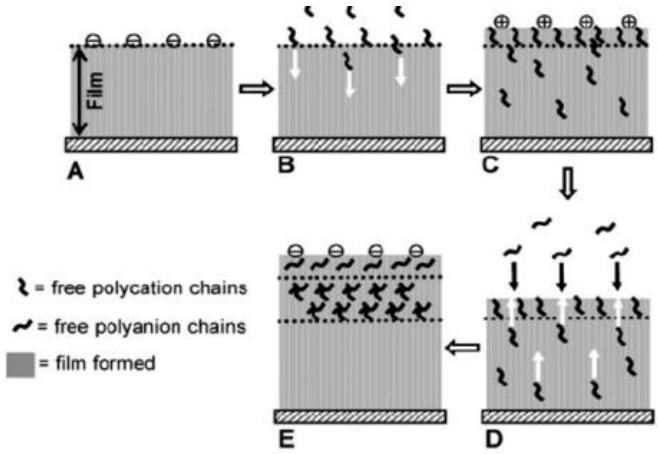

Figure 1.3 Molecular image of exponential growth mechanism. Reprinted with permission from ref 14. Copyright (2004) American Chemical Society.

constant, the absolute number of free chains is proportional to the film thickness. Thus, the number of complexes formed at the surface increases with the film thickness. As a result, the thickness increment increases with deposition cycle, and film growth becomes exponential.

In some multilayers, film growth evolves from exponential to linear.[15, 16] Hoda et al. proposed a model based on the limited contact time. The number of complexes (i.e., thickness) that can be formed depends on the contact time with a solution of polyanion (HA).[17] When the multilayer is thin, all the free polycations (PLL) will diffuse up to surface to form complexes. However, when the film becomes thick enough, only free polycations (PLL) that are within a distance from the surface can diffuse up to form complexes at a given time. Then, the number of complexes formed is constant regardless of the film thickness. As a result, a transition from exponential to linear growth takes place. However, Porcel et al. demonstrated that the transition from exponential to linear growth occurred at 10-12 deposition cycle regardless of contact time.[18] The authors proposed that the diffusion of polyions is limited due to the restructuring of multilayer rather than the short contact time. The origin of the transition is still under debate.

The internal structure of LbL assemblies is not just a stack of individual polyelectrolyte layers with clear interfaces. Early studies of PAH/ poly(styrene sulfonate) (PSS) LbL assemblies using neutron reflectivity showed that individual layers overlap with adjacent layers. Decher et al. proposed a concentration profile of polyelectrolyte composed of 10 layers in the vertical direction (Figure 1.4). In this model, each polyelectrolyte layer overlaps with five adjacent layers.[2]

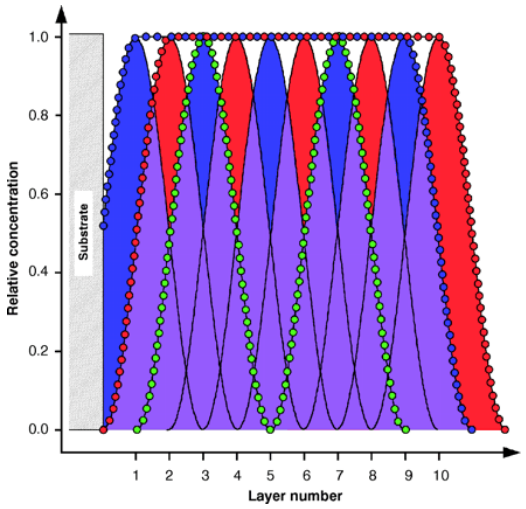

Figure 1.4 Schematic of a polyelectrolyte multilayer composed of 10 layers. The five blue layers and five red layers represent polyanion and polycation layers, respectively. Reprinted with permission from ref 2. Copyright (1997) The American Association for the Advancement of Science.

The structure of the film is related to the mode of film growth. Xu et al.[19] studied the film growth and structure as a function of assembly pH using LbL assembly of poly(2-(dimethylamino)ethyl methacrylate)/PMAA. Film growth changed from linear to exponential above pH 5.5. Neutron reflectometry results confirmed that the structure changed from a layered to highly intermixed structure as the growth mode changed from linear to exponential. Kharlampieva et al.[20] demonstrated that the strength of intermolecular interaction plays a role in internal structure for hydrogen-bonded LbL assemblies. The strongly hydrogen-bonded LbL assemblies of PVPON/PMAA showed relatively higher internal roughness compared to electrostatic LbL assemblies near the substrate. Furthermore, hydrogen-bonded LbL assemblies became more diffuse and mixed farther from the substrate. For relatively weak hydrogen-bonded LbL assemblies

of PEO/PMAA, films were completely interdiffused and did not show any layered structure.

Interpenetration of LbL assemblies increased as the ionic strength and temperature increased during assembly. Lösche et al.[21] reported that the internal roughness of PAH/PSS LbL assemblies increased with ionic strength. Gopinadhan et al.[22] reported that internal roughness of PAH/PSS LbL assemblies increased by a factor of three while film thickness increased 75% when assembly temperature was increased from room temperature to 45°C.

1.2.3 Advances in Assembly Technique

In contrast to the dip-assisted LbL assembly technique, other methods have been introduced to speed up the assembly process. Cho et al.[23, 24] demonstrated the spin-assisted LbL assembly of PAH and PSS. In this method, polymers were deposited on a substrate while spinning the substrate. The layer pair thickness of the spin-assisted film was six times larger than that of the film prepared by dipping. However, the thickness per layer is not necessarily higher compared to the conventional dipping method.[25, 26] Additionally, roughness was much lower for films prepared by the spinning process. The authors proposed that the elimination of water during spinning had two roles.[23] First, removal of water increases the polymer concentration. Second, electrostatic interaction between polyelectrolytes is not impaired by the water molecules in between. As a result, more efficient polymer adsorption is realized. The authors also showed that shear force induced by spinning results in a more stratified internal structure. Jiang et al. demonstrated compliant and robust freestanding film utilizing the advantage of spin-

assisted LbL assembly.[27] Despite the advantages of rapid processing, the spin-assisted method has limitations to substrate size and planarity.[28]

Another method is spray-assisted LbL assembly. Schlenoff et al.[29] demonstrated for the first time the buildup of LbL assemblies of PDAC/PSS using the spraying method. In this method, each polyelectrolyte solution is alternately sprayed on a vertical substrate for a short amount of time. Films prepared by both the conventional dipping and the spraying method showed similar chemical composition and ion transport properties. However, layer pair thickness was 50% less compared to films prepared by conventional dipping. Compared to the spin-assisted LbL process, the spray process can coat a larger surface area by moving either a spray gun or a substrate. Izquierdo et al.[28] explored the difference between spraying and dipping techniques using LbL assemblies of PAH/PSS. Spray-assisted deposition allowed for achieving regular multilayer growth and similar surface roughness in significantly shorter time. The authors explained the faster process of spray-assisted LbL assembly using the concept of "depletion layer" When a rinsing solution is replaced by the oppositely charge polyelectrolyte solution, the layer with very low polyelectrolyte concentration (depletion zone) forms near the surface of substrate. Thus, this depletion layer possesses the polymer concentration gradient. Polymer chains must diffuse through this depletion layer to adsorb on the substrate. In conventional dipping, the rinsing solution cannot be replaced instantaneously by the polyelectrolyte solution up to the deposition surface, and the polyelectrolytes are gradually depleted by the adsorption. Thus, the depletion layer is relatively thick. On the contrary, in the spraying method, the excess solutions are continuously drained by

gravity and relatively thin liquid film is formed on the deposition surface. Furthermore, new sprayed droplets continuously hit the surface and merge with the thin liquid film on the substrate, allowing us to assume that the polymer concentration in the liquid film is identical to the polymer concentration in the spraying tank. Therefore, the depletion layer is thin and close to the substrate's surface in spraying method. Due to this deposition mechanism, regular film growth is achieved in a short time.

1.2.4 Template-Assisted Fabrication of LbL Microtubes

Nanostructured materials have attracted considerable interest because the properties of nanomaterials can change significantly compared to the materials in bulk. It is suggested that properties of material properties can change significantly when the dimensions become close to the specific length scale of certain properties.[30] Since the discovery of carbon nanotubes, many researchers have focused on the development of one-dimensional nano- and microtubes.

LbL microtubes have attracted considerable interest because it is easy to control the thickness and composition can be controlled using various polymeric, inorganic, and metallic materials.[31, 32] One of the most popular methods of preparing LbL microtubes employs cylindrical pores in a substrate (Figure 1.5). Porous membranes such as track etched polycarbonate (PC) membranes and anodic aluminum oxide (AAO) membranes are commonly used. Liang et al. reported LbL microtubes of PAH/PAA and polyelectrolyte/metallic nanoparticles using a track etched PC membrane with cylindrical pores of 400 nm in diameter and 10 μm in length.[33] The PC membrane was selectively removed by using an organic solvent. Ai et al employed an AAO membrane

as a template to prepare LbL microtubes of PAH/PSS.[34] The authors overcame the reported challenge[35] of polyelectrolytes' clogging the pore mouth using a pressure-filter-template technique. The AAO membrane was placed between Millipore filters and polyelectrolyte solutions were squeezed through the membrane by applying pressure. PAH/PSS LbL microtubes of 60μm in length and 330 nm in diameter were demonstrated. Selection of materials for LbL microtubes is limited by the resistance to solvents, because different solvents are used to selectively remove PC and AAO membranes. Concentrated NaOH is used to dissolve AAO membrane and dichloromethane is used for track etched PC membranes.[34, 36]

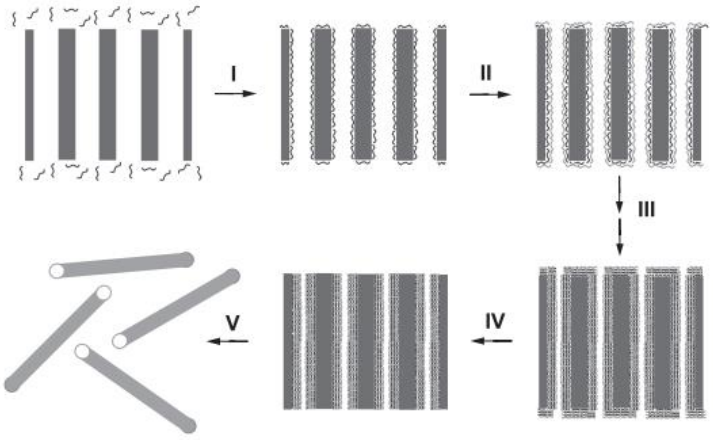

Figure 1.5 Schematic illustration of nano- and microtube tube production. I) adsorption of the first polyelectrolyte layer, II) adsorption of the second polyelectrolyte layer, III) adsorption of multiple layers, IV) removal of excess polyelectrolyte, V) membrane dissolution. Reprinted with permission from ref 33. Copyright (2003) Wiley-VCH Verlag GmbH & Co. KGaA, Weinheim.

It is reasonable to speculate that the growth of LbL assemblies in cylindrical pores would be different from the growth on a flat surface due to diffusion limitations arising from the difference in size of polyelectrolyte and cylindrical pore. Lazzara et al. investigated the in-situ LbL assembly of dendrimers in cylindrical AAO pores using optical wave guide spectroscopy.[37] It was shown that much higher salt concentration was required to achieve the same level of initial thickness in a pore as compared to a flat surface. It was also shown that regardless of initial pore diameter, when the diameter of pore opening became smaller than a critical value, the further film growth was inhibited. The critical pore opening diameter (26 nm) was much larger than the diameter of dendrimer (7 nm). The authors proposed that in addition to steric hindrance, electrostatic interaction is an important factor in the partitioning of polymer into pores. The transport limitations within pores were attributed to the difference in electric field within the pore and in the bulk, and to the electrostatic repulsion between polyelectrolytes deposited on the pore entrance and incoming polyelectrolytes.

Roy et al. studied the growth of PAH/PSS LbL assemblies on 100 - 500 nm track etched PC membrane by conventional dipping method focusing on the effect of molar mass and salt concentration.[38] Gas-flow porosimetry was used to estimate pore diameter in-situ. When the films were grown in small pores in the absence of salt or in large pores in the presence of salt, two growth regimes were demonstrated. In the first regime, the growth was comparable to that on a flat surface. In the second regime, the film growth became much slower, which was attributed to the overlapping of polymer chains across the pores.

1.3 Thermal Transitions in LbL Assemblies

In recent years, the thermal properties and behavior of LbL assemblies have gained considerable interests. The knowledge of thermal properties, especially glass transition temperature (T_g), is essential for both fundamental understanding and practical applications. The T_g's of LbL assemblies are categorized into T_g for "dry" and "hydrated" LbL systems.

The T_g of LbL films in the dry state was measured for the first time by Lutkenhaus et al.[39] The free-standing hydrogen-bonded LbL films of poly(ethylene oxide) (PEO) and PAA were removed from the low surface energy substrates and analyzed using differential scanning calorimetry (DSC). LbL films exhibited a well-defined, single T_g, suggestive of fully miscible blend. Furthermore, it was reported that the T_g increased as the assembly pH decreased.[40] It was suggested that the T_g increased due to the higher composition of PAA in the films to compensate for the lack of free carboxylic acid groups that could hydrogen-bond with PEO. On the other hand, with 0.1 M lithium triflate salt, the T_g remained constant regardless of assembly pH. The authors proposed that the ion-dipole interaction of lithium cations and PEO competes with PEO-PAA hydrogen bonding, thus shielding the hydrogen bonding interaction even when the assembly pH is varied. Contrary to hydrogen-bonded LbL assemblies, a "dry T_g" of electrostatic LbL assemblies has not been reported. LbL assemblies of PAH and PAA did not show a "dry T_g" regardless of assembly pH. Instead, two endothermic reactions (anhydride formation and amidation) were observed.[41] Jang et al. reported that the rate of amidation reaction was strongly influenced by the film thickness.[42] The enhanced

reaction rate was attributed to the catalytic contribution of hydroxyl groups on the substrate.

Recent interest in T_g of hydrated LbL assemblies arose from the thermal behavior of LbL microcapsules. For example, PDAC/PSS LbL microcapsules in aqueous media either swell or shrink as the incubation temperature increases.[43, 44, 45] PSS-capped microcapsules showed a pronounced shrinkage upon heating with the inflection temperature around 50-60 ℃. In contrast, PDAC-capped microcapsules swelled significantly upon heating until they ruptured at 55℃.[43] The authors proposed that whether the capsules swell or shrink is dictated by the competition of electrostatic and hydrophobic forces on the capsule. Hydrophobic forces that arise from the hydrophobicity of the polymer backbone favor shrinkage to reduce the interfacial area with water. Electrostatic repulsion forces that arise from electrostatic charges along the polymer chains favor swelling. The hydrophobic forces are dominant for PSS-terminated capsules, and the electrostatic repulsion forces are dominant for PDAC-terminated capsules. When the incubation temperature was increased above the T_g, the rate of polymer chain rearrangement increased rapidly, which leads to a more favorable configuration (i.e., via shrinking or swelling).

Thermal behavior of PAH/PSS LbL capsules and microtubes was also explained by the increased mobility of polymer chains at high temperature. PAH/PSS LbL capsules shrank at high temperature regardless of outermost layer.[45, 46] It was suggested that heating facilitates the transient disruption of ion-pairs and subsequent polymer chain rearrangement. The transformation of PAH/PSS LbL microtubes to microcapsules at

high incubation temperatures was explained by Rayleigh instabilities.[47] Thermal energy increases the mobility of polymer chains so that the transformation due to the Rayleigh instability can take place. However, no study on the thermal transition temperature of PAH/PSS has been reported.

Although thermal transitions seem to play an important role in the thermal behavior of LbL capsules and microtubes, the exact nature of the thermal transition of LbL assemblies in aqueous media is still uncertain. Mueller et al. measured the stiffness of PDAC/PSS LbL capsules terminated with PSS in the water as a function of temperature using atomic force microscopy (AFM) coupled with inverted fluorescence microscopy.[48] The authors suggested that it is a "glass-melt transition" considering the drastic decrease of Young's modulus from 100 MPa to order of MPa upon heating. Nazaran et al. showed that the lateral diffusion coefficient increased 1 – 2 orders of magnitude when the PDAC/PSS LbL films were heated to 65 ℃, suggestive of a glass-melt transition. The calorimetry studies give a different picture. Köhler et al. studied the thermal transition of PDAC/PSS LbL microcapsules terminated with PSS in aqueous media using micro DSC.[44] In this study, the thermal transition manifests as a second-order thermal phenomena, yielding a response much like a "glass" transition. Later, Vidyasagar et al. verified the second-order thermal transition for PDAC/PSS and PAH/PAA LbL freestanding films. [49, 50] For this reason the thermal transition observed for the hydrated PDAC/PSS LbL system has been called a "glass-melt" transition, or simply a "glass transition", in prior literature. The true nature of this thermal transition is still under debate.

The thermal transition of LbL assemblies was also studied using other techniques. Fortier-McGill et al. verified the higher mobility of PDAC-terminated capsules and through-film effect of PDAC by wide-line ^{2}H NMR spectroscopy.[51] The change in mobility for PDAC occurred around 25 ℃ and 35~45 ℃ for PDAC-terminated and PSS-terminated capsules, respectively. Recently, Vidyasagar et al. studied the glass-melt transition of electrostatic LbL assemblies using quartz crystal microbalance with dissipation (QCM-D).[49, 50] PDAC/PSS LbL films showed the odd-and-even effect.[49] For PDAC/PSS LbL films terminated with PDAC, dissipation showed a sudden increase at the glass-melt transition. In contrast, for PDAC/PSS LbL films terminated with PSS, dissipation decreased and frequency increased abruptly at the glass-melt transition. PDAC/PSS LbL assemblies showed glass-melt temperature when the salt concentration increased above the 0.25M NaCl.

The glass-melt transition of PAH/PAA LbL assemblies was also studied using QCM-D.[50] A glass-melt transition of PAH/PAA LbL films was characterized as the sudden increase of dissipation, coupled with an influx of the water into the film. No dependence on outermost layer was observed. PAH/PAA LbL films showed glass-melt temperatures of 40 - 50 ℃ for most assembly pH's investigated except for pH 7.0 where both polyelectrolytes were fully charged. In that case no transition was observed.

1.4 Thesis Overview

LbL assemblies have witnessed a significant progression both in fundamental understanding and applications. Although the knowledge of thermal properties,

especially thermal transition, is important for fundamental understanding and sophisticated design of LbL film, there has been limited work on the thermal properties of LbL assemblies. The object of this thesis is to investigate the thermal transitions of LbL assemblies in "dry state" and "hydrated state". Chapters II and III deal with the thermal transitions of LbL assemblies in dry state, and Chapters IV and V treat thermal transitions in hydrated state.

Chapter II presents the effect of film thickness on thermal properties of hydrogen-bonded LbL assemblies. It is well known that the T_g of homopolymers shifts when the film thickness decreases below 100 nm.[52] The growth of LbL assemblies is nonlinear in the early stage of growth.[53] Thus, the thermal properties of LbL assemblies can change depending on the film thickness. In Chapter II, thermal properties of hydrogen-bonded LbL assemblies of PEO/PAA and PEO/poly(methacrylic acid) (PMAA) in the dry state was explored using modulated differential scanning calorimetry (DSC) and temperature-controlled ellipsometer for relatively thick films and submicron films, respectively.

Chapter III presents the comparison of thermal transitions of LbL assemblies that were prepared by spray- and dip-assisted deposition methods. The spray-assisted LbL deposition method reduces the process time significantly compared to the conventional dip-assisted method. The structure and properties of LbL assemblies prepared by dip- and spray-assisted deposition methods can be different[54, 55, 56] because the polymer adsorption does not reach equilibrium due to the short contact time in spray-assisted deposition method.[28] In Chapter III, thermal properties of hydrogen-bonded LbL

assemblies of PEO/PAA and PEO/PMAA fabricated using the spray-assisted and dip-assisted LbL methods are compared.

Chapter IV examines the temperature-triggered shape-transformation of LbL microtubes in aqueous media. PDAC/PSS LbL microcapsules have exhibited swelling or shrinking upon heating.[43] PAH/PSS LbL microtubes have transformed into microcapsules upon heating.[47] It has been suggested that transformation upon heating is associated with the thermal properties of LbL assemblies. In Chapter IV, shape transformation of LbL microtubes consisting of a weak polyelectrolyte system, PAH and PAA, was studied as a function of incubation temperature. LbL microtubes were fabricated on the pores of polycarbonate (PC) membranes. Released (freely floating in the solution) LbL microtubes and unreleased (remaining within the membrane) were incubated as a function temperatures. An electron microscope and confocal laser scanning microscope were used to examine the shape change of LbL microtubes.

Chapter V presents the study on the thermal transition of LbL films in aqueous media using electrochemical impedance spectroscopy (EIS). EIS has been used to study the interfacial and transport properties of LbL films. EIS studies have shown that the charge transfer resistance depends on the surface charge of LbL films.[57] The permeability and swelling of LbL films were successfully studied using EIS.[58] Recently, temperature-controlled EIS was used to probe the T_g of polymer brush in the aqueous media.[59] Thus, LbL films could show distinct variations in electrochemical behavior associated with a thermal transition via EIS. However, there is only one study that investigated EIS of PAH/PSS over very limited temperature range (15-45 °C).[60] In

Chapter V, we study the structure of PDAC/PSS LbL assemblies in aqueous media as a function of temperature using EIS with a redox-active probe. The effect of assembly salt concentration, film thickness, and identity of the outermost layer on the thermal transition temperature is investigated.

Finally, Chapter VI summarizes the results and suggests possible future works.

CHAPTER II

EFECT OF THICKNESS ON THE THERMAL PROPERTIES OF HYDROGEN-BONDED LBL ASSEMBLIES*

2.1 Introduction

Understanding thermal properties, especially the glass transition temperature (T_g), is essential in order to design a desired layer-by-layer (LbL) assembly and manipulate its properties. LbL assemblies have found a wide variety of applications such as in biomedical devices,[61] fuel cells,[62] batteries,[63] antireflection coatings,[64] and antimicrobial coatings[65] since their introduction by Iler[1] and later Decher.[2, 66] The LbL technique is based upon the alternate exposure of a substrate to positively and negatively charged species or to hydrogen-bond donors and acceptors in solution (or dispersion). The type of adsorbing species is not limited to polymers but may also include inorganic fillers[67] or biological molecules.[68] Internal structure and properties of LbL assemblies are finely tuned by factors such as type of adsorbing species,[69] assembly and post-assembly treatment pH,[70, 71] assembly temperature,[72, 73] added salt type and concentration,[74] and solvent.[75] Although both the LbL film buildup mechanism and its internal structure have been rigorously studied using various methods ranging from confocal laser scanning microscopy[13] to X-ray reflectivity[76] and neutron scattering,[21]

* Reprinted with permission from "Effect of thickness on the thermal properties of hydrogen-bonded LbL assemblies" by Choonghyun Sung, Ajay Vidyasagar, Katelin Hearn, and Jodie L. Lutkenhaus, *Langmuir* **2012**, 28, 8100−8109, Copyright (2012) American Chemical Society

thermal properties such as glass transitions, heat capacities, and coefficients of thermal expansion have not been sufficiently studied and are relatively unknown.

To date, glass transitions in LbL assemblies have been reported for a handful of systems, which may be categorized into T_g's for "dry" or "hydrated" LbL systems. A T_g-like transition for ion-pairing LbL systems, such as for poly(diallyldimethylammonium chloride)/poly(styrene sulfonate), has been observed in hydrated conditions using micro-differential scanning calorimetry (micro-DSC),[44] NMR spectroscopy,[51] and shrinking/swelling of LbL capsules.[43] The diffusion coefficient of ferricyanide probes within these same hydrated films significantly increased with increasing temperature.[77] It is generally thought that the "hydrated T_g" arises from the dissociation/association of ion pairs and chain relaxation. We have yet to observe a T_g for analogously dry ion-pairing LbL films. For example, our group investigated the thermochemical properties of dry poly(allylamine hydrochloride)/poly(acrylic acid) (PAH/PAA) LbL assemblies using modulated DSC[41] by isolating free-standing films from a low energy surface.[39] No T_g was observed for the dry film; instead, the film underwent thermal crosslinking via amidation.

In contrast to ion-pairing LbL assemblies, hydrogen-bonded LbL assemblies in the dry state can possess a distinct T_g, similar to that of miscible hydrogen-bonded complexes.[39, 40, 78] Hydrogen-bonded LbL assemblies of poly(ethylene oxide) (PEO) and PAA or poly(methacrylic acid) (PMAA) have been explored as solid polymer electrolytes and pH-responsive microcapsules.[40, 79, 80, 81] Assembly pH, which controls the ionization of polyacids, is considered an important parameter for hydrogen-bonded

LbL assembly. DeLongchamp and Hammond[79] explored PEO/PAA and PEO/PMAA LbL assemblies as solid polymer electrolytes and showed that LbL film assembly occurs below a critical pH (3.5 for PEO/PAA and 4.5 for PEO/PMAA systems). Sukhishvili and Granick[8] demonstrated that LbL films of PEO/PAA and PEO/PMAA deconstructed upon immersion in solution above the critical pH. Lutkenhaus et al. measured the bulk T_g of PEO/PAA LbL films (> 1μm thick) assembled at various pH values.[39, 40] Dry PEO/PAA LbL assemblies exhibited a single well-defined T_g between that of its pure components. The appearance of a single T_g, rather than two, indicated that PEO/PAA LbL films behave similarly to miscible blends, rather than stratified, phase-separated layers. Furthermore, it was reported that the T_g of PEO/PAA LbL films increased from 25 to 52 ℃ as the assembly pH decreased from 3.0 to 2.25; the increase was attributed to the tendency of PAA to hydrogen bond with itself instead of PEO at lower pH values.[39]

Because LbL films are often studied as ultrathin films (< 100 nm thick), it is important to consider the effect of thickness on their materials properties with regard to the substrate on which they are assembled. One common misconception regarding LbL assemblies is that they are comprised of stratified, unmixed layers; however, numerous studies[2, 13, 21, 76] have verified a highly interpenetrated layer structure such that these films can be suitably treated as miscible blends. Therefore, we will consider LbL assemblies as a single homogeneous film rather than a collection of stratified layers for the present investigation unless otherwise noted. Confinement effects observed for neutral homopolymers could potentially occur for LbL assemblies. For example, the effect of thickness on the T_g of ultrathin or "confined" neutral homopolymer films has

been of great interest for a number of years and has been discussed in many reviews.[52, 82, 83, 84] Keddie et al. measured the T_g of supported polystyrene films using ellipsometry, and it was found that T_g decreased relative to bulk values at thicknesses below 100 nm as film thickness decreased.[85] This result was attributed to a mobile, liquid-like layer at the surface of the film.[86] It was also demonstrated that T_g varied depending on vertical location within the film using a fluorescent probe method.[87] Depending on the type of polymer and the supporting substrate's surface chemistry, T_g can increase or decrease with respect to decreasing film thickness. For example, Keddie et al.[88] also showed that the T_g of poly(methyl methacrylate) (PMMA) increased for silicon with native oxide support and decreased for a gold-coated support. Fryer et al.[89] investigated the T_g of PMMA thin films on both polar and nonpolar substrates, finding that T_g decreased relative to bulk values for thin films on nonpolar hexamethyldisilizane-treated substrates but increased for polar silicon oxide substrates.

In comparison, few investigations of thickness-dependant thermal properties exist for LbL assemblies.[42, 78] It should be noted that the thickness of LbL assemblies is controlled by varying the number of adsorption steps or "layer pairs." Jang et al.[42] studied the influence of thickness on the crosslinking kinetics of PAH/PAA LbL assemblies supported on silicon; for thicknesses below 200 nm, the amidation crosslinking temperature and activation energy decreased with decreasing film thickness.[42] The enhanced reaction kinetics was attributed to the catalytic contribution of hydroxyl groups on the silicon substrate. Recently, Gu et al.[78] measured the T_g of PEO/PAA LbL assemblies of varying thicknesses using shear modulated force

microscopy (SM-FM); however, SM-FM measures the T_g of the film's surface and not that of the entire film.[90] Gu et al. found that as film thickness decreased, so did T_g. The authors attributed the T_g-depression to changes in the surface's composition and surface heterogeneity during the assembly process. When the PEO/PAA LbL film was sufficiently thick (over 15 layer pairs), only the T_g of the outermost layer (PAA, in that case) was observed.

Here, we investigate the effect of thickness on the thermal properties of dry hydrogen-bonded LbL assemblies of PEO/PAA and PEO/PMAA using modulated DSC and temperature-controlled ellipsometry. Modulated DSC of free-standing LbL assemblies facilitates the study of bulk films (> 500 nm), while temperature-controlled ellipsometry probes much thinner films (< 200 nm). These techniques capture thermal information regarding the entire LbL assembly, rather than only the surface. The T_g-value, it's breadth, and it's strength are qualitatively related the LbL films' composition, structure, and extent of hydrogen-bonding. Quartz crystal microbalance with dissipation (QCM-D) is also used to determine the films' composition. This study represents the first application of temperature-controlled ellipsometry to determine T_g's in LbL assemblies and should be widely applicable to other LbL systems. Results are discussed with regard to assembly structure and molecular interactions with the substrate's surface.

2.2 Experimental Section

2.2.1 Materials

Poly(ethylene oxide) (PEO, Mw = 4,000,000 g/mol), poly(acrylic acid) (PAA, Mw = 50,000 g/mol), and poly(methacrylic acid) (PMAA, Mw = 100,000 g/mol) were purchased from Polysciences, and were used as received. Linear polyethylene imine (PEI, Mw = 25,000 g/mol) was purchased from Sigma Aldrich. Solutions of 20 mM concentration, based on the molar mass of the repeat unit, were prepared by dissolving the polymer in 18.2 MΩ water (Milli-Q, Millipore) and then by pH adjustment using either HCl or NaOH. Teflon® substrates and silicon wafers were purchased from McMaster-Carr and Wafer World, respectively. Teflon® substrates were used for the preparation of free-standing LbL assemblies for modulated DSC. Teflon® substrates were cleaned by sonication in 18.2 MΩ water and then ethanol for 15 min each. Silicon wafers were used as substrates for ellipsometry measurements. Silicon wafers were cleaned by immersion in piranha solution (3:1 sulfuric acid to hydrogen peroxide) for 15 min, followed by thorough rinsing in 18.2 MΩ water. *Caution: Piranha solution is extremely corrosive, and proper caution should be taken.* Immediately before assembly, silicon wafers were oxygen plasma-treated for 5 min.

2.2.2 Layer-by-Layer Film Assembly

All LbL films were assembled using a programmable slide stainer (HMS series, Carl Zeiss Inc.). Substrates were dipped in 20 mM PEO solution for 15 min followed by three separate rinses with agitation in 18.2 MΩ·cm water for 2 min, 1 min, and 1 min, respectively. Then, the substrates were immersed in either 20 mM PAA or PMAA

solution for 15 min followed by another three rinsing steps as described previously. This process was repeat n times to yield n layer pairs, denoted as $(PEO/PAA)_n$, for example. All solutions were maintained at pH 2.5 throughout the entire study to suppress the ionization of PAA and PMAA. Thickness measurements were performed using profilometry (KLA - Tencor Instruments P-6). All samples were dried in a convection oven at 40 ℃ for 30 min before measurements. Three different points were measured for each sample.

2.2.3 Modulated Differential Scanning Calorimetry (Modulated DSC)

Thermal properties of bulk samples were characterized using modulated DSC (Q200, TA instruments). Samples were obtained by peeling or flaking dry LbL assemblies from their Teflon® substrate to obtain a free-standing film. Samples were dried in a vacuum oven at 40 ℃ overnight. 5 to 10 mg of sample was loaded into Tzero aluminum pans with lids (TA Instruments). Samples were scanned using a heat-cool-heat method. Unless otherwise stated, samples were first heated from room temperature to a predetermined temperature (140 ℃ for PEO, PAA, PEO/PAA LbL assemblies and 250 ℃ for PMAA and PEO/PMAA LbL assemblies), held there isothermally for 5 min, cooled down to a desired temperature, and held there isothermally for 5 min, respectively. Finally, the sample was heated again to a predetermined temperature. Cooling and heating rates, temperature modulated amplitude, and period were fixed at 3 ℃/min, 0.636 ℃, and 40 seconds, respectively. All data reported here were taken from the second heating cycle unless noted otherwise. The T_g was taken as the inflection point. The standard deviation was taken as the error

2.2.4 Ellipsometry

Thickness and refractive index of thin LbL films on silicon substrates were monitored as a function of temperature using a single-wavelength (λ = 623.8 nm) LSE Stokes ellipsometer (Gaertner). The samples were affixed to a hot stage (Thermo Scientific) using thermally conductive paste (Omega Engineering Inc.). Measurements were performed in a nitrogen-purged custom-made quartz cell to prevent moisture uptake. The angle between the quartz window and hot stage was the same as the incident angle of the laser, 70°. The programmed temperature was calibrated by measuring the surface temperature of a silicon substrate atop the hot plate using a thermocouple. PEO and PAA films were heated to 140 ℃, held isothermally for 5 min, cooled to 30 ℃ and 70 ℃, respectively, held again for 15 minutes, and heated once more. PMAA films were heated to 250 ℃, held isothermally for 15 min, cooled to 90 ℃, held for isothermally for 15 min, and heated once more. PEO/PAA LbL assemblies were first heated to 140 ℃ and held isothermally for 5 min. Samples were then cooled to 104 ℃, held isothermally for 15 min, and then cycled between 30 ℃ and 104 ℃. PEO/PMAA LbL assemblies were first heated to 250 ℃ and held isothermally for 15 min to induce thermal crosslinking. Samples were then cooled to 180 ℃, held isothermally for 15 min, and then cycled between 90 ℃ and 180 ℃. All samples were cooled or heated by changing the temperature in 2 ℃ increments every 3 min, yielding an overall rate of 0.67 ℃/min. Data were acquired at the end of each time increment. The T_g was identified from the intersection of lines extrapolated from low and high temperature regions of thickness vs.

temperature curves.[85, 91] The thermal expansion coefficient (α) of LbL films was calculated using the following Equation 2.1[91]

$$\alpha = -\frac{1}{h_{avg}}\left[\frac{d(1/h)}{dT}\right] \tag{2.1}$$

where h_{avg} is average film thickness and d(1/h)/dT is estimated using linear regression of thickness vs. temperature data within a given temperature range. α_{glass} denotes the thermal expansion coefficient below T_g, and α_{rubber} denotes the thermal expansion coefficient above T_g.

2.2.5 Quartz Crystal Microbalance with Dissipation

LbL film growth was monitored using a Q-Sense E1 QCM-D system. Gold-plated AT-cut quartz crystals were first plasma-treated for 10 min followed by immersion in a 5:1:1 mixture of water/NH_4OH/H_2O_2 70 ℃ for 10 min. Then, the crystals were dried using nitrogen and plasma-treated as before. Prior to LbL assembly, 1 mg/mL PEI solution was flowed over the crystal for 17 min, followed by a 6 min rinse with 18.2 MΩ·cm water. PEI was used as the first layer only for QCM-D experiment. For LbL assembly, the PEI-coated crystal was alternately exposed to solutions of 2 mM PAA (or PMAA) and 2 mM PEO solution for 17 min. A 6 min rinsing step was applied after each exposure to polymer solution. The pH of all solutions and rinses was adjusted to 2.5. This procedure was repeated until the desired number of layers was achieved. QCM-D measures the resonant frequency change (Δf) and dissipation change (ΔD) upon adsorption of material to the quartz crystal.[92, 93] Δf is correlated to mass change, and ΔD is correlated to the stiffness or viscoelasticity of the adsorbed material. In this study, the

Voigt model was used to model the hydrogen-bonded LbL film to account for its viscoelastic nature.[94, 95] All calculations were performed by taking overtones n = 3 to 13 into consideration using QSoft and Q-Tool software (Q-sense).

2.3 Results

The thermal properties of PEO/PAA and PEO/PMAA LbL assemblies of varying thickness were compared to that of their homopolymer constituents using modulated DSC and temperature-controlled ellipsometry. Results regarding homopolymers are presented first. Then, LbL film growth, bulk LbL film thermal properties, and thin LbL film thermal properties are presented.

2.3.1 PEO, PAA, and PMAA Homopolymers

Prior to the analysis of LbL films, homopolymers PEO, PAA, and PMAA were examined using modulated DSC (Figure 2.1). By using this technique, it is possible to separate the total heat flow into reversing and non-reversing heat flow curves.[96] Reversing heat flow is associated with thermal events such as glass transitions and melting. Non-reversing heat flow is associated with processes such as curing or crosslinking, evaporation, and enthalpic relaxation. Modulated DSC was chosen over conventional DSC for this investigation because of its ability to detect weak glass transitions.

In the reversing heat flow curve, PEO (Figure 2.1a) has a T_g at -52 ℃ and a melting peak at 67 ℃, whereas PAA (Figure 2.1b) has a broad T_g at 129 ℃. The sharp up-turn starting at 135 ℃ in the non-reversing curve for PAA is attributed mainly to the loss of bound water and the beginnings of anhydride crosslinking. PAA's T_g is

somewhat higher here than prior reports[39] because we have cycled to a higher temperature, which induces some amount of crosslinking that elevates the T_g. For PMAA, two large endothermic peaks were observed at 117 and 214 ℃ in the non-reversing scan of the first heating cycle (Figure 2-1c). The first peak is attributed to the

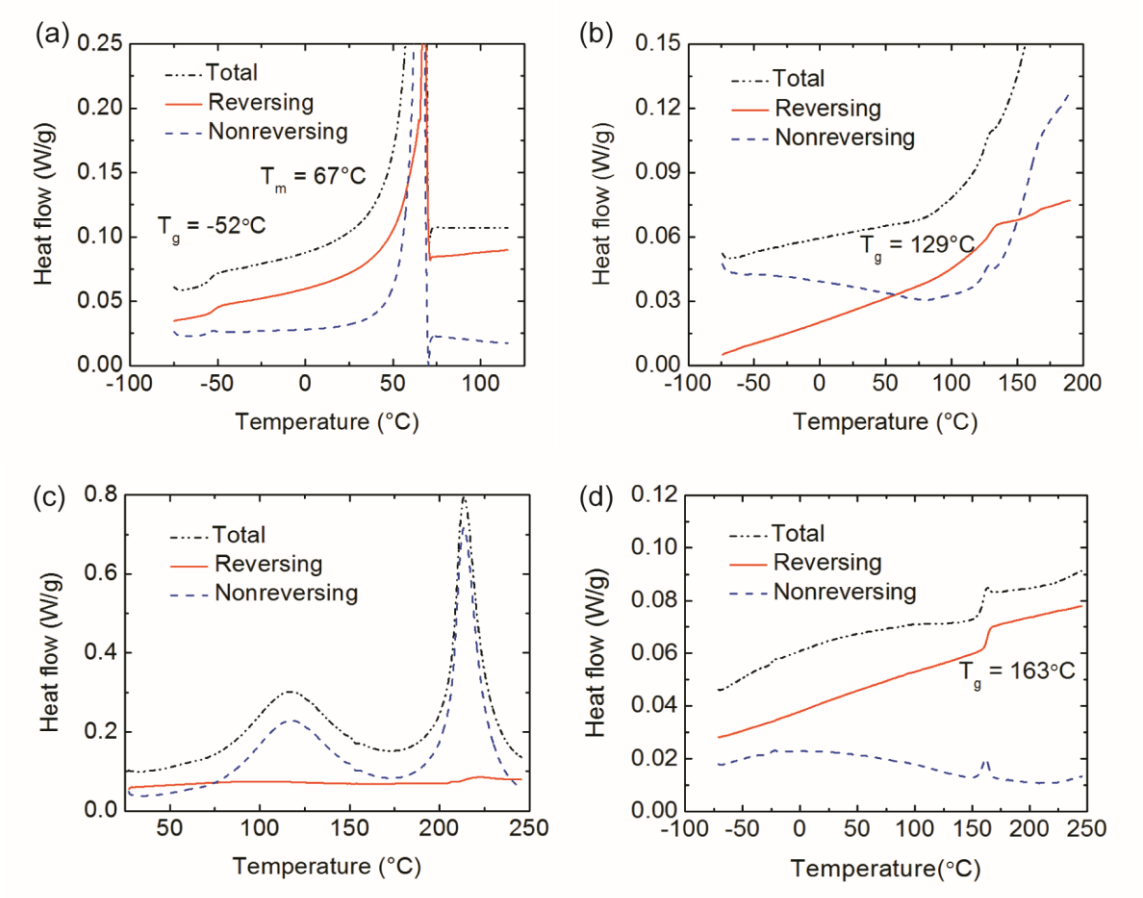

Figure 2.1 Modulated DSC thermograms of (a) PEO (2nd heating cycle), (b) PAA (2nd heating cycle), (c) PMAA (1st heating cycle), and (d) PMAA (2nd heating cycle). The heating rate, modulation amplitude, and period were 3 ℃/min, 0.636 ℃, and 40 sec, respectively.

release of bound water, and the second peak corresponds to the release of the water due to the formation of anhydride crosslinks.[97, 98] The onset temperature of the anhydride reaction was 170 ℃ for PMAA. In the second heating cycle (Figure 2.1d), a T_g was observed at 163 ℃ in the reversing heat flow curve. The glass transition appears only after the anhydride crosslinking reaction had taken place, and is consistent with prior reports.[98] Table 2.1 summarizes the thermal properties of homopolymers measured using modulated DSC.

Ellipsometry is often used to measure changes in refractive index or film thickness, and is a sensitive probe of thermal transitions in thin films. Whereas DSC measures heat capacity, ellipsometry monitors changes in refractive index and thickness. For example, as a thin film is heated it may expand, resulting in measurable increase in film thickness related to the film's coefficient of thermal expansion, α. At the glass transition α changes, which results in a change in the slope of a thickness-temperature curve.

Homopolymer PEO, PAA, and PMAA thin films (~100 nm) were prepared via spin-coating, and film thickness was measured as a function of temperature using ellipsometry. All data shown were obtained during the second heating stage. PEO thickness increased linearly with temperature, and an abrupt increase in thickness was observed upon melting at 56 ℃ (Figure 2.2a). The thickness of PAA also increased linearly as temperature increased; however, thickness decreased for temperatures over 130 ℃ (Figure 2.2b). No clear T_g for PAA was detected using ellipsometry, which may be a result of its broad glass transition range coupled with the loss of bound water.

Table 2.1 Thermal transitions of homopolymers and LbL assemblies measured using modulated DSC and ellipsometry

Sample	T_g (°C)	ΔT (°C)	ΔC_p (J $g^{-1}°C^{-1}$)	$\alpha_{glass} \times 10^4$ ($°C^{-1}$)	$\alpha_{rubber} \times 10^4$ ($°C^{-1}$)
PEO[a] (bulk, powder)	-52.4 ± 0.2	7.5 ± 0.6	0.16 ± 0.02	-	-
PEO[b] (94±8 nm)	-	-	-	5.3 ± 0.4 ($< T_m$)	11 ± 3 ($> T_m$)
PAA[a] (bulk, powder)	129 ± 1	24 ± 6	0.46 ± 0.07	-	-
PAA[b] (86 nm)	-	-	-	2.08 ± 0.04	-
PMAA[a] (bulk, powder)	163.2 ± 0.3	4.8 ± 0.5	0.18 ± 0.01	-	-
PMAA[b] (106 nm)	138 ± 2	-	-	1.97 ± 0.07	5.47 ± 0.05
PEO/PAA[a] (bulk, 7.2 μm)	47 ± 2	17 ± 3	0.37 ± 0.09	-	-
PEO/PAA[b] (149 nm)	41 ± 3	-	-	4.1 ± 0.4	6.0 ± 0.2
PEO/PAA[b] (33 nm)	50 ± 4	-	-	6 ± 2	10 ± 3
PEO/PMAA[a] (bulk, 7.4 μm)	138 ± 2	20 ± 1	0.21 ± 0.02	-	-
PEO/PMAA[b] (163 nm)	120 ± 3	-	-	2.8 ± 0.3	6.7 ± 0.3
PEO/PMAA[b] (30 nm)	127 ± 4	-	-	10 ± 1	17 ± 2

a. Measured using modulated DSC, b. Measured using ellipsometry

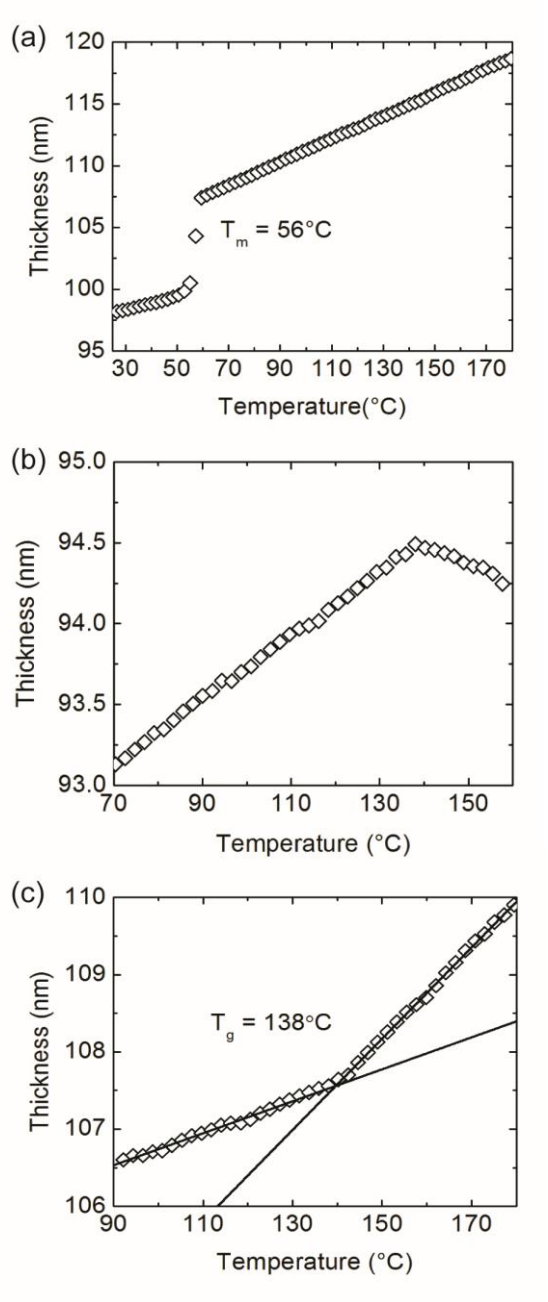

Figure 2.2 Thickness vs. temperature data for (a) PEO, (b) PAA, and (c) PMAA. Polymer films on silicon with native oxide were heated at a rate of 0.67 °C/min in a nitrogen environment. Data shown are taken from the second heating scan.

On the other hand, PMAA has a clear T_g at 138 ℃, (Figure 2.2c), after it had been thermally crosslinked. Coefficients of thermal expansion were calculated from data shown in Figure 2.2 using Equation 2.1 and are summarized in Table 2.1. For a ~100 nm PEO film, α was similar in magnitude to a reported value of 7.1×10^{-4} for bulk PEO;[99] prior reports of α for PAA and PMAA were not found in available literature.

The T_m's and T_g's measured using ellipsometry were notably lower than that measured using modulated DSC. Lower T_g's may be attributed to dissimilar measurement techniques,[100] dissimilar heating and cooling rates,[101] and substrate/surface effects.[102] Beaucage et al. observed an ellipsometric T_g 25 ℃ lower (for a 300 nm thick poly(styrene) film) than the calorimetric bulk T_g during heating, which they attributed to stresses and strains generated within film upon prior cooling.[91] On the other hand, substrate/surface effects may play a role, even for a 100 nm film. For example, the T_g of a 100 nm poly(4-hydroxy styrene) film grafted to a silicon oxide surface was more than 50 ℃ higher than that of bulk.[102] As a control, we measured the T_g of a 100 nm polystyrene film, which should be near bulk T_g according to Keddie et al,[85] and our ellipsometric T_g was 7 ℃ lower than the bulk calorimetric T_g for identical scan rates. As another control, we measured the calorimetric T_g of PMAA using scan rates of 0.67 and 3 ℃/min; the T_g decreased by only 1 ℃ for the slower scan rate. These controls suggest that the differences are likely a result of our different measurement techniques, rather than the different scan rates.

2.3.2 PEO/PAA and PEO/PMAA LbL Assemblies

Profilometry was used to monitor the evolution of thickness with respect to the number of layer pairs deposited for each type of dip-assisted LbL assembly (Figure 2.3). Following an initial nonlinear growth period for the first ten layer pairs, linear growth was observed for PEO/PAA and PEO/PMAA LbL assemblies (156 and 213 nm/layer pair, respectively). This type of growth profile is consistent with previous studies,[8, 78, 79] where a linear growth profile was observed following an "induction period" of exponential growth. Whereas Sukhishvili and Granick reported film fouling for PEO/PMAA LbL assemblies,[8] we were able to assemble PEO/PMAA LbL films in excess of 50 layer pairs, which may be explained by considering the effect of PEO molecular weight. As shown for hydrogen-bonding complexes, both the degree of complexation and the stability constant increases as the molecular weight of PEO increases.[103, 104] Here, we use a PEO molecular weight of 4,000 kg/mol whereas the prior report used 594 and 327 kg/mol, suggesting that our present PEO/PMAA LbL assemblies may be more stable and have a higher degree of hydrogen bonding. Another reason for our ability to grow PEO/PMAA LbL assemblies is that we have chosen a pH below the "modulation window" in which only partial film growth is possible.[79]

QCM-D was used to monitor the assembly of the LbL film's first few layer pairs (Figure 2.4). Hydrated film thickness and composition were calculated from using a Voigt model (Figure 2.5). Because QCM-D provides in-situ measurement of polymer adsorption from solution, the thickness presented in Figure 2.5 is considered a "hydrated"

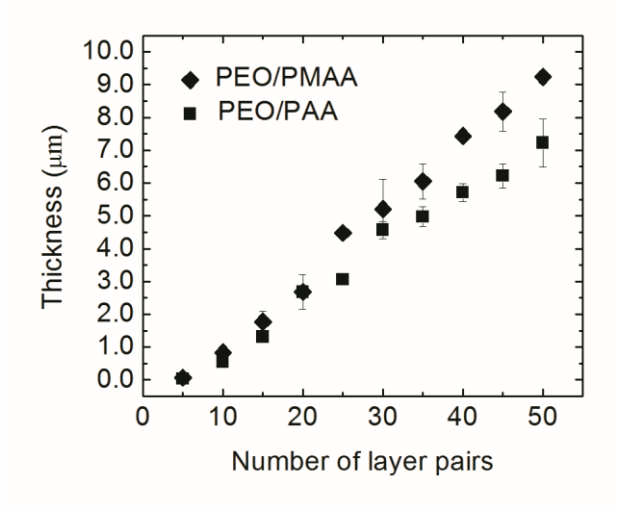

Figure 2.3 Dry PEO/PAA and PEO/PMAA LbL assembly thickness as a function of the number of layer pairs as measured by profilometry. Data shown are taken from "as-made" samples without any thermal treatment.

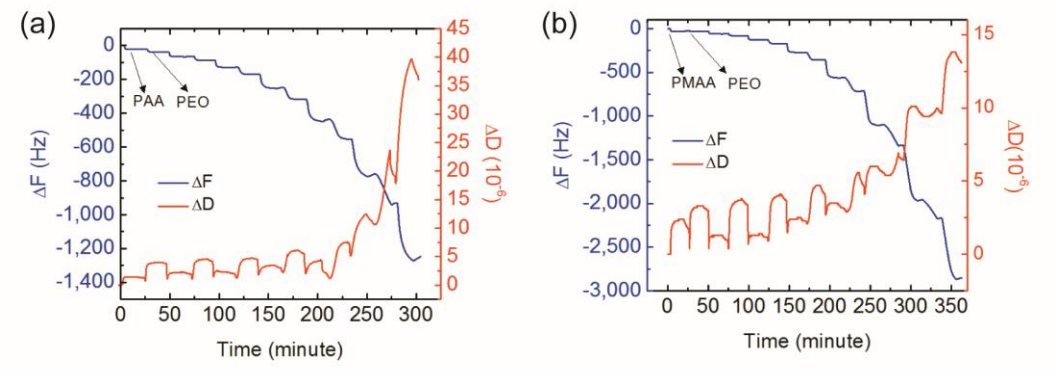

Figure 2.4 LbL buildup as measured by QCM-D for (a) PEO/PAA and (b) PEO/PMAA LbL assemblies.

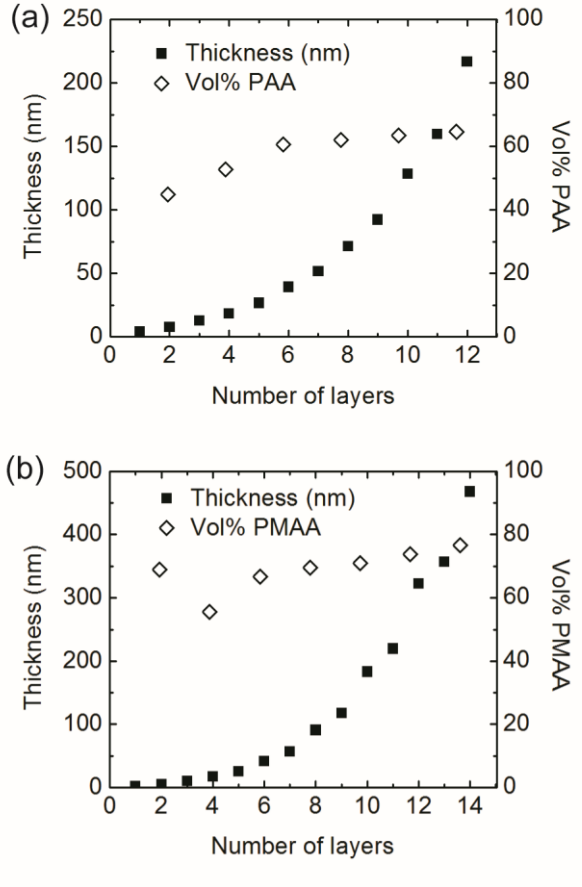

Figure 2.5 Hydrated film thickness and composition as a function of layer number for (a) PEO/PAA and (b) PEO/PMAA LbL assemblies calculated from QCM-D data using a Voigt viscoelastic model. Odd layers are PEO, and even layers are PAA or PMAA.

thickness. The first layer reported here is PEO adsorbed upon a PEI/PAA bilayer. Thus, every odd layer is a PEO layer and every even layer is a PAA or PMAA layer. Both PEO/PAA and PEO/PMAA LbL assemblies show exponential growth in the early stages of assembly. The percentage of PAA and PMAA by volume was calculated by dividing the sum of the thickness of the even layers by the total thickness of the film. The PAA or

PMAA content generally increases as the film builds up, and content saturates after 6 to 8 layers to 65 v% and 77 v% for PAA or PMAA-containing films, respectively. Applying the dry densities of the materials (PEO 1.2, PAA 1.1, PMAA 1.2 g/cm^3), the mol % of PAA and PMAA was estimated to be 50 mol % and 63 mol % by monomer unit respectively for films greater than eight layers (i.e., four layer pairs).

Modulated DSC was used to probe the thermal properties of dry, free-standing LbL assemblies (Figure 2.6). The thinnest free-standing film we could obtain was ~500 nm in thickness. PEO/PAA LbL assemblies of 30 layer pairs (4.6 ± 0.3 μm) were cycled between 140 and -80 ℃ (Figure 2.6a). A single T_g at 47 ± 4 ℃ was present in the reversing heat flow curve, accompanied by enthalpic relaxation in the nonreversing heat flow curve. This T_g is consistent with a previous report by Lutkenhaus et al., where a PEO/PAA LbL film assembled at pH 2.5 had a T_g of 40 ± 7 ℃.[39, 40]

PEO/PMAA LbL assemblies were cycled between 250 and -80 ℃; Figures 2.6b and c show the second heating scan for 30 and 10 layer pairs (5.2 ± 0.9 μm and 0.83 ± 0.01 μm), respectively. Both types of PEO/PMAA LbL films exhibited a weak T_g around 140 °C only after the sample's first heating cycle, where thermal crosslinking similar to that of homopolymer PMAA was observed. Anhydride formation was confirmed using FT-IR spectroscopy (Figure 2.7). Before heat treatment, FT-IR spectra show peak at 1694 and 1255 cm^{-1} which corresponding to COOH group. After heat treatment at 250℃ for 5min, the formation of anhydride is confirmed by the appearance of peak at 1002, 1752 and 1799 cm^{-1}.[97, 98] Interestingly, PEO/PMAA LbL films of 10 layer pairs display a

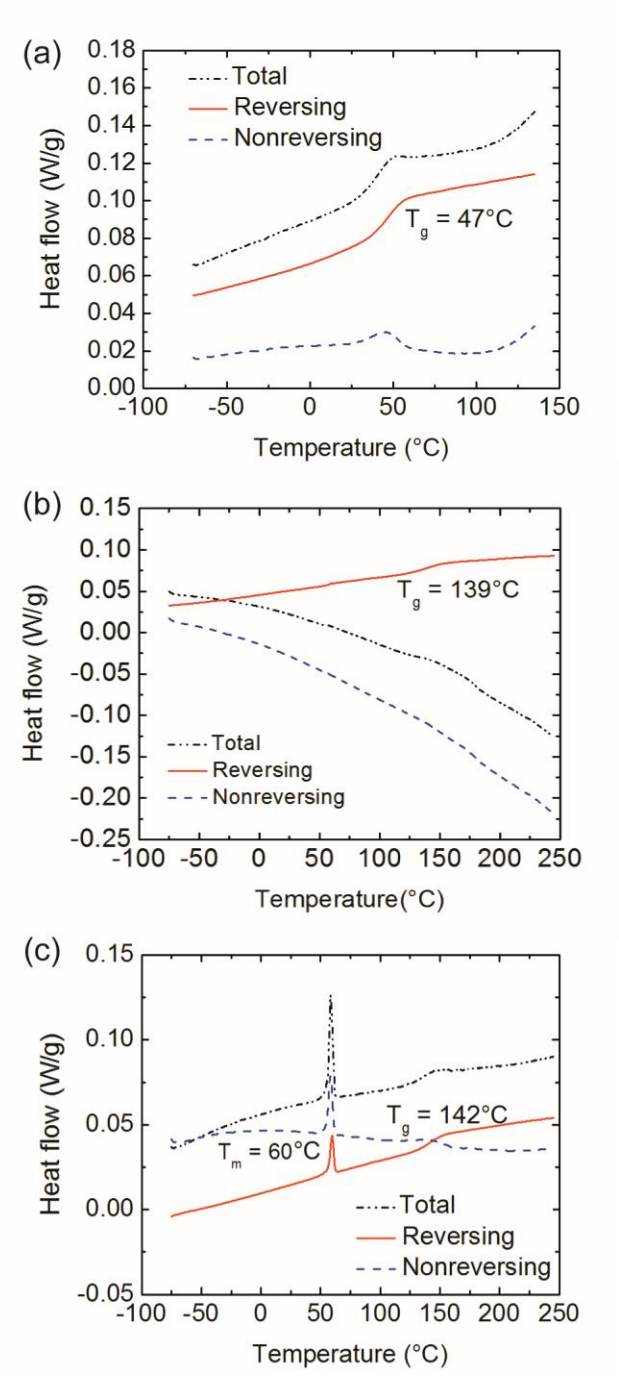

Figure 2.6 Modulated DSC thermograms of (a) $(PEO/PAA)_{30}$, (b) $(PEO/PMAA)_{30}$, and (c) $(PEO/PMAA)_{10}$ LbL assemblies, second heating scan. The heating rate, modulation amplitude, and period were 3 °C/min, 0.636 °C, and 40 sec, respectively.

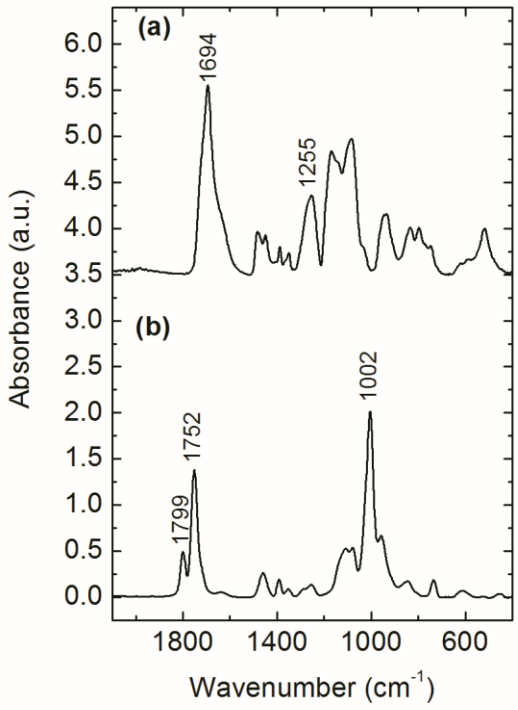

Figure 2.7 ATR/FT-IR spectra of PEO/PMAA LbL assemblies of (a) before heat treatment and (b) after heat treatment at 250℃, 5min.

melting peak in addition to a glass transition. Of note, the melting peak did not appear during the first cycle, where the anhydride reaction takes place, but appears in subsequent cycles. Considering this, we attribute the melting peak to PEO that phase separated during thermal crosslinking of PMAA in the first heating cycle. Also, the melting peak appears in samples of about 20 layer pairs or less (< 2.68 μm). For 20 layer pairs, two out of three samples exhibited a melting peak, and for 10 layer pairs, all samples tested displayed a melting peak. The average enthalpy of melting increased from 2.7 J/g to 7.2 J/g as the number of layer pairs decreased from 20 to 10, which

suggests that the mass fraction of crystalline PEO domains increases as film thickness decreases. The corresponding crystallinity (X_c) of PEO was calculated based on the following Equation 2.2[105]

$$X_c = \frac{\Delta H}{\Delta H^o} \tag{2.2}$$

where ΔH was the enthalpy of melting of PEO fraction in LbL film and ΔH^o was enthalpy of meting of 100% crystalline PEO (188 J/g).[105] Assuming that 23 wt% of the PEO/PMAA LbL film is PEO (estimated from QCM-D experiments), the percentage of crystalline PEO domains in the film increases from 6.2% to 16.7% as the number of layer pairs decreased from 20 to 10.

The effect of thickness on the T_g of LbL films was studied using modulated DSC for varying number of layer pairs (10, 20, 30, 50, 100 for PEO/PAA and 10, 20, 30, 40, 50 for PEO/PMAA, respectively). For a PEO/PAA LbL film (Figure 2.8a), the T_g increases by about 4 ℃ as thickness decreases from 15 µm to 540 nm. However for a PEO/PMAA LbL film (Figure 2.8b), there is no clear trend between T_g and film thickness. Of note, even the PEO/PMAA LbL film of 1 µm thickness (10 layer pairs) that exhibited PEO melting had a T_g similar to that of a 9 µm thick film (50 layer pairs) that did not exhibit PEO melting. Thus, the presence of the PEO crystalline domains does not seem to affect the T_g of the PEO/PMAA LbL assembly.

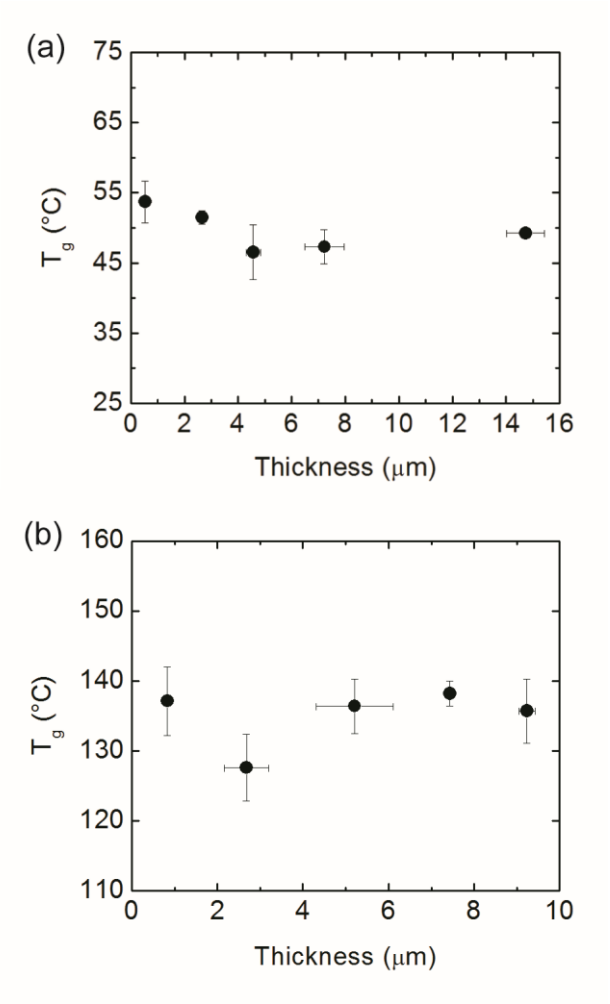

Figure 2.8 Effect of thickness on the T_g of (a) PEO/PAA and (b) PEO/PMAA LbL assemblies. T_g's are taken from the second heating scan using modulated DSC. In some cases, the error was smaller than the data symbol

The temperature range of the transition region (ΔT) and change in heat capacity during the glass transition (ΔC_p) were obtained from the reversing heat flow curve (Figure 2.9). In both PEO/PAA and PEO/PMAA LbL assemblies, ΔT and ΔC_p did not change much with respect to film thickness. ΔT of PEO/PAA LbL assemblies ranges

from 15 to 20 ℃, and the onset temperature (T_{onset}) was ~40℃ and the end temperature was (T_{end}) ~60℃ (Figure 2.10a). ΔT of PEO/PMAA LbL films ranges from 20 to 30 ℃, and is much larger than the ranges of both PEO and PMAA homopolymers (6 ℃). For the PEO/PMAA LbL film, the average T_{onset} was 124 ℃, and the average T_{end} was 149 ℃, respectively (Figure 2.10b). For both LbL films studied, T_{onset} and T_{end} did not vary much with respect to thickness. In Figure 2.9, ΔC_p of PEO/PAA LbL films was ~0.4 J/g·℃, and that of PEO/PMAA LbL films was 0.25 J/g·℃. This data confirms that PEO/PMAA LbL assemblies have a broader and weaker T_g relative to PEO/PAA LbL assemblies.

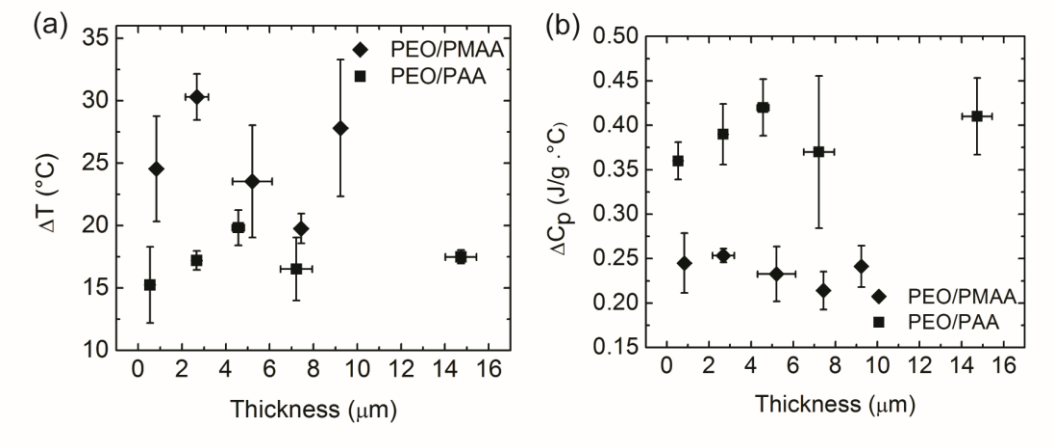

Figure 2.9 Effect of thickness on the (a) glass transition temperature range (ΔT) and (b) heat capacity change (ΔC_p) of PEO/PAA and PEO/PMAA LbL assemblies measured using modulated DSC.

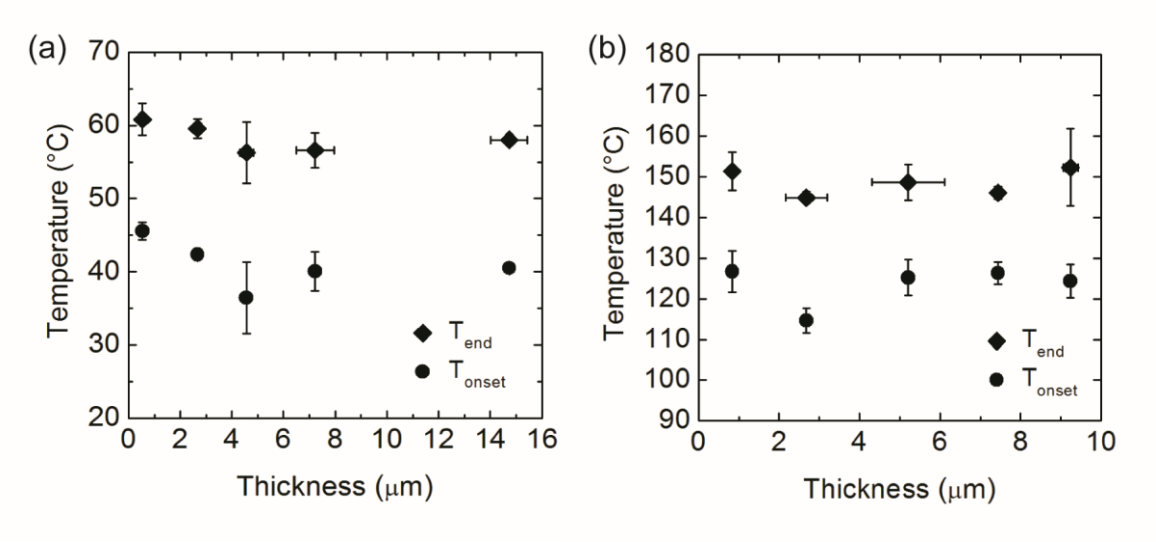

Figure 2.10 The onset and end temperatures for the glass transition of (a) PEO/PAA and (b) PEO/PMAA LbL assembly measured using modulated DSC.

LbL assemblies below 200 nm in thickness were analyzed using temperature-controlled ellipsometry (Figure 2.11). The T_g's were identified using thickness-temperature data from the second heating scan. The T_g's of PEO/PAA and PEO/PMAA LbL films of similar thickness (~100 nm) were 42 ± 2 and 125 ± 4 ℃, respectively. The T_g can be also identified using refractive index (Figure 2.12)

The T_g's of dip-assisted LbL films as a function of film thickness were obtained using temperature-controlled ellipsometry (Figure 2.13). Below 30 nm and above 200 nm thickness, the T_g could not be identified due to the limited sensitivity of our set-up combined with error introduced by surface roughness. The number of layer pairs was varied from 5 to 8 and 4 to 7 for PEO/PAA and PEO/PMAA LbL assemblies, respectively. In the case of PEO/PAA LbL films, the T_g increases by 9 ℃ as thickness

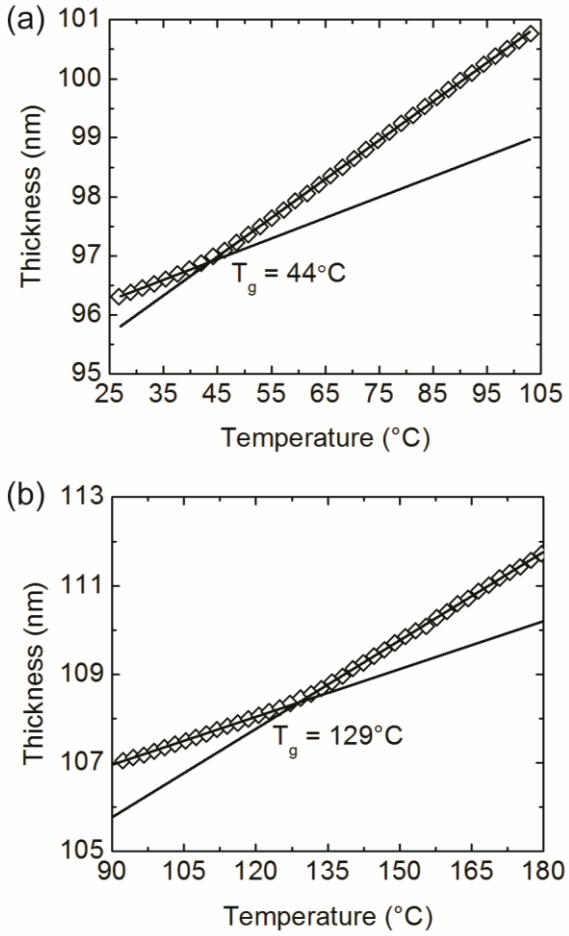

Figure 2.11 Thickness vs. temperature data for (a) $(PEO/PAA)_7$ and (b) $(PEO/PMAA)_6$ LbL assemblies on silicon measured using ellipsometry. Samples were heated at a rate of 0.67 °C/min in a nitrogen environment. Second heating scans are shown.

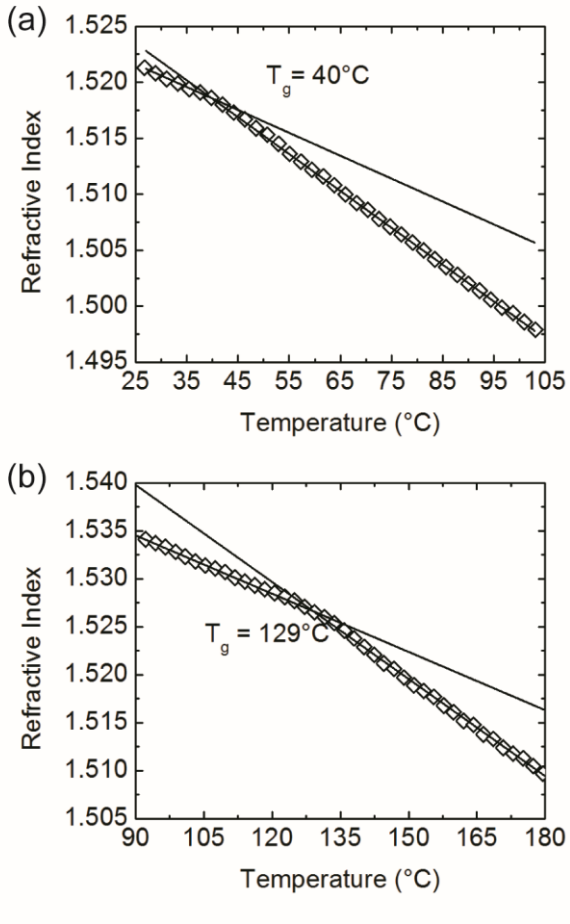

Figure 2.12 Refractive index vs. temperature for (a) $(PEO/PAA)_7$ and (b) $(PEO/PMAA)_6$ LbL assemblies measured using ellipsometry

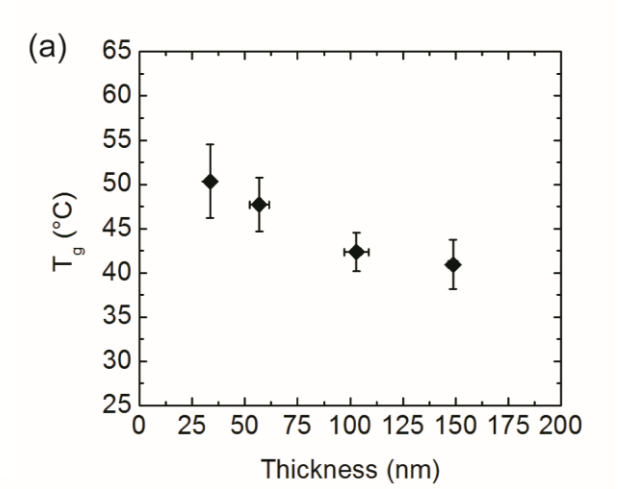

Figure 2.13 Effect of dry film thickness on the T_g of (a) PEO/PAA and (b) PEO/PMAA LbL assemblies identified using temperature-controlled ellipsometry.

decreases from 149 to 33 nm. In contrast to PEO/PAA LbL films, the T_g of PEO/PMAA LbL films remains fairly constant regardless of thickness. Both trends were similar to those observed for modulated DSC, although the temperatures measured do not exactly match, which may be attributed to the differing measurement techniques as discussed before. For all PEO/PMAA LbL films investigated using ellipsometry, an abrupt

increase in thickness coinciding with the melting peak observed in modulated DSC was observed during the second heating scan (Figure 2.14).

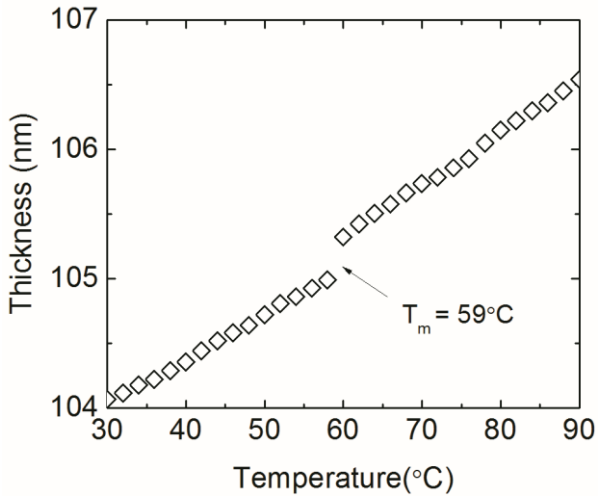

Figure 2.14 Thickness as a function of temperature for a $(PEO/PMAA)_6$ LbL assembly showing the PEO melting region measured using ellipsometry.

Figure 2.15 shows the effect of thickness on α for the LbL assembly. α_{glass} denotes the thermal expansion coefficient below T_g, an α_{rubber} denotes the thermal expansion coefficient above T_g. In both PEO/PAA and PEO/PMAA LbL films, α_{glass} and α_{rubber} generally increase as film thickness decreases. This is contrary to the ellipsometric study of polystyrene by Keddie et al., where α_{glass} increased with decreasing film thickness, while α_{rubber} remained constant.[85] In another study of polystyrene,[106] α_{rubber} decreased instead and α_{glass} was constant. Of note, the error range for both α_{glass} and α_{rubber} increased as the film thickness decreased as shown in Figure 2.15.

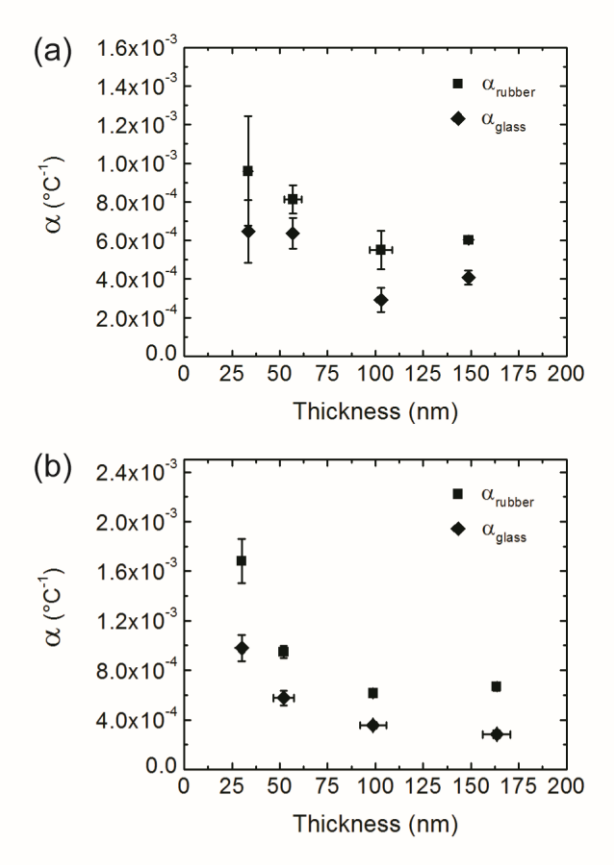

Figure 2.15 Thermal expansion coefficients (α) of (a) PEO/PAA and (b) PEO/PMAA LbL assemblies of varying film thicknesses.

2.4 Discussion

The LbL assemblies' composition, internal layer structure, and extent of hydrogen bonding are qualitatively related to the T_g, it's breadth, and it's strength. First we will discuss the T_g with regard to PEO/PAA or PEO/PMAA LbL composition; then, we will discuss the interpenetration or stratification of layers as suggested by T_g data. Also, the extent of hydrogen bonding between PEO and PAA or PEO and PMAA will be

presented. Finally, we will discuss our results as they relate to their dependence on film thickness.

Both PEO/PAA and PEO/PMAA LbL assemblies possess a single T_g between that of their pure components. Assuming that the film is a miscible blend and assuming that the composition of a thick LbL film is the same as the saturated composition observed in QCM-D, then one can predict a T_g for each bulk LbL assembly using the Fox Equation as a crude prediction;[101] this equation yields T_g's of 34 ℃ and 82 ℃ for PEO/PAA and PEO/PMAA LbL assemblies, respectively. The Fox Equation under-predicts T_g's in bulk LbL films, likely because interactions between the two polymer constituents stiffens the network and elevates T_g.

The breadth of the transition, ΔT, is related to the extent of layer interpenetration or heterogeneity of the structure. In Table 2.1 and Figure 2.9, ΔT of a PEO/PMAA LbL assembly is slightly larger compared to that of a PEO/PAA LbL assembly. A larger ΔT could be the result of inhomogeneous regions of slightly different compositions brought about by the breakage of hydrogen bonds and subsequent film restructuring during the first heating cycle for PEO/PMAA LbL assemblies. Or, the larger ΔT could indicate that PEO/PMAA LbL assemblies exhibit slightly less layer interpenetration relative to PEO/PAA LbL assemblies. The former hypothesis is more likely, considering that neutron reflectivity studies of PEO/PMAA LbL assemblies (without thermal crosslinking) conducted by Kharlampieva et al. show a completely interpenetrated structure throughout the film.[20]

The strength of the transition, ΔC_p, is related to the number of segments that are available for thermal activation.[100, 107] For example, as crosslinking increases, fewer mobile segments are available and ΔC_p decreases. The ΔC_p of a bulk PEO/PMAA LbL film was smaller than that of a bulk PEO/PAA LbL film, indicating that PEO/PMAA films have a smaller number of mobile segments; this lower mobility is likely caused by anhydride crosslinking between PMAA segments that stiffens the film.

Because PEO/PMAA LbL assemblies undergo substantial changes between the first and second heating scans, it is pertinent to discuss them here in further detail. In the first modulated DSC heating scan, PEO/PAA LbL assemblies show a single clear T_g, whereas PEO/PMAA LbL assemblies do not. This difference can be explained by considering analogous hydrogen-bonding complex literature. Both the degree of complexation between and the stability constant of PEO and PMAA are much larger than that of PEO and PAA because PEO/PMAA complexes are stabilized by additional hydrophobic interactions from PMAA's methyl group.[108, 109] The large degree of complexation in PEO/PMAA LbL assemblies may result in a stiff network that is highly crosslinked via hydrogen-bonds, resulting in significantly reduced chain mobility and the absence of a T_g in the first heating scan.

However, the PEO/PMAA LbL film does exhibit a T_g in the second heating scan once the anhydride crosslinking reaction has taken place. It is likely that hydrogen-bonds between PEO and PMAA break during anhydride crosslinking, which results in some amount of phase separation allowing for the appearance of a T_g in subsequent heating scans. A previous study verified that hydrogen-bonding between PEO and PMAA

essentially disappeared and that anhydride bonds were formed when PEO/PMAA complexes were heated over 200 °C.[110] Further evidence of phase separation in thermally crosslinked PEO/PMAA LbL assemblies is provided by the appearance of PEO melting in films of 20 layer pairs (< 2.68 μm) or less, Figure 2.6c. Melting is more evident in thinner films, which may suggest that the internal structure of the film is perhaps more stratified than a thicker film or that PEO phase separates into crystalline domains more easily in thinner films. The latter hypothesis is more likely in light of neutron reflectivity data that indicates that 230 nm PEO/PMAA LbL films (without anhydride crosslinking) are completely mixed.[20]

The effect of thickness on the T_g was studied using both modulated DSC and ellipsometery. T_g, ΔC_p, and ΔT did not change much for thick LbL films (540 nm to 15 μm) studied via modulated DSC, with the small exception of PEO/PAA LbL films. The T_g of PEO/PAA LbL films show more noticeable changes as thickness decreases below 100 nm as confirmed using ellipsometry, where the T_g increased by about 9 °C. The T_g of PEO/PMAA LbL films did not show a noticeable shift for any of the thicknesses investigated. The thermal expansion coefficients, α_{glass} and α_{rubber} both increased with decreasing thickness in both types of LbL assemblies.

Several factors such as composition, number of hydrogen bonds, and confinement effects may explain the elevated T_g in ultrathin PEO/PAA LbL assemblies. Let us first consider the films' composition as measured using QCM-D. Figure 2.5 shows that the volume fraction of PAA increases in the initial stages of LbL film growth until it reaches a steady-state volume fraction after 3-4 layer pairs had been deposited.

Because our ellipsometry measurements were taken on films 5-8 layer pairs thick, the measured films may be assumed to have identical compositions from sample to sample. Thus, composition is not likely the primary explanation for our observed results. Of note, the differences in thickness between Figure 2.5 and Figure 2.12 arise from differences in hydrated vs. dry thickness.

Another possible explanation for the increase in the T_g of ultrathin PEO/PAA LbL assemblies could be that the number of hydrogen bonds increases per unit volume. Hydrogen-bonds act as non-covalent crosslinks and reduce chain mobility, thus elevating T_g. Considering that samples explored here are in the regime where composition is relatively constant with respect to layer pair, one might conclude that the number of hydrogen bonds is also relatively constant with respect to thickness. Therefore, this hypothesis is also not a primary explanation for the observed phenomena.

Instead, the most likely explanation is that the T_g of PEO/PAA LbL assemblies increase with decreasing thickness because of substrate effects. In previous reports, an increase in T_g was reported for poly-(2)-vinylpyridine[111] and PMMA[88] on silicon with decreasing film thickness, which was attributed to favorable interactions between the polymer film and substrate. These favorable interactions outweighed surface effects, leading to an increase in T_g. In our study, PEO, which is the first adsorption layer, has favorable hydrogen bonding interactions with the native oxide surface bearing hydroxyl groups. Because the first few layers adsorb heterogeneously,[78] it is likely that PAA also contacts the substrate, leading to additional favorable hydrogen-bonding interactions with the substrate. No increase in T_g was observed for PMAA-containing films, which

might be explained by PMAA's higher degree of hydrophobicity, leading to less favorable interactions with the substrate relative to PAA-containing films.

In comparison to a recent study on ultrathin PEO/PAA LbL assemblies by Gu et al.,[78] our results are quite different. Gu reports that the T_g of PEO/PAA LbL assemblies decreases from 75 to 8 ℃ as the number of layer pairs decreases from 15 to 5, whereas we report here that the T_g increases from 41 to 50 ℃ as the number of layer pairs decreases from 8 to 5. This stark difference is explained by considering the method of measurement. Gu uses SM-FM, which probes the properties of a surface, meaning that the reported T_g is that of the surface and not that of the entire film. They report that the surface contains heterogeneous regions of PAA and PEO phases for films of low layer pair number, ~5. As the number of layer pairs increases, say to 15, the surface becomes a homogenous layer of the last polymer to be deposited. For this reason, the apparent T_g of a 15 layer pair film measured via SM-FM approaches the T_g of the last polymer deposited, in that case PAA. In our present report, both modulated DSC and ellipsometry probe the entire film, allowing for us to access thermal information related to the film as a whole.

2.5 Conclusion

The thermal properties of PEO/PAA and PEO/PMAA LbL assemblies of varying thicknesses have been studied using modulated DSC and temperature-controlled ellipsometry. The T_g of PEO/PAA LbL films increases significantly with decreasing film thickness, which is attributed to favorable interactions between the film and the substrate.

PEO/PMAA LbL films exhibited a T_g only after thermal crosslinking to produce anhydride bonds between PMAA chains. PEO/PMAA LbL films have a T_g that is independent of thickness, which is attributed to PMAA's hydrophobic nature and less favorable interactions with the substrate. Interestingly, PEO melting was observed for PEO/PMAA LbL films of 20 layer pairs, indicating that some degree of phase separation occurs after the thermal crosslinking step. Crosslinked PEO/PMAA LbL assemblies had a significantly weaker T_g relative to that of PEO/PAA LbL assemblies, indicating that PEO/PMAA LbL assemblies have fewer mobile segments participating in the transition.

The thermal expansion coefficients of both LbL assemblies increased with decreasing film thickness. Our work provides a new understanding of the structure of and substrate effects in hydrogen-bonded LbL assemblies. Our ongoing work with electrostatic LbL assemblies suggests that QCM-D can be used to detect the T_g's, which we also plan to explore in hydrogen-bonding LbL systems. This work also presents temperature-controlled ellipsometry as a versatile means to access glass transitions in LbL assemblies, and it is expected to be relevant to many other LbL systems.

CHAPTER III

A COMPARISON OF THERMAL TRANSITIONS IN DIP- AND SPRAY-ASSISTED LAYER-BY-LAYER ASSEMBLIES*

3.1 Introduction

Spray-assisted layer-by-layer (LbL) assemblies have a rapidly expanding array of applications, and a fundamental understanding of their internal structure is crucially needed to keep pace. Here, we use thermal analysis to understand differences between LbL assemblies made via dipping and spraying. Hydrogen-bonded LbL assemblies containing poly(ethylene oxide) (PEO) and a complementary polyacid are of particular focus in this study.

In the conventional dip-assisted deposition method, LbL assemblies are fabricated by alternately immersing a substrate into solutions or dispersions of complementary species with rinsing steps in between.[2] The spray-assisted deposition method was first introduced to dramatically speed up the process,[29] and is well described by a recent review.[112] In this method, solutions are sprayed onto a vertical substrate. A large surface area is coated uniformly in a significantly shorter time. For example, Nogueira et al. demonstrated that spray-assisted LbL deposition of optical coatings was

* Reprinted with permission from "A comparison of thermal transitions in dip- and spray-assisted layer-by-layer" by Choonghyun Sung, Katelin Hearn, Dariya K. Reid, Ajay Vidyasagar, Katelin Hearn, and Jodie L. Lutkenhaus, *Langmuir* **2013**, 29, 8907−8913, Copyright (2013) American Chemical Society

4 times faster than dipping.[113] Other forms of spray-assisted LbL assembly (simultaneous spray, step-by-step) have been recently demonstrated.[114, 115]

However, the structure and properties of LbL assemblies prepared by dip-assisted and spray-assisted methods are not necessarily the same. In general, the spray-assisted method gives a smaller film thickness at the same number of deposition cycles.[28] LbL assemblies of strong polyelectrolytes prepared by spraying do not exhibit the introductory period of initial slow film growth that usually appears for films prepared by dipping.[116] In addition, there are contradictory neutron reflectivity studies on the interfacial roughness of LbL films prepared by spraying.[56, 117] Krogman et al. compared a metal ion reactive thin LbL film prepared by dipping and spraying.[55] Spray-assisted LbL films contained two times higher metal ion concentration compared to dip-assisted films. To date, there are no comparative studies on the thermal properties of LbL films prepared by dipping and spraying. This knowledge is critical for the future translation of LbL films from dip- to spray-assisted LbL assembly.

In our prior work, we investigated the effect of thickness on the thermal properties of hydrogen-bonded LbL assemblies made via dipping.[118] PEO/polyacrylic acid (PAA) LbL assemblies had a single T_g that increased as the film thickness decreased below 100 nm. The single T_g indicated that the two polymers were miscible, and that the layers were highly interpenetrated, complementing prior neutron reflectivity work.[20] The T_g varied depending on the pH of assembly, showing as much as a 20 ℃ degree variation as pH increased from 2.0 to 3.0.[40]

Here, we compare the growth and thermal properties of spray-assisted PEO/PAA and PEO/polymethacrylic acid (PMAA) LbL assemblies made at varying pH-values to their analogs made via dipping. These two systems are specifically selected because it is has been shown that they have an observable T_g under dry conditions. We hypothesize that spray-assisted LbL assemblies are more stratified and heterogeneous than their dip-assisted analogues. By examining the glass transition temperature, the breadth of the transition, and the strength of the transition, we qualitatively examine microheterogeniety and local composition within the LbL films.

3.2 Experimental Section

3.2.1 Materials

Poly(ethylene oxide) (PEO, Mw = 100,000 g/mol), poly(methacrylic acid) (PMAA, Mw = 100,000 g/mol), poly(glycidyl methacrylate) (PGMA, Mw= 25,000 g/mol) were purchased from Polysciences. Poly(acrylic acid) (PAA, Mw = 100,000 g/mol) and 1,1-mercaptoundecanoic acid were purchased from Sigma Aldrich. Silicon wafers were purchased from Wafer World.

3.2.2 Substrate Preparation

First, silicon wafers were cleaned with piranha solution (3:1 sulfuric acid to hydrogen peroxide) for 15 min. *Caution: Piranha solution is extremely corrosive, and proper caution should be taken.* After oxygen plasma-treatment for 5 min, the silicon wafer was immersed in 0.1% PGMA/methyl ethyl ketone (MEK) solution for 3 min and held at 110℃ for 30 min.[119] Without surface treatment, PEO/PAA LbL assemblies

showed agglomerations and uneven thickness similar to previous reports.[79, 119] After cooling to room temperature, excess PGMA was removed by rinsing with MEK. The PGMA-coated silicon wafer was then immersed in 20 mM PAA or PMAA (based on the repeat unit molecular weight) solution in 18.2 MΩ·cm (Milli-Q) water for 20 min followed by placing on a hotplate at 110℃ for 30 min. Excess PAA or PMAA was removed by rinsing with water.

3.2.3 Dip-Assisted LbL Assembly

PEO, PAA, and PMAA were separately dissolved in 18.2 MΩ·cm water at a concentration of 20 mM based on the repeat unit molecular weight. All solutions including rinse water were adjusted to the same pH using HCl or NaOH. LbL assemblies were prepared using an automated slide stainer (HMS series, Carl Zeiss). PAA (or PMAA)-coated silicon wafers were dipped in PEO solution for 15 min followed by three water rinses for 2, 1, and 1 min, respectively. Then, the substrates were dipped into PAA (or PMAA) solution for 15 min followed by another three water rinses as before. This process was repeated n times to yield n layer pairs, denoted as (PEO/PAA)n, for example.

3.2.4 Spray-Assisted LbL Assembly

Identical solutions of the same concentration and pH were used in the spray-assisted LbL method. LbL films were assembled using an automated spraying system (Svaya Nanotechnologies). PAA (or PMAA)-coated silicon wafers were placed vertically 20 cm from the spray nozzle. First, PEO solution was sprayed for 10 sec and drained for 10 sec. Then, rinse water was sprayed for 10 sec followed by 10 sec of

draining. PAA or PMAA solutions were sprayed and rinsed according to the same protocol. All samples were dried in a convection oven at 40℃ for 30 min.

3.2.5 Profilometry

Thickness and root-mean-square roughness were measured using profilometry (KLA - Tencor Instruments P-6) and taken as the step height of a film scratched using a razor blade. The reported value was taken as the average of a minimum of three measurements and the error was taken as the standard deviation.

3.2.6 Atomic Force Microscopy (AFM)

AFM was performed using a Nanoscope IIIa (Digital Instruments) to investigate surface morphologies of the LbL films. Measurements were performed in tapping mode at a set point of 1 - 2 V and a scan rate of 1.0 Hz under atmosphere. Ca. 5 µm thick samples were used for all the measurements. Root-mean-square (RMS) roughness was measured in three different areas. The measured value was taken as the average of a minimum of three measurements and the error was taken as the standard deviation.

3.2.7 Ellipsometry

Film thickness was also measured using an LSE Stokes ellipsometer (Gaertner Scientific). The refractive index used for ellipsometer measurements was 1.5.[120, 121] Incremental thickness of each polymer layer was measured after the deposition of each layer and its rinsing steps. Composition was estimated from Equation 3.1, where the vol % of PAA (or PMAA) was estimated from incremental thickness measured in layer n, where n was the last layer pair deposited. Films of thickness 70 - 250 nm were used for

the estimation of polymer composition, and the reported composition was taken as the average of three separate samples.

$$\text{Vol \% PAA(or PMAA)} = \left.\frac{\text{PAA layer thickness}}{\text{PEO layer thickness} + \text{PAA (or PMAA)layer thickness}}\right|_{n} \quad (3.1)$$

3.2.8 Modulated Differential Scanning Calorimetry (Modulated DSC)

The thermal properties of LbL assemblies were characterized using modulated DSC (Q200, TA instruments). Samples were obtained by peeling the LbL film away from silicon substrates. The thickness of LbL assemblies used was around 5 μm. Samples were dried in a vacuum oven at 40℃ overnight. 5-10 mg was used for measurement. Unless otherwise stated, samples were first heated from room temperature to a predetermined temperature (110 ℃ for PEO/PAA LbL assemblies and 250 ℃ for PEO/PMAA LbL assemblies), held there isothermally for 5 min, cooled down to a desired temperature, and held there isothermally for 5 min, respectively. Finally, the sample was heated again to a predetermined temperature. Cooling and heating rates were at 3 ℃/min. The temperature-modulated amplitude was 0.636 ℃, and the period was 40 sec. Modulated DSC conditions were chosen based on our previous study.[118] These predetermined temperatures were chosen based on our previous study.[118] The first cycle served to remove residual water and to give the sample a well-defined thermal history. For PEO/PAA, 110 ℃ was chosen as the maximum temperature because it was found to be sufficient for removing residual water and yielding reproducible T_g's in subsequent cycles. However, for PEO/PMAA, a maximum cycling temperature of 110 ℃ proved insufficient because no T_g was observed in second and third cycles; instead, reproducible

T_g's were observed in second and third cycles when using a maximum cycling temperature (e.g. T = 250 °C) that lay above temperature of PMAA anhydride formation. (In the first cycle, two large endothermic peaks owing to the release of bound water and anhydride reaction of PMAA appeared). It is important to note that the observed PEO/PMAA T_g is different from the true T_g of the corresponding pristine film because of the required heat treatment. The T_g's of PEO/PAA LbL films were obtained from the second heating scan. T_g's of PEO/PMAA LbL films were obtained from the cooling scan following the first heating scan because reliable detection of the T_g was difficult due to the presence of a secondary T_g arising from PMAA homopolymer. The T_g was taken as the inflection point. The glass transition's temperature range or broadness (ΔT) was calculated as the difference between the transition's onset and final temperature.

3.3 Results and Discussion

3.3.1 LbL Film Growth

The thickness of dry LbL assemblies was measured as a function of layer pairs using profilometry (Figure 3.1a, b). Both PEO/PAA and PEO/PMAA LbL assemblies showed linear growth profiles. The layer pair thickness, calculated from the slope of the growth profile, was consistently smaller for spray-assisted LbL assemblies as compared to dip-assisted LbL assemblies (Figure 3.1c); for example, dip-assisted PEO/PAA LbL films assembled at pH 2.0 were about 2.4 times thicker than sprayed counterparts. Also, the layer pair thickness of PEO/PAA LbL films exhibited more of a pH-dependence than

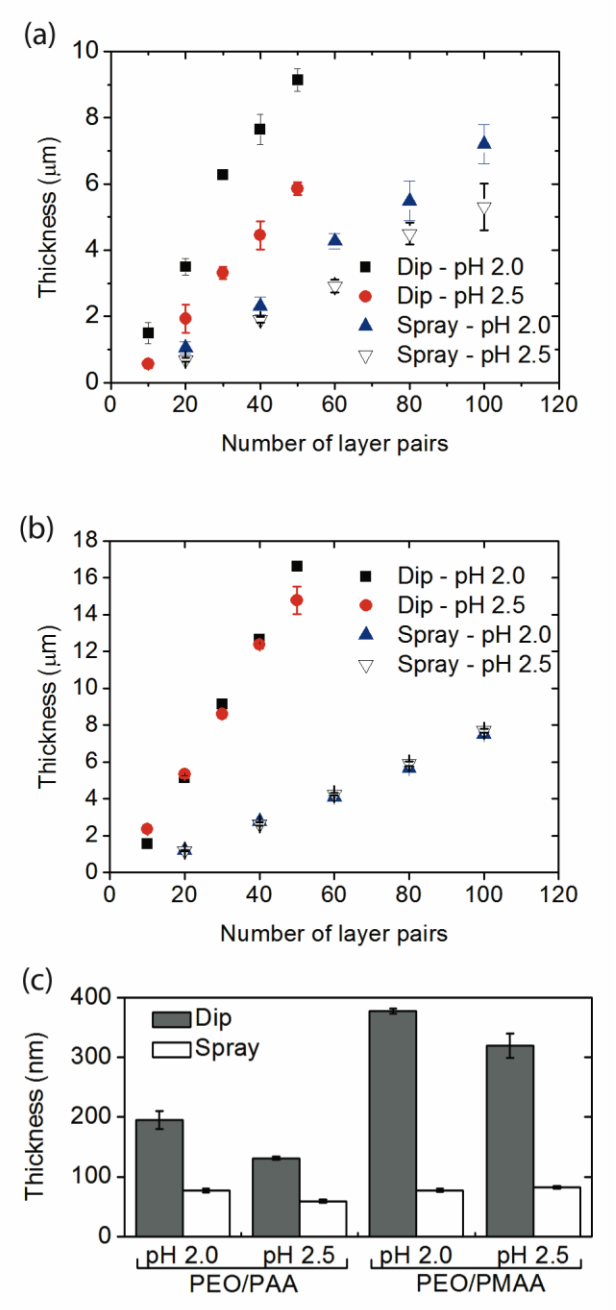

Figure 3.1 Dry film thickness of LbL assemblies of (a) PEO/PAA, (b) PEO/PMAA as a function of the number of layer pairs measured using profilometry, and (c) layer pair thickness obtained from (a,b). Films were prepared by dip-assisted and spray-assisted LbL deposition methods at pH 2.0 and 2.5.

PEO/PMAA films; PEO/PAA LbL films assembled at pH 2.0 were about 1.4 times thicker than their counterparts deposited at pH 2.5, whereas PEO/PMAA LbL films did not exhibit any remarkable dependence on pH.

The effect of pH on the properties of dip-assisted PEO/PAA LbL films has been previously studied.[40] PAA is known to undergo both inter and intramolecular hydrogen bonding, and it was shown that the fraction of inter-molecular (and intramolecular) hydrogen bonding PAA groups (i.e., COOH groups that hydrogen-bonded with PEO) decreased (and increased, respectively) as the assembly pH decreased from 3.0 to 2.0 in dip-assisted PEO/PAA LbL assemblies. As a result, thickness increased and saturated at pH values lower than 2.5 as the assembly pH decreased. Also in that prior study, the T_g consistently increased as the assembly pH decreased even when the pH value was lower than 2.5.

In this present study, as assembly pH changed from 2.5 to 2.0, the layer pair thickness increased while the T_g remained fairly constant. An increased layer pair thickness implies that the PEO/PAA LbL film assembled at pH 2.0 possessed chains bearing more loops, trains and tails, which could be a result of increased intramolecular PAA hydrogen bonding, relative to pH 2.5. This result is in contrast to our previous study,[40] where no dependence was observed below pH 2.5. The source of the contrasting results might be due to the different PEO molar masses utilized. In the previous study, the molar mass of PEO was 4,000,000 g/mol, and a molar mass of 100,000 g/mol was used in our present study. DeLongchamp et al. demonstrated that the growth of PEO/PAA LbL films is heavily influenced by the molecular weight of PEO.[79] It was

suggested that low molar mass PEO may not possess sufficient polyvalency of interacting ether oxygens to fully satisfy the protic surface and reverse the surface chemical identity. Such might be the case for our present work. On the other hand, the layer pair thickness of PEO/PMAA LbL films shows less of a pH dependence. PMAA has a more tightly coiled structure due to the hydrophobic nature of its methyl groups as compared to PAA. Also PMMA can be more insensitive at lower pH's than PAA, because the pK_a of PMAA (6-7)[122] is higher than that of PAA (5.5-6.5).[123]

3.3.2 Surface Morphologies of LbL Assemblies

Surface morphologies of LbL assemblies were examined using AFM and optical microscopy (Figure 3.2). Both dip-assisted and spray-assisted PEO/PAA LbL films possessed similarly smooth surface morphologies (Figure 3.2a, b). On the contrary, strikingly different surface morphologies were observed in PEO/PMAA LbL assemblies. Dip-assisted films showed micro-scale surface structures, but spray-assisted films showed a very smooth surface (Figure 3.2c, d). Root-mean-square (RMS) roughness was measured for samples about 5 μm in thickness using AFM (Figure 3.2e). For PEO/PAA LbL assemblies, dip-assisted films showed slightly lower RMS roughness than spray-assisted films. In contrast, for PEO/PMAA LbL assemblies, spray-assisted films demonstrated significantly lower RMS roughness than dip-assisted LbL assemblies. Optical images of LbL assemblies support this observation (Figure 3.2 inset and Figure 3.3). The roughness of the dip-assisted PEO/PMAA LbL film decreased slightly as assembly pH increased, however no strong conclusions could be made since they were nearly within error of each other.

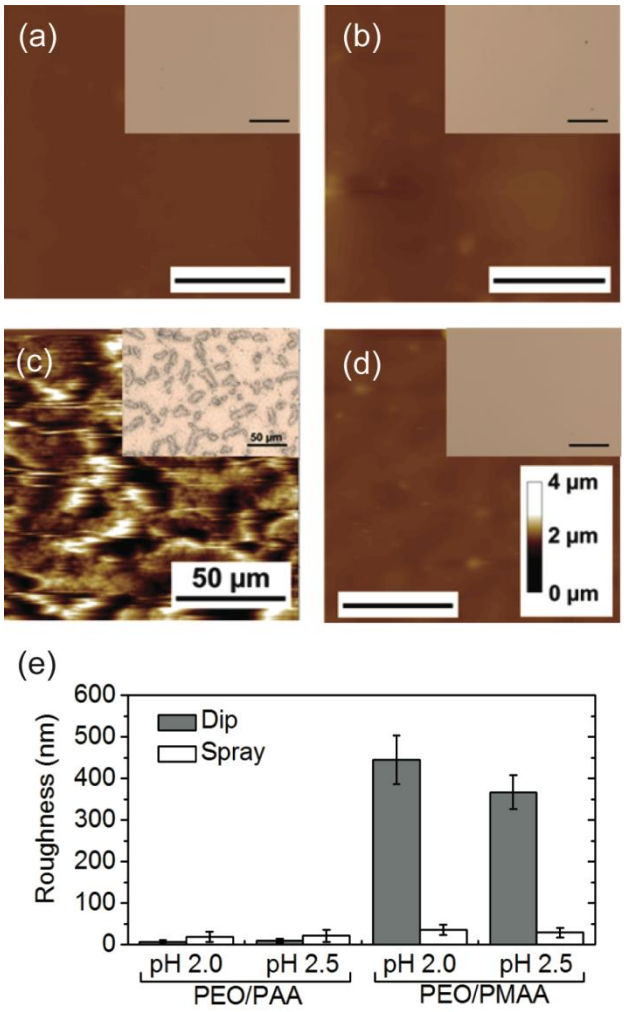

Figure 3.2 AFM images (135 µm × 135 µm) of (a, b) PEO/PAA LbL assemblies and (c, d) PEO/PMAA LbL assemblies prepared at assembly pH 2.0, and (e) root-mean-square roughness of various ~5 µm thick LbL assemblies measured using AFM. Films were prepared using (a, c) the dip-assisted method and (b, d) the spray assisted method. The same scale bars apply to all the images (a-d). All scale bars represent a length of 50 µm. The insets are corresponding optical microscopy images.

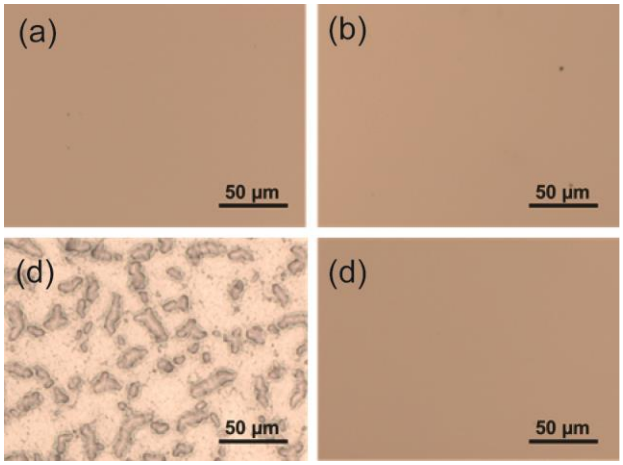

Figure 3.3 Optical images of (a, b) PEO/PAA LbL assemblies and (c, d) PEO/PMAA LbL assemblies prepared at assembly pH 2.0. Films were prepared using (a, c) the dip-assisted method and (b, d) spray assisted method.

To evaluate local roughness, AFM was performed over a small area (5 µm × 5 µm) to evaluate the local roughness (Figure 3.4) and compared to AFM images obtained over a large area (Figure 3.2). Both dip- and spray-assisted PEO/PAA LbL films show undulations about ~25 nm in height on the surface at higher magnification, which were not observable at low magnification. For PEO/PMAA LbL assemblies, both dip- and spray-assisted films at high and low magnifications showed similar corresponding surface morphologies.

RMS roughness was calculated from the higher magnification AFM images (Figure 3.4e). Most films exhibited a fairly smooth surface with the exception of dip-assisted PEO/PMAA LbL assemblies, consistent with the result of Figure 3.2e. However, the roughness of dip-assisted PEO/PMAA decreased from 445 nm to 36 nm when

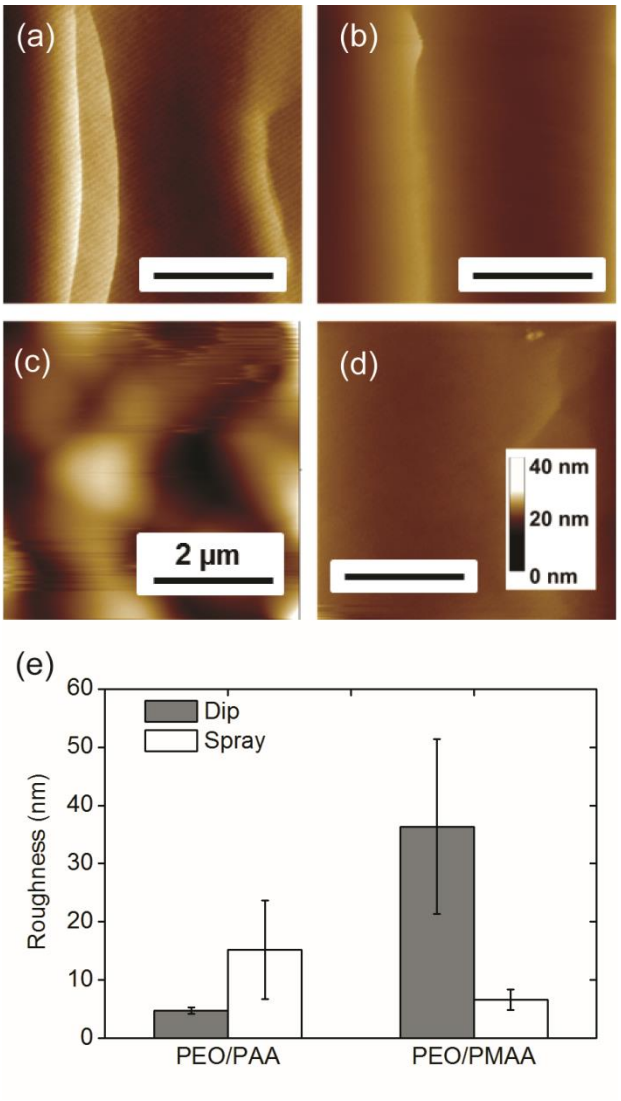

Figure 3.4 AFM images (5 µm × 5 µm) of (a, b) PEO/PAA LbL assemblies and (c, d) PEO/PMAA LbL assemblies prepared at assembly pH 2.0, and (e) root-mean-square roughness of ~ 5 µm thick LbL films measured using AFM. Films were prepared using (a, c) the dip-assisted method and (b, d) the spray assisted method. All the films were assembled at pH 2.0. All scale bars represent a length of 2 µm.

measured from a 135 µm × 135 µm vs. 5 µm ×5 µm scan area, respectively. This result suggests that dip-assisted PEO/PMAA LbL films are smoother locally than they are over a larger surface area, which is supported by the optical micrograph in Figure 3.2c, where features tens of microns in size were visible.

The exceptionally rough surfaces of dip-assisted PEO/PMAA LbL assemblies likely arise from PMAA, which exhibits a more tightly coiled conformation than PAA due to PMAA's hydrophobic interactions arising from the α-methyl group in its backbone.[124] Micro-scale surface roughness induced by hydrophobic interations has been observed in other dip-assisted LbL assemblies. Seo et al. observed large surface grains in LbL assemblies of hydrophobically modified PEO and PAA, where PEO-based micelles were responsible for the surface morphology.[125] Micro-scale corrugated surface morphologies were also reported in LbL assemblies of poly[2-(dimethylamino)ethyl methacrylate] and PAA prepared at pH values where films grew exponentially.[25] In that case, the uneven surface was caused by extensive interdiffusion and large-scale surface segregation.

However, the micro-scale surface texture of PEO/PMAA LbL assemblies disappears for the spray-assisted LbL method. It is possible that polymer chains have limited time to penetrate into the film and rearrange on the surface to develop the surface morphology. However, increasing the spraying time from 10 sec to 30 sec resulted in no statistical or visual difference in roughness (Figure 3.5). This suggests that either the time scale of penetration is longer than 30 sec or that another reason for the smooth surface exists. Alternatively, Krogman et al. have suggested that the convective action of

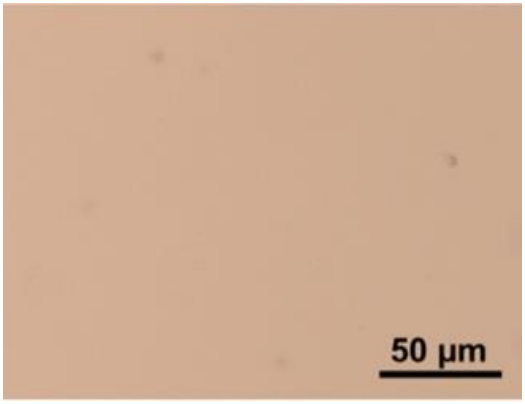

Figure 3.5 Optical microscope image of a PEO/PMAA spray-assisted LbL film using 30 sec of spraying. The surface appears relatively featureless, much like a similar sample produced with 10 sec of spraying (Figure 3.3d).

spraying may cause chain spreading while limiting interpenetration, leading to smoother films.[55] Smoothing of micro-scale surface morphologies was also observed for spin-assisted LbL assembly,[26] which was explained by the short contact time and shear forces arising from the spinning process. Like spin-assisted LbL assembly, spray-assisted LbL assembly is typified by its short contact time.

Dewetting has been observed in nanoscale LbL films,[126, 127, 128, 129] so it is important to clarify whether or not the surface morphologies observed here are attributed to dewetting or another phenomena. For example, Zimnitsky et al. showed that below a critical thickness (10 ~ 100 nm depending on the substrate) pores in PAH/PSS LbL films formed due to dewetting.[126] Another report describes the salt-induced dewetting of hydrogen-bonded LbL films as thick as 500 nm to 1 µm.[129] In our case, the film thickness was about 5 µm and thick enough to suppress dewetting. In our study, we used

a specially treated silicon wafer as the substrate, where PAA or PMAA had been chemically grafted to the surface to prevent dewetting and enhance LbL growth and adhesion. Generally, dewetting phenomena is accompanied by the formation of regularly sized pores in the polymer film.[130] Dewetting-induced pore formation has been also reported in LbL assemblies, which we do not observe.[126, 127, 128, 129] Instead, we believe that the observed micrometer-scale features are attributed to phase separation rather than dewetting, discussed later.

3.3.3 Thermal Properties of LbL Assemblies

The thermal properties of dry LbL films were studied using modulated DSC. Figure 3.6 shows typical thermograms of spray-assisted LbL films prepared at assembly pH 2.5. Dip-assisted LbL films also showed similar thermal behavior. PEO/PAA LbL assemblies showed a well-defined single T_g at 15 ℃ with a small amount of enthalpic relaxation when cycled between -90 and 110 ℃ (Figure 3.6a). PEO and PAA homopolymers had T_g's at -51 and 123 ℃, respectively.

A slightly different temperature profile was applied to PEO/PMAA LbL assemblies, which exhibited a well-defined T_g only after thermal crosslinking (i.e., anhydrie reaction).[118] For only PEO/PMAA LbL assemblies, samples were first heated to 250 °C to induce the formation of anhydride bonds from PMAA's carboxylic acid groups. Similar thermal treatments are required for even homopolymer PMAA to observe a T_g.[98, 118] No change in LbL surface morphology was observed after anhydride

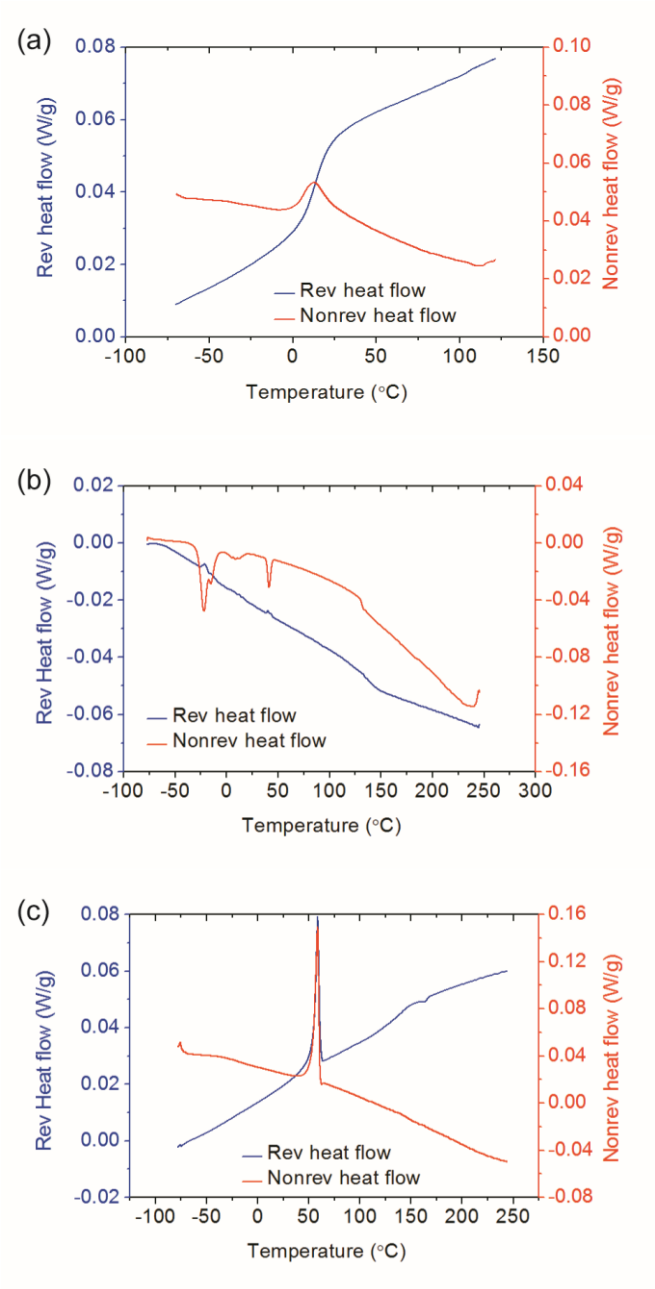

Figure 3.6 Modulated DSC thermograms of (a) PEO/PAA (2nd heating cycle), (b) PEO/PMAA (1st cooling cycle), and (c) PEO/PMAA (2nd heating cycle) spray-assisted LbL assemblies. Dip-assisted LbL assemblies had similar thermograms.

formation. In a subsequent cooling scan, exothermic peaks were observed around -10 to -20 ℃ and around 42 ℃ (Figure 3.6b). These exothermic peaks were attributed to the crystallization of phase-separated PEO domains, and occurred at much lower temperatures, likely because of interactions with PMAA.[131] Initial samples did not show any evidence of PEO melting. Therefore, this phase separation most likely occurred during the first heating scan, when anhydride crosslinking took place.

In the second heating scan for PEO/PMAA spray-assisted LbL films (Figure 3.6c), an endothermic peak due to the melting of PEO appeared, as well as a glass transition. The T_g of the spray-assisted PEO/PMAA LbL film was detected at 139 ℃, but overlapped with another small transition (Figure 3.7), which coincided with the T_g (163 ℃) of PMAA homopolymer after anhydride formation. The appearance of two

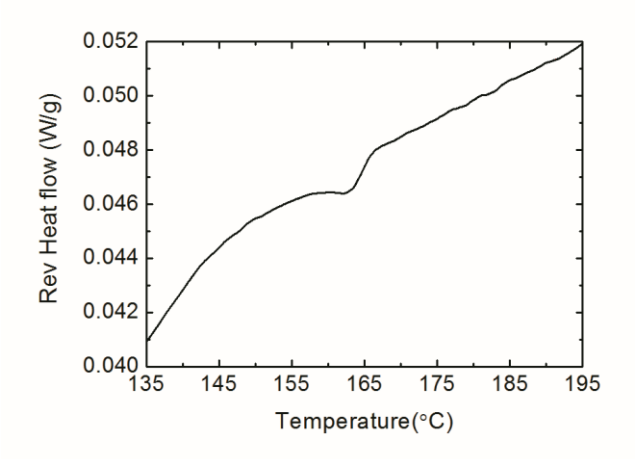

Figure 3.7 Modulated DSC thermogram of PEO/PMAA spray-assisted LbL assemblies (2nd heating cycle).

glass transitions was another indication of phase separation. This small transition was more distinct at pH 2.5 than pH 2.0, indicating that phase separation is more severe at pH 2.5 where the degree of ionization of PMAA is larger.

The fact that the first heating and cooling scans were distinctly different from each other suggests that the internal structure of the film changes upon heat treatment. From this study, we have shown that phase separation and PMAA crosslinking occurs during the first heating cycle. It is true that crosslinking should reduce the mobility of PMAA chains, possibly preventing further reorganization of the LbL assembly in subsequent cycles. However, a T_g was consistently observed in second and third cycles, which we attributed to PMAA-rich domains. The fact that a glass transition is observed at all suggests that the PMAA is not completely crosslinked.

Because LbL assemblies are often thought to be similar to complexes, it is important to briefly discuss the behavior of analogous hydrogen-bonded complexes. It is known that PEO/PAA complexes are less stable than PEO/PMAA complexes, which remain intact over a wider pH-range.[103, 124] Therefore, it can be argued that phase separation should be more pronounced in PEO/PAA LbL films with weaker hydrogen bonding. However, a comparable PEO/PAA LbL system heated to 170℃ (which is sufficient to induce anhydride formation[40, 41]) showed no evidence of subsequent PEO crystallization. Perhaps PEO/PMAA LbL films are more susceptible to phase separation because anhydride formation increases PMAA's hydrophobicity as more carboxylic acid groups are eliminated. In our present work, the thermal crosslinking presumably serves to remove hydrogen-bonding groups and increase the film's hydrophobicity, which

disrupts the configuration of the PEO/PMAA LbL film. This crosslinking reaction removes the PEO/PMAA LbL film far from that of a traditional PEO/PMAA complex, so it may be unwise to compare the present crosslinked system with an uncrosslinked complex.

In our previous study of dip-assisted PEO/PMAA LbL assemblies, PEO phase separation appeared for film thicknesses only below 2.68 μm.[118] However, here, the phase separation of PEO appeared for all films studied even though their thicknesses were around 5 μm. This difference could be due to the molecular weight of PEO, as discussed earlier. Here, we used a lower molar mass PEO to facilitate spraying, but this clearly results in more phase separation upon thermal heat treatment.

Figure 3.8 shows the T_g's and their broadness (ΔT's) for LbL assemblies obtained from the Modulated DSC themograms. The T_g was taken as the inflection point of the reversing heat flow. ΔT was calculated as the difference between the T_g's onset and the final temperature. In both PEO/PAA and PEO/PMAA LbL assemblies, the T_g's were similar for both deposition methods at a given assembly pH. In contrast, the broadness of the transition, which is related to the heterogeneity of the structure,[118] was consistently larger for the spray-assisted LbL films (Figure 3.8c). This difference indicates that spray-assisted LbL films have a less-interpenetrated structure relative to dip-assisted LbL films. In the dip-assisted method, polymers have sufficient time to adsorb and diffuse into the film. However, in the spray-assisted method, polymers tend to interact mostly with the film's surface due to the limited time for diffusion and rearrangement.[55]

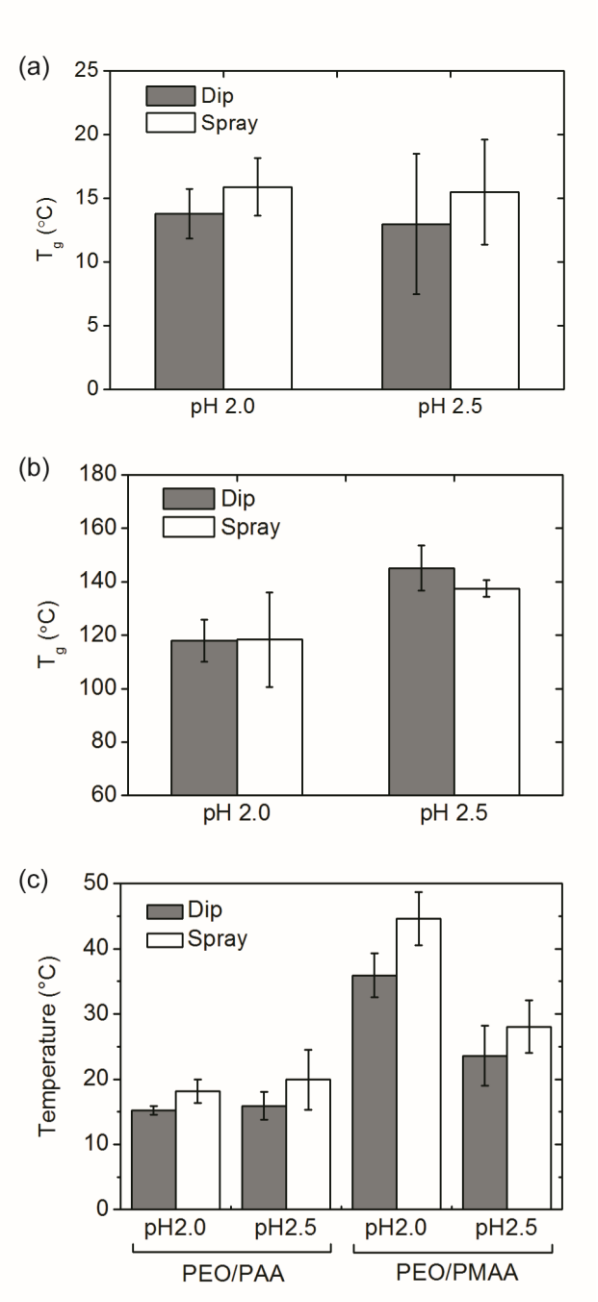

Figure 3.8 Glass transition temperatures of (a) PEO/PAA LbL assemblies, (b) PEO/PMAA LbL assemblies prepared by dipping and spraying, as well as (c) the transition's temperature range, ΔT. All assemblies investigated were ca. 5 µm thick.

Regardless of pH, the T_g of PEO/PAA LbL assemblies remained constant at 13-15℃ for both dip- and spray-assisted LbL methods (Figure 3.8a). The constant T_g suggests that the composition of the PEO/PAA LbL film is invariant with respect to deposition method and to assembly pH. Indeed, the volume fraction of PAA within both dip- and spray-assisted PEO/PAA LbL assemblies was estimated to be about 61 vol% PAA for assembly pH 2.0 (Figure 3.9).

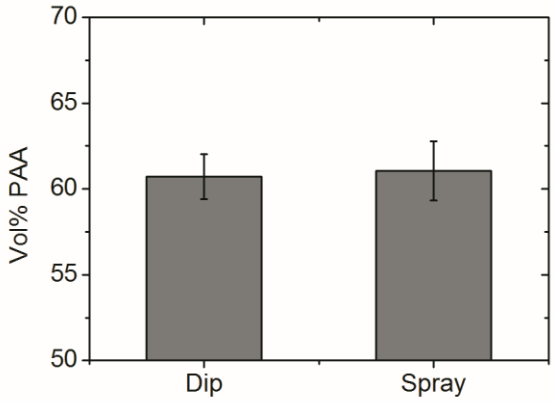

Figure 3.9 Volume percent PAA within dip- and spray-assisted PEO/PAA LbL films as determined using ellipsometry. The pH of assembly was 2.0. The incremental thickness, Δt_{PEO} and Δt_{PAA}, was measured after every layer PEO and PAA layer deposited, respectively. Volume percent PAA was calculated as $\Delta t_{PAA}/(\Delta t_{PAA}+\Delta t_{PEO})*100\%$.

On the other hand, PEO/PMAA LbL films exhibited markedly different behavior (Figure 3.8b). For dip-assisted PEO/PMAA LbL assemblies, the T_g increased from 118 ± 8 to 145 ± 8 °C as the assembly pH increased from pH 2.0 to 2.5. For spray-assisted

PEO/PMAA LbL assemblies, the T_g increased from 118 ± 18 to 137 ± 3 °C as the assembly pH increased from pH 2.0 to 2.5, although the two were within error of each other. The increase in T_g with increasing assembly pH indicates that either the PMAA content increases or that the nature of PMAA's microenvironment within the LbL film changes with increasing assembly pH. Considering that the PMAA content does not change much from pH 2.0 to pH 2.5 (Figure 3.10), the former supposition may be discarded. As for the latter supposition, the local PMAA composition, or the microenvironment, may depend on the degree of phase separation.

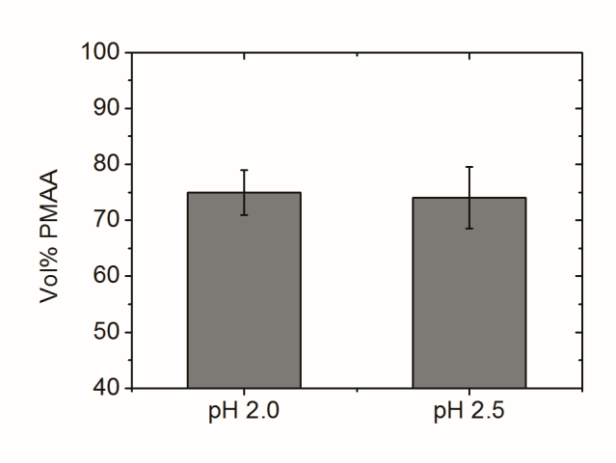

Figure 3.10 Percent PMAA by volume in dip-assisted PEO/PMAA LbL assemblies as calculated using ellipsometry.

As a qualitative measure of phase separation, one may compare the enthalpy of melting (ΔH_m) of PEO domains within PEO/PMAA LbL assemblies (Figure 3.11). At pH 2.5, ΔH_m is about four times higher than that of films assembled at pH 2.0, which suggests that larger amounts of PEO phase separate for assembly pH 2.5; this, in turn, leads to PMAA-rich domains have a higher local PMMA content and higher T_g. The narrowing of the T_g and subsequent decrease in ΔT also provided further evidence for the enrichment of PMAA in PMAA-rich domains as assembly pH increased from 2.0 to 2.5. We speculate here that the pH dependence may be attributed to either PMAA's slight change in ionization (PMAA pKa ≈ 6-7)[122] or differing amounts of inter and intramolecular hydrogen bonding.

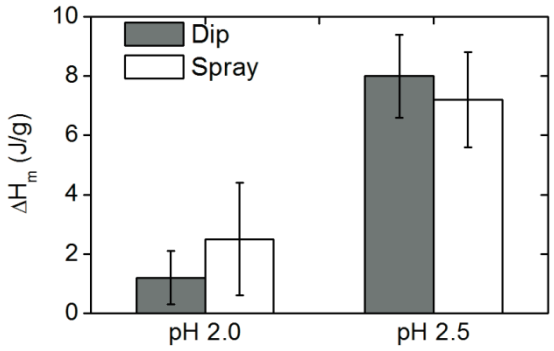

Figure 3.11 Enthalpy of melting of PEO/PMAA LbL assemblies taken from the second modulated DSC heating scan.

3.4 Conclusion

In summary, we have demonstrated that it is possible to prepare LbL assemblies of comparable thermal properties using the dip- and spray-assisted LbL assembly. Although the T_g's were similar regardless of the deposition method, spray-assisted LbL films possessed slightly broader glass transitions. These differences likely arise from the short contact times afforded by the rapid assembly of LbL films via spraying. Interestingly, spray-assisted PEO/PMAA LbL assemblies showed different surface morphologies from dip-assisted assemblies, and underwent phase separation following a high-temperature treatment. The extent phase separation was dominated by the pH of assembly, rather than the mode of fabrication. We expect that more dramatic differences in the thermal properties of dip and spray-assisted LbL assembly could arise from the use of inorganic particles, and will be a subject of future work.

CHAPTER IV

TEMPERATURE-TRIGGERED SHAPE-TRANSFORMATIONS IN LAYER-BY-LAYER MICROTUBES*

4.1 Introduction

LbL assembly is a versatile technique used to build functional thin films and nanostructures for applications ranging from energy to health.[2, 31, 132] Oppositely charged polyelectrolytes are alternately adsorbed onto various substrates with rinsing steps in-between. An LbL assembly's growth, structure, and properties can be fine-tuned using polymer chemistry and assembly conditions such as pH and salt concentration.[133, 134] Besides polyelectrolytes, other materials such as inorganic and metallic nanoparticles as well as biomacromolecules may act as the adsorbing species.[132, 135]

LbL microcapsules and microtubes have emerged as promising materials for drug delivery.[136, 137, 138, 139] Using sacrificial spherical particles or porous templates, an LbL assembly is deposited, resulting in microcapsules or microtubes, respectively, following template dissolution.[140] Hollow LbL microcapsules consisting of poly(diallyldimethyl-ammonium chloride) (PDAC) and poly(styrene sulfonate) (PSS) have exhibited a characteristic response upon heating – either shrinking or swelling,

* Reprinted with permission from "Temperature-triggered shape-transformations in layer-by-layer microtubes" by Choonghyun Sung, Ajay Vidyasagar, Katelin Hearn, and Jodie L. Lutkenhaus, *J Mater. Chem. B* **2014**, 2, 2088–2092, Copyright (2014) The Royal Society of Chemistry,

depending upon the outermost layer and the balance of hydrophobic and electrostatic forces.[43, 44, 141, 142] Elsewhere, PAH/PSS LbL microcapusles have exhibited shrinkage upon heating.[45, 46, 143, 144] This behavior was tied to a "glass-melt" transition.[43, 44]

We recently identified this transition using quartz crystal microbalance with dissipation (QCM-D), in which it was demonstrated that the transition is accompanied by a large flux of water into or out of the LbL assembly depending on whether it shrinks or swells.[49, 50] The transition itself exhibits many features typical of a glass transition temperature (T_g), (sigmoidal heat capacity, dramatic changes in mechanical properties and diffusion). We have also found that LbL assemblies containing weak polyelectrolytes PAH and PAA undergo a glass transition in water for most assembly pH values with the exception when both polyelectrolytes are fully charged. It should be noted that this transition has been called a "glass transition" or a "glass-melt transition", but the underlying process is likely very different from a traditional glass transition because ion pairs and water are involved.

Considering that hollow LbL capsules have shown dramatic changes in size in response to temperature, we hypothesized that LbL microtubes would exhibit an analogous unique response. Hollow LbL capsules retain their spherical shape during the transition, but LbL microtubes may not. Early work by He *et al.* showed that PAH/PSS microtubes transform to spheres and hollow capsules upon high-temperature incubation, although only a limited temperature range and only free microtubes were explored.[47]

Here, we investigated the temperature-triggered shape transformation of released and unreleased PAH/PAA LbL microtubes in water as a function of temperature and

time. The PAH/PAA LbL system is of particular interest because it offers future opportunities as a pH-responsive material. The temperature-response of unreleased LbL microtubes (in which the tubes remain in the template) is of interest because the substrate/film interface plays an additional role. Drastically different transformations are observed for the two scenarios. Results are discussed in the context of LbL film structure, properties, and surface interactions. To our knowledge, this is the first investigation of temperature-triggered changes in shape for LbL microtubes consisting solely of weak polyelectrolytes.

4.2 Experimental Section

4.2.1 Materials

Poly(allylamine hydrochloride) (PAH, MW = 58,000 g/mol) was purchased from Sigma Aldrich and poly(acrylic acid) (PAA, MW = 50,000 g/mol) was purchased from Polysciences. Fluorescein isothiocyanate dextran ((FITC-dextran), MW = 10,000 g/mol) was obtained from Sigma Aldrich. All chemicals were used without further purification. PAH and PAA solutions were prepared at a concentration of 10 mM, based on the molar mass of repeat the unit, by dissolving the polymer in 18.2 MΩ·cm water (Milli-Q, Millipore). The assembly pH of the solution was adjusted using HCl and NaOH. Track-etched polycarbonate (PC) membranes (Nucleopore^{TM}) were purchased from Whatman. The membrane's pore size and thickness were 1 μm and 10 μm, respectively.

4.2.2 Preparation of FITC-Labeled PAH (FITC-PAH)

Briefly, 33.6 mg (corresponding to a ratio of 1 FITC molecule for every 100 PAH repeat

units) of FITC was dissolved in 400 ml of PAH solution (2 mg/mL in 3:1 methanol-water mixture) and gently stirred overnight.[145, 146] The remaining FITC was removed by extensive dialysis against pure 3:1 methanol-water mixture. Then, the mixture was dialyzed against water for solvent exchange. Dialysis was performed until there was no trace of methanol in the dialysis solution as confirmed by FT-IR spectroscopy (Alpha FT-IR spectrometer, Bruker optics). For LbL assembly, as-made FITC-PAH solution was diluted to 10 mM and pH-adjusted as noted previously.

4.2.3 LbL Microtube Preparation

All samples were assembled using a programmable slide stainer (HMS series, Carl Zeiss Inc.). Polyelectrolyte microtubes were fabricated using a PC membrane as a porous template. PC membranes were first immersed in 10 mM PAH solution for 15 min followed by three separate rinses in pure water for 2 min, 1 min, and 1 min. Then, the PAH-coated membranes were dipped in the 10 mM PAA solution for 15 min followed by another three water rinses as described previously. This process was repeated *n* times to yield *n* layer pairs, denoted as $(PAH/PAA)_n$ for example. $(PAH/PAA)_nPAH$ denotes the case where PAH is the last layer. Assembly pH-values of 7.5 and 3.5 was used for PAH and PAA, respectively. Following LbL assembly, the LbL-coated membranes were dried overnight at room temperature. Both surfaces of the PC membranes were oxygen plasma-etched for 10 min to remove the film deposited on the membrane surface.[36] PAH/PAA LbL hollow tubes were released by selective dissolution of the membrane in dichloromethane (DCM) followed by sonication for 3 min. Then, PAH/PAA LbL microtubes were washed with fresh DCM three times and ethanol twice followed by re-

dispersion in water at pH 5.5. Then PAH/PAA LbL microtubes were dialyzed against pH 5.5 water for 17 hr to remove residual solvent. PAH/PAA LbL microtubes released from a single membrane were dispersed in 3 ml of water.

4.2.4 High Temperature Incubation

The microtube-in-water suspension (or microtube-in-membrane) was incubated in a temperature-controlled water bath for various times. All samples were sonicated for 3 min prior to incubation. For the incubation at 121 ℃, an autoclave (Steris, Amsco Lab250) was used.

4.2.5 Electron Microscopy

Scanning electron microscopy (SEM) images were obtained using a JEOL JSM-7500F at an acceleration voltage of 5 kV. A few drops of suspension were cast onto a silicon wafer, dried at room temperature, and sputtered with Pt for SEM observation. Transmission electron microscopy (TEM) images were collected using a JEOL 1200 EX operating at a voltage of 100 kV. The suspension was cast and dried on carbon-coated Cu grids for TEM measurements. The length and outer diameter of microtubes were measured from SEM images. We measured at least 30 microtubes and avoided the microtubes that curved significantly because the reading of the dimensions can be affected.

4.2.6 Modulated differential scanning calorimetry (Modulated DSC)

The thermal properties of bulk PAH/PAA LbL assemblies were characterized using modulated DSC (Q200, TA instruments). PAH/PAA LbL assemblies were assembled on Teflon® substrates, dried in vacuum oven at 30℃ overnight, and isolated

from the substrate. 18 wt% hydrated samples in pH 5.5 water were prepared according to our previous investigations.[49] Hydrated samples were first prepared by weighing the dried film in Tzero hermetic pans and by adding excess pH 5.5 water. Then, the samples were dried at 40℃ to evaporate water until a water content of 18 wt% of the dried film weight was achieved. The total sample weight was around 8-10 mg. Hydrated samples were left at room temperature for 24 hour before measurement. Modulated DSC measurements were performed by employing a heat-cool-heat cycle between 10 ℃ and 115 ℃ with amplitude of 1.272 ℃ for a period of 60 s. All thermal properties were obtained from the second heating scan.

4.2.7. Confocal Laser Scanning Microscopy (CLSM)

Optical images of microtubes in water were obtained using CLSM (Leica TCS SP5) with a 63x oil immersion objective. For effective visualization of microtubes, either FITC-PAH or FITC-dextran were used as a fluorescent labels.

4.3 Results and Discussion

To study the transformation of LbL microtubes in water, two different experimental routes were employed, Figure 4.1. In Route A, a PAH/PAA LbL film is deposited onto an ion track-etched polycarbonate template. Film deposited on the template's surface is removed, the membrane is dissolved, and the released microtubes are purified via dialysis. The microtubes are then incubated at the time and temperature of interest, and dried for further analysis. In Route B, the LbL-coated membrane is incubated in water at the desired temperature. The microtubes are then released from the

membrane for further analysis. The main difference between the two routes is whether microtubes are incubated when freely suspended (Route A) or when bound to the membrane pore (Route B).

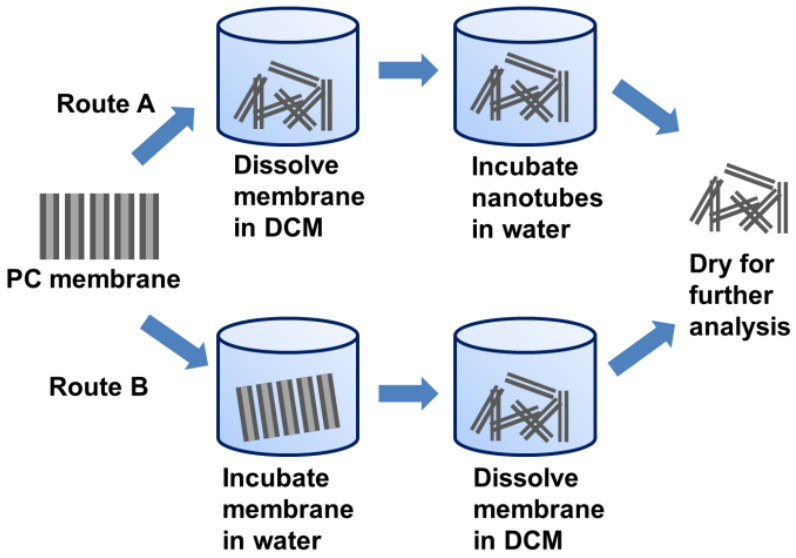

Figure 4.1 A schematic illustration of the two routes. In route A, microtubes are released from the membrane and then incubated. In route B, the unreleased microtubes are incubated and then released.

4.3.1 Route A. Incubation of Released LbL Microtubes

Figure 4.2 shows images of microtubes prior to high temperature incubation. Figure 4.2a and b show typical scanning electron microscopy (SEM) and transmission electron microscopy (TEM) images of $(PAH/PAA)_{10}$ microtubes released from the template using dichloromethane (DCM). (The subscript in $(PAH/PAA)_{10}$ is indicative of

the number of layer pairs deposited). The microtubes' length (10 μm) and diameter (1 μm) were comparable to the original dimensions of the template's pores. The tubular structure is clearly present in the TEM image shown in Figure 4.2b, from which the average wall thickness was estimated to be 110 nm. Following dialysis in water to remove residual DCM, the microtubes appear to soften and contract to 5.1 μm in length and 1 μm in diameter (Figure. 4.2c). Confocal laser scanning microscopy (CLSM) of the dialyzed microtubes in water also shows the microtubes' contraction and wall-thickening to 390 nm, Figure 4.2d and Figure 4.3. Many of the microtubes appear to retain their hollow shape.

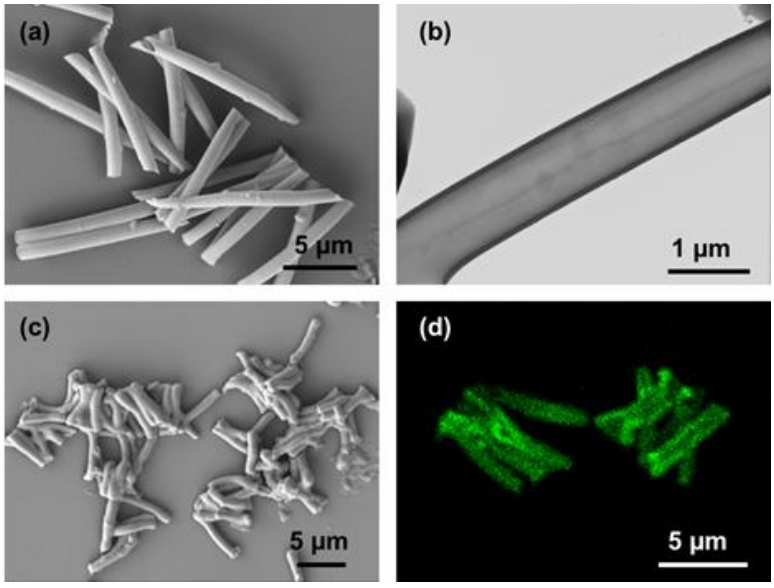

Figure 4.2 (a) SEM and (b) TEM images of microtubes released from the sacrificial membrane using dichloromethane, (c) SEM image of the microtubes after dialysis in water, and (d) CLSM image of microtubes in water at room temperature.

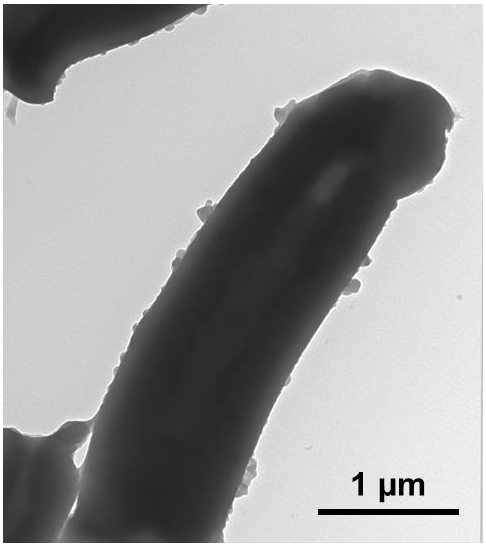

Figure 4.3 TEM images of $(PAH/PAA)_{10}$ microtubes incubated at 25℃.

The effect of high temperature incubation on the transformation of the LbL microtubes in water was investigated for varying incubation temperatures ranging from room temperature to 121 ℃ (Figure 4.4). At all incubation temperatures, except 121 ℃, the incubation time was 1 hour. At 121 ℃, the incubation temperature was 45 min. Generally, as the incubation temperature increased, the microtubes contracted and the outer diameter increased. LbL microtubes incubated at 85 ℃ and 95 ℃ did not exhibit a hollow tubular structure as confirmed using TEM (Figure 4.5a and b), and the majority of the incubated microtubes appear to have closed ends. At 121 ℃, fairly spherical/ellipsoid shapes are observed as shown in Figure 4.4c and d. These results suggest that this transition from open to closed structures might be applicable for the encapsulation of small molecules. The transformation is irreversible; even after 1 week the ellipsoid shapes remained intact.

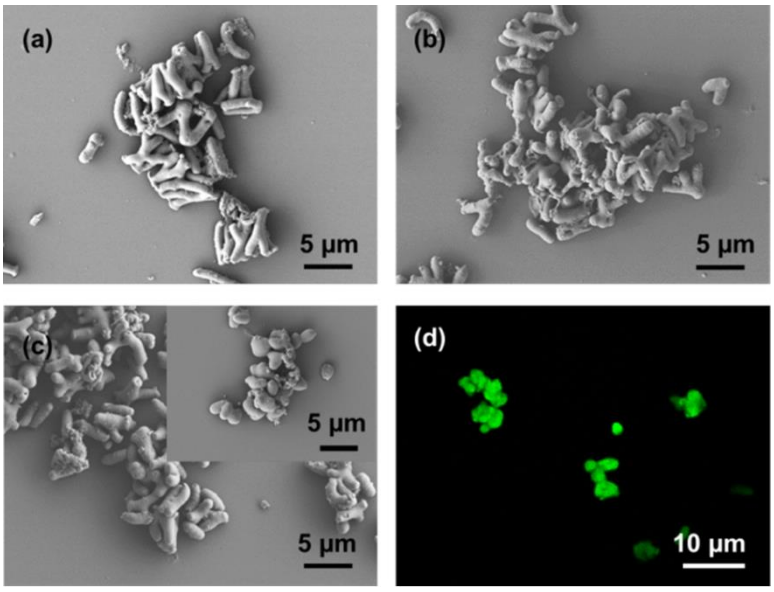

Figure 4.4 SEM images of the microtubes incubated at (a) 70, (b) 95, and (c) 121 ℃. CLSM image of the microtubes in water after incubated at 121 ℃.

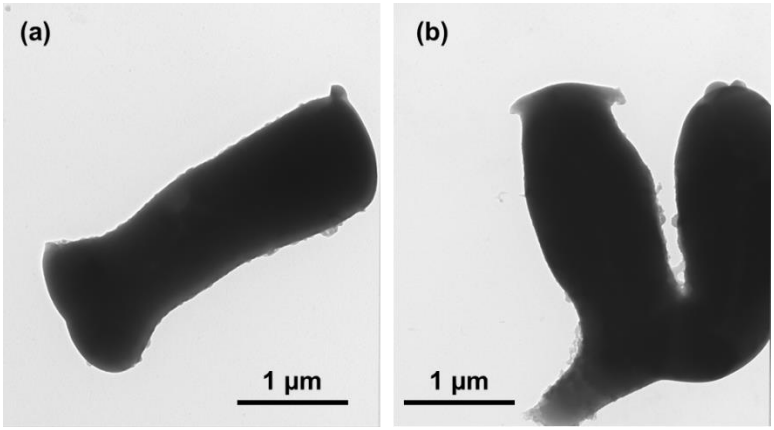

Figure 4.5 TEM images of $(PAH/PAA)_{10}$ microtubes incubated at (a) 85, and (b) 95 ℃.

To study the effect of incubation time, microtube suspensions were incubated for varying times at a fixed temperature, 70℃ (Figure. 4.6). Generally, the microtubes shorten and fatten as incubation proceeds. After 5 hr, the shape became similar to that of the samples incubated at 121 ℃ for 45 min. This demonstrates that incubation time can be used to control the transformation at low incubation temperatures. However at 121 ℃, the transformation rapidly proceeded within the first 15 min.

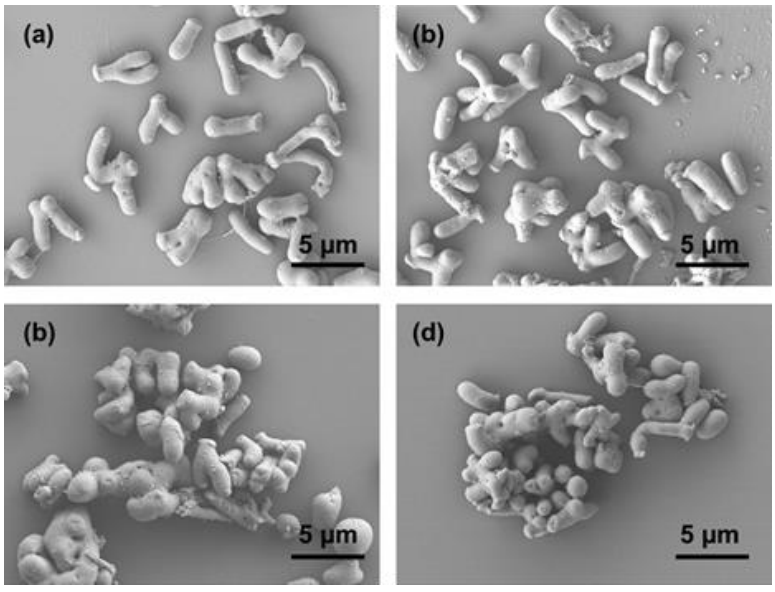

Figure 4.6 SEM images of $(PAH/PAA)_{10}$ microtubes incubated at 70 ℃ for (a) 15 min, (b) 30 min, (c) 2 hr, and (d) 5 hr.

To quantify the effect of the incubation temperature and time, the length and outer diameter of microtubes were measured from multiple SEM images. Figure 4.7a shows the effect of incubation temperature on the microtube dimensions. As the incubation temperature increased, the microtubes' length decreased and diameter increased. Above 85 ℃, the length remained fairly constant. However, the microtubes'

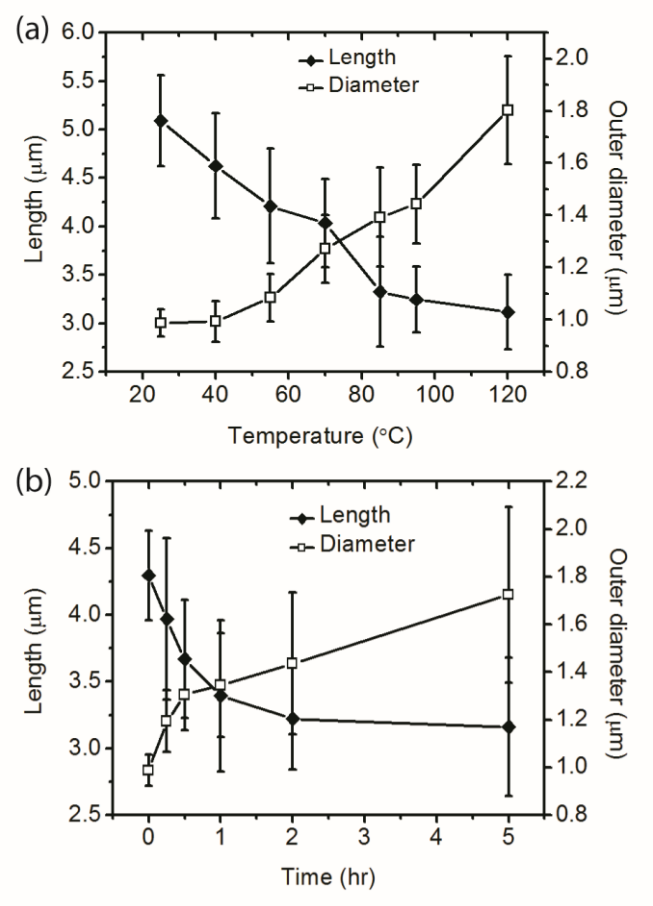

Figure 4.7 Length and outer diameter of $(PAH/PAA)_{10}$ microtubes as a function of (a) incubation temperature (incubation time as noted in main text) and (b) incubation time at 70 ℃.

outer diameter increased linearly as the incubation temperature increased. It should be noted that some microtubes incubated at temperatures greater than 95 ℃ merged to form larger structures (evident in Figrue 4.4c and d), resulting in increased error for the outer diameter. Figure 4.7b shows the effect of incubation time on the microtube dimensions at a fixed incubation temperature of 70 ℃. The microtubes' length decreased rapidly in the first hour and leveled off after 2 hr of incubation. The microtubes' outer diameter also increased with incubation time.

The temperature-triggered transformation of microtubes did not depend on the microtubes' innermost layer. For instance, $(PAH/PAA)_{10}PAH$ microtubes showed similar results to $(PAH/PAA)_{10}$ (Figure 4.8 and 4.9). This result is in contrast to the known odd-even effect for PDAC/PSS LbL microcapsules discussed previously. The lack of odd-even effect for PAH/PAA LbL microtubes suggests that hydrophobic forces dominate upon incubation, in which the PAH/PAA microtube contracts regardless of the identity of the inner layer. The aspect ratio of the microtubes decreases from about 5 to about 1.7 as incubation temperature increases from room temperature to 121 ℃. The reduction in aspect ratio further supports the idea that hydrophobic forces dominate, in which a reduction in water/tube contact area occurs upon incubation. At extended times and temperatures, the tubes merged with each other, further reducing the contact area and increasing the apparent volume (Figure 4.10).

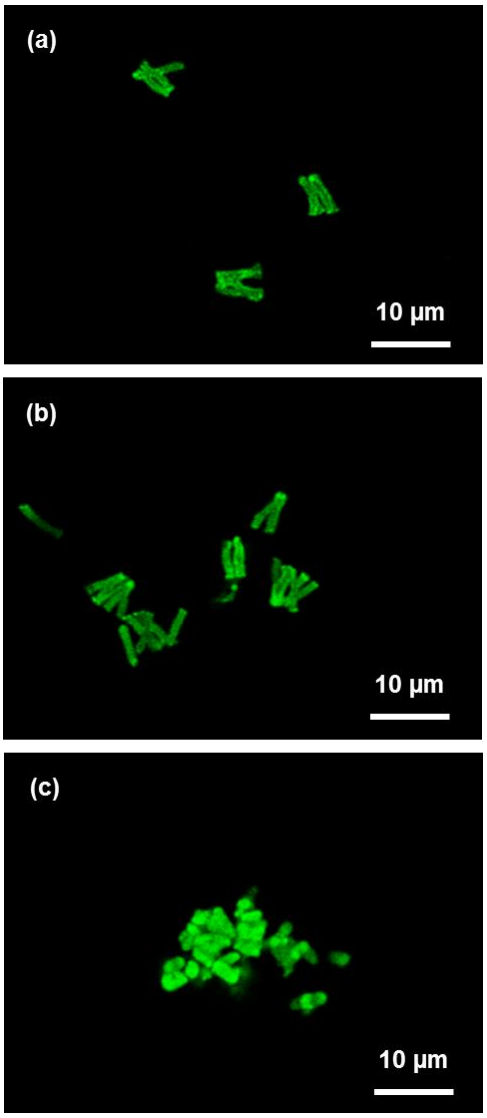

Figure 4.8 Confocal microscopy images of $(PAH/PAA)_{10}PAH$ microtubes in water (a) after dialysis and after incubation at (c) 40 and (d) 95 ℃.

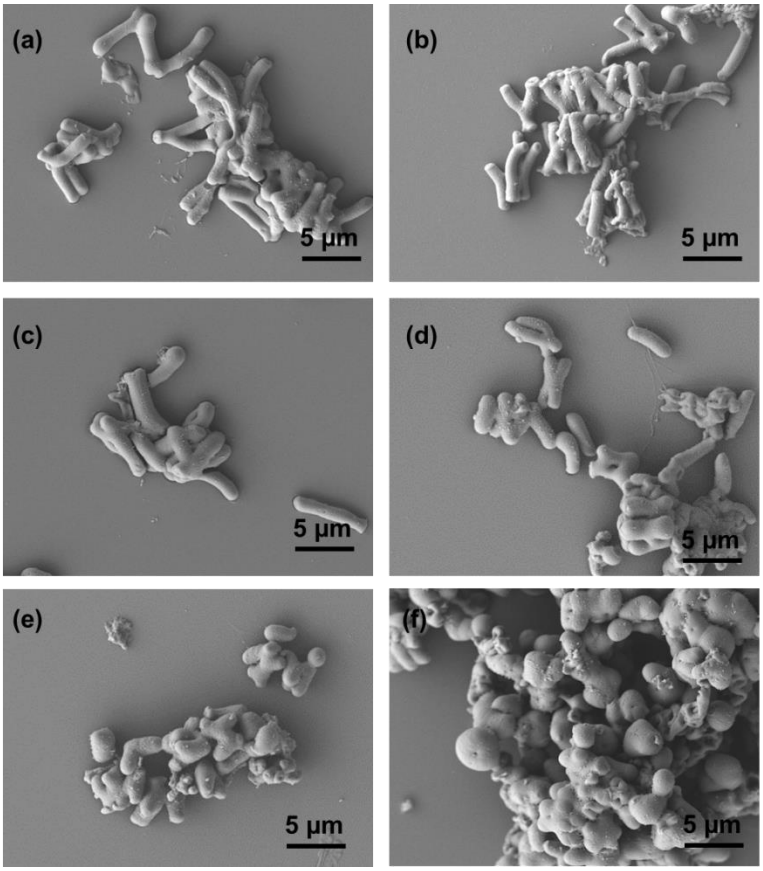

Figure 4.9 SEM images of $(PAH/PAA)_{10}PAH$ microtubes (a) after dialysis, and after incubation at (b) 40, (c) 55, (d) 70, (e) 95, and (f) 121 ℃.

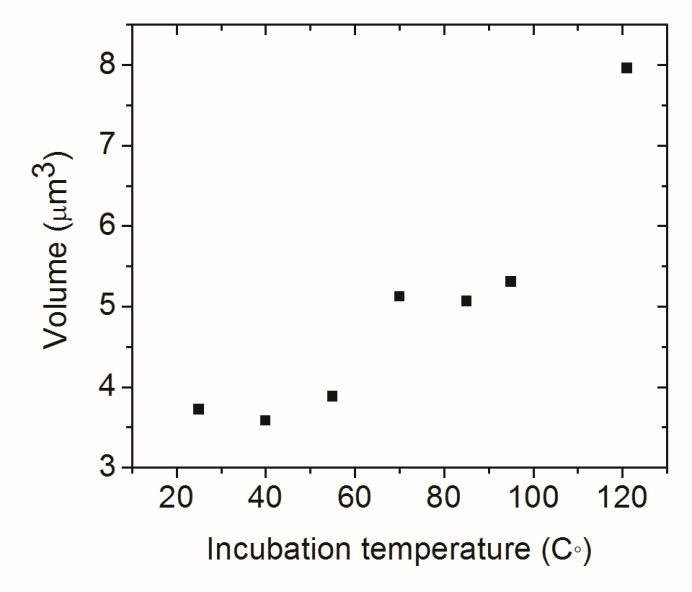

Figure 4.10 Microtube volume as a function of incubation temperature calculated from SEM images.

4.3.2 Route B. Incubation of Unreleased LbL Microtubes

After depositing LbL assemblies onto porous templates, the LbL-coated templates were incubated at varying temperatures in water. Then, the incubated membranes were selectively dissolved in DCM to release the resulting microtubes (Figure 4.11). As the incubation temperature increased, perforations appeared at a fairly regular spacing, whereas the microtubes' length remained unchanged. Above 70 ℃ the number of perforations greatly increased, whereas at lower incubation temperatures they were observed infrequently. The center-to-center spacing between the perforations was 3.5 ± 0.8 μm, and the perforation's diameter was 1.5 ± 0.3 μm for microtubes incubated

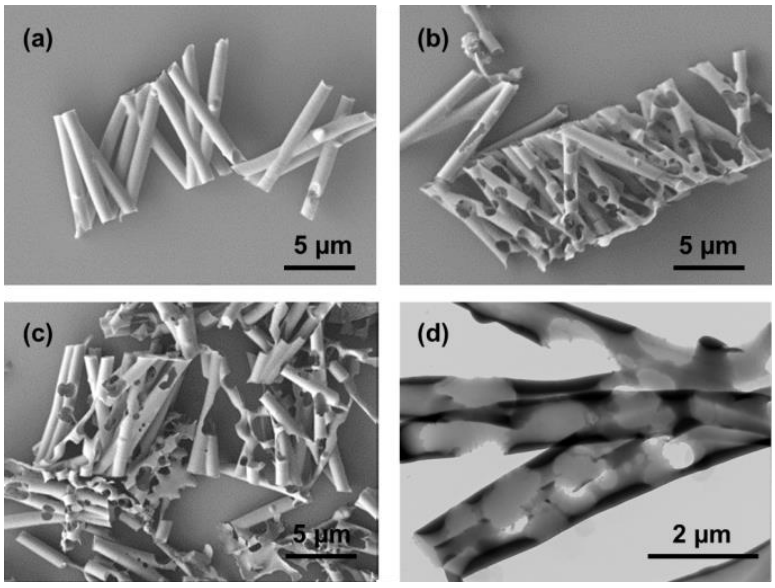

Figure 4.11 SEM images of microtubes that had been incubated in water at temperatures of (a) 40, (b) 75, (c) 85 ℃ during which the microtubes were confined to the template, and (d) TEM image of microtubes incubated at 85℃. Microtubes were released and dried from DCM.

at 70 ℃. From the pronounced darkening in the microtubes' wall (Figure 4.11d vs. Figure 4.2b) it appears that the microtube wall thickens as the perforations form. The temperature at which the perforations regularly appear coincides with the thermal transition temperature (T_{tr} = 71 ± 7 ℃) as measured using modulated differential scanning calorimetery (Figure 4.12 and Table 4.1).

The regularity and periodicity of the observed perforations is suggestive of Rayleigh instabilities. When the free surface of a liquid cylinder undulates with a wavelength larger than the perimeter of the cylinder, the liquid cylinder responds by decreasing the surface area and the amplitude of undulation grows. Eventually, the liquid

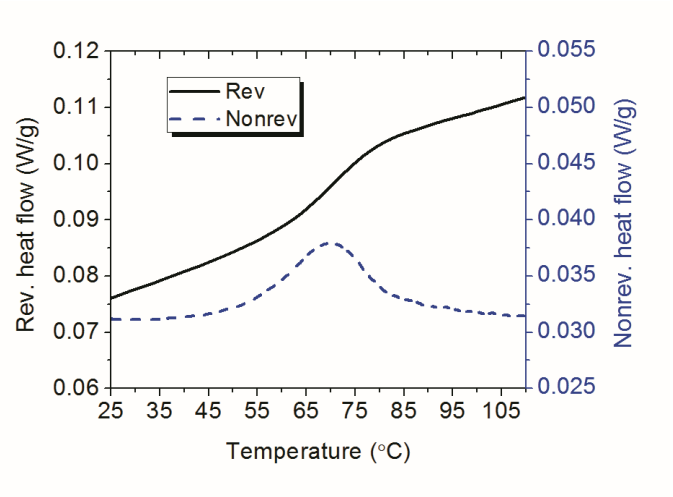

Figure 4.12 Modulated DSC thermogram of a hydrated $(PAH/PAA)_{100}$ freestanding film.

Table 4.1 Thermal properties of freestanding PAH/PAA films obtained from the modulated DSC thermogram shown in Figure 4.12.

	T_{init} (°C)	T_{final} (°C)	T_{tr} (°C)	ΔT (°C)	ΔCp (J/(g ·°C))
$(PAH/PAA)_{100}$	59 ± 9	80 ± 10	71 ± 7	17 ± 5	0.5 ± 0.1
$(PAH/PAA)_{100}PAA$	62 ± 5	83 ± 5	73 ± 6	20.0 ± 0.5	0.49 ± 0.06

*T_{tr} is the thermal transition temperature. ΔT is the temperature range of thermal transition, T_{init} and T_{final} is initial and final temperature of transition. ΔC_p is the heat capacity change during the transition.

cylinder disintegrates into droplets.[147] For a thin liquid film inside a capillary of radius R, the wavelength (spacing between voids) is $\lambda=8.89R$.[148] For our 1 µm diameter microtubes, the characteristic wavelength is 4.4 µm, whereas our actual spacing is 3.5 ±

0.8 μm. The two values show good agreement, and any minor discrepancy might arise from electrostatic interactions[47] or the finite wall thickness of the microtube.[149] Our results compare well to Rayleigh instabilities observed for nanotubes of poly(methylmethacrylate) (PMMA), polystyrene (PS), PMMA/PS blends, and poly(styrene-b-2-vinylpyridine), in which periodic holes were observed upon thermal annealing.[149, 150, 151, 152, 153, 154]

Transformation of the microtubes due to Rayleigh instabilities is driven by lower viscosity at higher incubation temperatures. According to the theory of Rayleigh instabilities, characteristic time (τ) for the fastest growing mode of thin liquid film in a capillary is described by Equation 4.1[149]

$$\tau = \frac{12\mu R^4}{\gamma h^3} \tag{4.1}$$

where μ is viscosity, R is the pore radius, γ is surface tension, and h is the thickness of the initial film thickness. The main factor that determines the temperature-dependence of τ is the viscosity. For example, the viscosity of polystyrene above the glass transition temperature decreases exponentially by the Arrhenius relation with activation energy ~70 kcal/mol,[155] and γ decreases linearly with temperature. μ is proportional to exp(35,000/T), and γ in dyne/cm is 40.7-0.072(T-293), where T is the absolute temperature[156] As the temperature increases 10℃, τ for polystyrene film decreases more than 10 times driven by the decrease of viscosity.

It is curious that we should observe drastically different transitions in shape for released and unreleased LbL microtubes. The materials and assembly are identical, as

are the incubation conditions. The remaining factor, then, is the interaction between the templates' pore wall and the LbL assembly. Rayleigh instabilities are driven by surface energy; therefore, microtubes produced by the two Routes should have very different surface energies. In the case of Route A, microtubes are fully surrounded by water during incubation. The cylinder-to-sphere transition shares similarities to the predictions of Nichols et al. in which a critical length-to-diameter ratio of 7.2 was derived.[157] Below this critical ratio, a single tube transforms into a single sphere; above the ratio, multiple particles are formed. In our case the length-to-diameter ratio is 10, which is only slightly above the critical ratio. Thus, it is possible that the microtubes formed via Route A desire to form Rayleigh instabilities upon incubation, but are too short to do so.

In the case of unreleased microtubes prepared from Route B, there exist attractive interactions between the pore wall and the layer-by-layer assembly. These interactions possibly pin the microtube's outer wall to the pore wall, thus drastically changing the surface energy. Upon incubation, the LbL microtube desires to contract, but its interaction with the wall prevents it from doing so. Instead, to minimize the surface energy, Rayleigh instabilities form during the incubation process for the unreleased microtubes.

He et al. reported the transformation of PAH/PSS LbL microtubes to microcapsules, when microtube suspensions were incubated at 121 ℃ for 20 min.[47] This system consists of a weak polyelectrolyte and a strong polyelectrolyte. Rayleigh instabilities were suggested as a possible mechanism. In light of the discussion above and the results found herein, Rayleigh instabilities are indeed a possible cause. The

change in wall thickness was not reported and only a limited range of temperature and time was explored, so further work is required to fully understand the PAH/PSS system.

There remains a question as to whether mass is conserved for the PAH/PAA microtube over the course of the transition. PDAC/PSS microcapsules exhibited mass loss during incubation, but it is not known if PAH/PAA microtubes behave similarly. Our prior work with QCM-D of PAH/PAA LbL films indicates that mass changes slightly at the thermal transition, but this was associated with flux of water into and out of the film rather than loss of polyelectrolyte.[50]

Because the PAH/PAA LbL microtubes consists solely of weak polyelectrolytes, we expect that they should exhibit pronounced changes in shape in response to pH. For instance, LbL microtubes arrays have exhibited pronounced swelling in response to pH.[36] The dual pH/temperature-response of our microtubes will be a subject of further exploration.

4.4 Conclusion

The temperature-triggered transformation of released and unreleased PAH/PAA microtubes in water was studied. Released microtubes contract into spheres and ellipsoids and unreleased microtubes exhibit Rayleigh instabilities upon incubation. In both cases, the transformation occurred near the T_g for hydrated PAH/PAA LbL assemblies. These results suggest that the surrounding media, whether it is water or a solid pore wall, can have a strong influence on the temperature-response of an LbL microtube. This temperature-triggered transformation has potential applications for the

encapsulation of drugs, small molecules, and separations. Because this system is comprised of weak polyelectrolytes, it also bears the possibility of dual pH/temperature-responsive behavior.

CHAPTER V

THERMAL TRANSITIONS IN HYDRATED LAYER-BY-LAYER ASSEMBLIES OBSERVED USING ELECTROCHEMICAL IMPEDANCE SPECTROSCOPY*

5.1 Introduction

Layer-by-layer (LbL) assemblies offer immense promise for a variety of applications ranging from energy to life science.[138, 158, 159] These functional coatings and films are fabricated from the alternate adsorption of oppositely charged polyelectrolytes,[2] metallic or inorganic nanoparticles,[160, 161] and biological species,[68] for which structure and properties are modulated using assembly pH, salt concentration, and temperature.[133, 134] The sensitivity of an LbL film to assembly conditions as well as external stimuli can be attributed to the weak nature of non-covalent interactions (electrostatic, hydrogen bonding, van der Waals) existing between the two adsorbing species. As it will be shown here, temperature is a particularly intriguing parameter in that some LbL films respond dramatically in aqueous media. The reasoning behind this phenomenon is not well understood, and is explored herein using electrochemical impedance spectroscopy.

* Reprinted with permission from "Thermal transitions in hydrated layer-by-layer assemblies observed using electrochemical impedance spectroscopy" by Choonghyun Sung, Katelin Hearn, and Jodie L. Lutkenhaus, *Soft Matter* **2014**, 10, 6467-6476, Copyright (2014) The Royal Society of Chemistry

Understanding the nature of an LbL assembly's thermal transition in the hydrated state is of particular interest because many applications, such as drug delivery and separations, are found in aqueous media. For example, leveraging the thermal transition is crucial for temperature-responsive LbL films, capsules, and microtubes.[43, 44, 162] Further, it has been proposed that the mode of the film growth (linear *vs.* exponential) is influenced by the viscoelastic properties of film, which may be related to whether the film was assembled below or above its thermal transition temperature.[14, 49] The thermal transition itself has been clearly observed via atomic force microscopy (AFM) coupled with fluorescence microscopy,[48] calorimetry,[44] ^{2}H NMR spectroscopy,[51] and quartz crystal microbalance with dissipation (QCM-D).[49, 50] The majority of studies have focused upon a pair of strong polyelectrolytes, poly(diallyldimethylammonium chloride) (PDAC) and poly(styrenesulfonate) (PSS) assembled in the presence of salt.

For this LbL system, the thermal transition manifests as a reversible second-order thermal phenomena, yielding a response much like a glass transition. Upon heating through the transition, a significant drop in stiffness, an increase in viscoelasticity, and an increase in chain motion have been reported.[48, 49, 51] For this reason the thermal transition observed for the hydrated PDAC/PSS LbL system has been called a "glass-melt" transition, or simply a "glass transition", in prior literature. In light of our forthcoming publication, which contains simulations of the thermal transition, we now understand that the transition is related to the rearrangement of water molecules around ionic groups on the polyelectrolyte, leading to enhanced polyelectrolyte mobility. This reasoning is supported by the observation that the same systems, when dry, do not have

thermal transitions.[41, 49] Hydrated complexes also possess this transition, albeit at a lower temperature.[163]

Electrochemical impedance spectroscopy (EIS) has been widely used to study the interfacial and transport properties of polymer films, and offers new opportunities to assess the nature of thermal transitions in LbL assemblies. EIS has been used to monitor the swelling and shrinking of polymer hydrogels[164] and to investigate the chain conformation of polymer brushes.[165] LbL properties, such as permeability and swelling, have also been characterized using EIS for various pH values and salt concentrations.[57, 166, 167] EIS studies also provide a deeper understanding of LbL film structure and transport when investigated with the aid of a redox-active label, such as ferro/ferricyanide. It has been proposed that the redox probes hop between "reluctant" exchange sites within the LbL film.[168, 169] Pardo-Yissar *et al.* showed that Donnan inclusion and Donnan exclusion strongly affected the charge transfer resistance.[57] When the charge of the redox active probe matched that of the film's outermost layer, Donnan exclusion occurred and the charge transfer resistance increased. Conversely, for the case of opposite charge, Donnan inclusion occurred, and the charge transfer resistance was negligible, consistent with a neutralized porous film structure.[57] Barreira *et al.* suggested sophisticated models for the impedance response, considering an inhomogeneous LbL film structure characterized by spots or capillaries at the electrode-film interface where electrochemical transport is favored.[167]

Temperature-controlled EIS studies on LbL assemblies are relatively rare. Silva *et al.* investigated thermal behavior over a limited temperature range (15 to 45 ℃) for

polyallylamine/PSS LbL assemblies.[60] It was reported that the diffusion coefficient increased and film resistance decreased with increasing temperature, but no thermal transition was observed, possibly because of the limited temperature range investigated. Elsewhere, Alonso-Garcia *et al.* measured the glass transition temperature of grafted polyelectrolyte brushes using temperature-controlled EIS.[59] The glass transition temperature of the brushes coincided with a discontinuity in the charge transfer resistance and diffusion coefficient with respect to temperature. Motivated by these results, we hypothesized that LbL films would show distinct variations in electrochemical behavior associated with a thermal transition via EIS.

In this work, we study the structure of PDAC/PSS LbL assemblies in aqueous media as a function of temperature using EIS with a redox-active probe. The effect of assembly salt concentration, film thickness, and identity of the outermost layer on the thermal transition temperature is investigated. A modified Randles circuit is used to quantitatively analyze the impedance spectra in terms of charge transfer resistance, capacitance, and Warburg impedance. It is found that some circuit elements are particularly responsive to temperature, which is interpreted in the context of the nature of the thermal transition. To our knowledge, this is the first report of temperature-controlled EIS in which the thermal transition of PDAC/PSS LbL assemblies is demonstrated. EIS is particularly powerful in that it allows one to probe the structure of the film itself at a variety of frequencies and time scales.

5.2 Experimental Section

5.2.1 Materials

Poly(diallyldimethylammonium chloride) (PDAC, Mw =350,000 g/mol) and poly(styrene sulfonate salt) (PSS, Mw= 500,000 g/mol) were purchased from Sigma Aldrich. Indium-tin oxide (ITO) coated glass was purchased from Delta Technologies. Potassium hexacyanoferrate(II) trihydrate ($K_4[Fe(CN)_6]\cdot 3H_2O$) and potassium ferricyanide(III) ($K_3[Fe(CN)_6]$) were purchased from Alfa Aesar and Sigma Aldrich, respectively.

5.2.2 Preparation of Layer-by-Layer Assemblies

PDAC/PSS LbL assemblies were prepared on ITO- coated glass using a programmable slide stainer (HMS series, Carl Zeiss Inc.). ITO-coated glass was cleaned by immersion in a water/NH_4OH/H_2O_2 (5:1:1) mixture at 70℃ for 15 min followed by plasma-cleaning for 5 min. ITO-coated glass slides were immersed in PDAC solution for 15 min followed by three rinses with 18.2 MΩ·cm water for 2, 1, and 1 min. Then, the substrates were immersed in PSS solution for 15 min, followed by three water rinses as before. The cycle was repeated n times to form a $(PDAC/PSS)_n$ LbL film in which the subscript describes the number of layer pairs. The polymer solution's concentration was fixed at 1 mg/ml. Two NaCl concentrations, 0.5 M and 1.0 M, were used in this study for both water rinse baths and polyelectrolyte solutions. These adsorption processes were repeated as desired. The LbL films were dried in a convection oven at 70 ℃ for 15 min, and stored in a sealed vial until further use.

5.2.3 Electrochemical Characterization

Electrochemical impedance measurements were performed in a standard three-electrode cell using Ag/AgCl (4M KCl) as the reference electrode (Pine Research Instrumentation) and platinum wire of 0.3 mm diameter (Alfa Aesar) as the counter electrode. LbL-coated, ITO-coated glass slides were used as working electrodes (Delta Technologies). The active area of the working electrode immersed in supporting electrolyte was 2.1 cm^2. The supporting electrolyte was an aqueous solution of NaCl in which the concentration was matched to that used for assembly to avoid the possibility of salt annealing. In the case of bare ITO, the NaCl concentration was 0.5 M. $K_3[Fe(CN)_6]$ and $K_4[Fe(CN)_6]$ (5 mM each) were used as redox-active probes. The electrochemical cell was held at 25 ℃ and purged with nitrogen for 30 min. Impedance measurements (Solartron 1287) were performed every 5 ℃ up to 80 ℃ after being held isothermally at a given temperature for 15 min under nitrogen purge. The DC potential was set to the open circuit potential and the AC amplitude was 10 mV. Frequency was scanned from 10^4 Hz to 0.02 Hz. Impedance data were modeled using commercial software (Zview, Scribner Associates, Inc.), which uses a complex nonlinear least squares fitting method. EIS measurements were done for three separate samples at a given condition, and the error was taken as the standard deviation.

5.2.4 UV-Vis Spectroscopy

LbL films on the quartz cuvette slides were immersed in supporting electrolyte similar to that used for EIS measurements. UV spectra were obtained (Hitachi U-4100) at an absorbance of 226 nm to monitor the relative amount of PSS.[5]

5.2.5 Surface Morphology and Film Thickness

Surface morphologies of PDAC/PSS LbL films were investigated using atomic force microscopy (AFM) (Dimension Icon AFM, Bruker Corporation). Measurements were performed in tapping mode under dry conditions at a scan rate of 1.0 Hz. LbL film thickness was measured using profilometery (D-100, KLA Tencor) and/or ellipsometry (LSE stokes, Gaertner) after drying the samples at 65 ℃ for 30 min. Three separate samples were used for the thickness measurements, and standard deviation was taken as the error.

5.3 Results and Discussion

5.3.1 Nyquist Plots and Electric Circuit Modeling

Figure 5.1 shows typical electrochemical impedance spectra in the form of Nyquist diagrams for ITO electrodes with and without PDAC/PSS LbL coatings at varying temperatures. Bode plots are given in Figure 5.2. LbL films made at 0.5 and at 1.0 M NaCl were explored; we also attempted to evaluate films made without salt, but we encountered issues associated with salt annealing during exposure to the aqueous electrolyte to which some salt is necessary for the measurement. The Nyquist plots for the LbL-coated electrodes show semicircles in the high frequency region and, for higher temperatures, a roughly 45° straight line in the low frequency region associated with a Warburg impedance (semi-infinite diffusion). On the other hand, for the bare ITO electrode, only a single 45° straight line was observed. It is clear that the appearance of semicircles in the Nyquist plots is due to the presence of the LbL film.

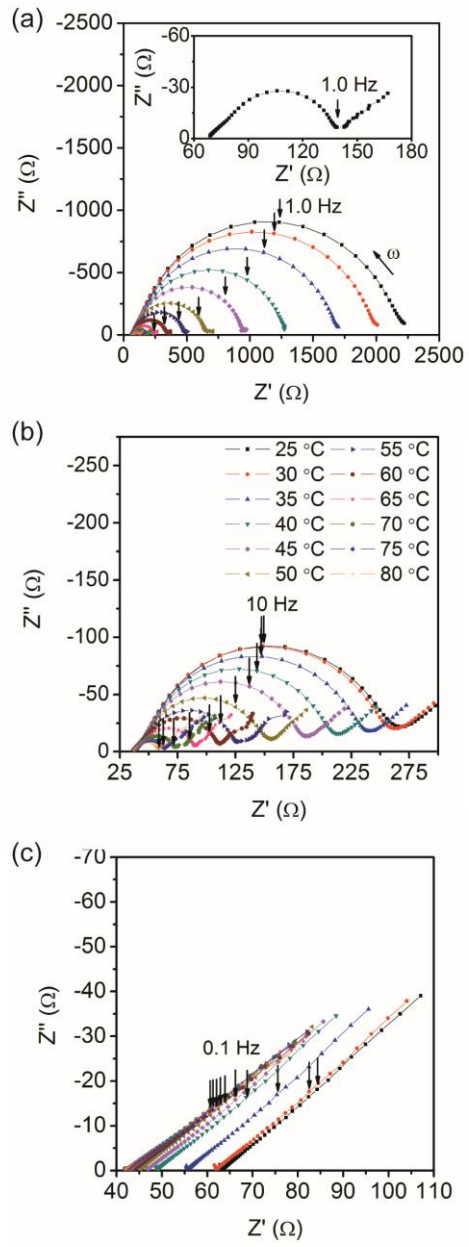

Figure 5.1 Nyquist plots of electrochemical impedance spectra taken at different temperatures for an ITO electrode modified with (a) $(PDAC/PSS)_{11}$ assembled at 0.5 M NaCl (~100 nm) and (b) $(PDAC/PSS)_7$ assembled at 1.0 M NaCl (~125 nm), as well as (c) an unmodified ITO electrode. The inset of Figure 5.1a is the magnification of the impedance response measured at 75 ℃ for $(PDAC/PSS)_{11}$ assembled at 0.5 M NaCl. The legend in (b) applies to all panels. Solid lines are provided to guide the eye. The electrolyte consisted of NaCl in water, in which the concentration of NaCl was matched to the assembly conditions so as to minimize salt annealing.

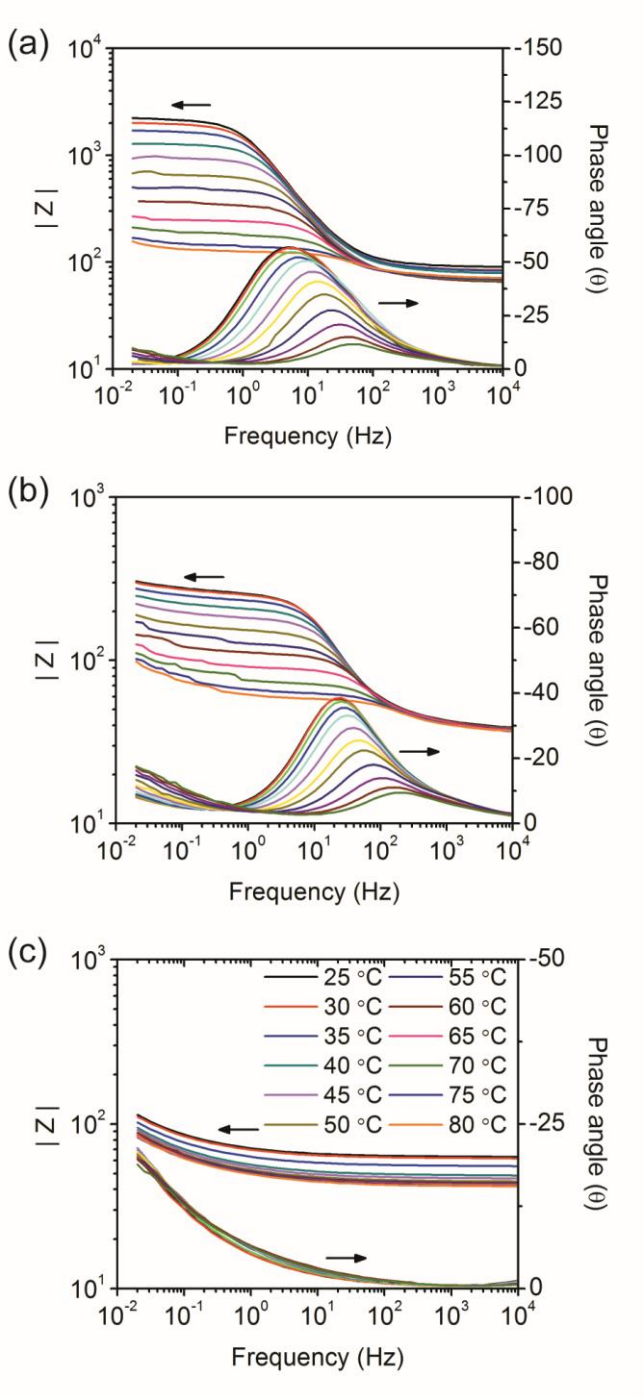

Figure 5.2 Bode plots for the ITO electrode modified with (a) $(PDAC/PSS)_{11}$ LbL film assembled at 0.5M NaCl, (b) $(PDAC/PSS)_7$ LbL film assembled at 1.0M NaCl, and for (c) bare ITO electrode. The legend in panel (c) applies to all panels.

For PDAC/PSS LbL films assembled at 0.5 M NaCl, the semicircle's diameter decreased and became skewed as the temperature increased (Figure 5.1a). At room temperature, the semicircle was nearly perfect in semicircular shape, but the skewedness became distinct at 75 ℃ as shown in the inset of Figure 5.1a. A Warburg impedance was not clearly detected at low temperatures, indicating kinetic control, but as the temperature increased a Warburg impedance appeared, indicative of facile kinetics and diffusion control.[58]

As for the impedance spectra of PDAC/PSS LbL films assembled at 1.0 M NaCl, the semicircle's diameter also decreased with increasing temperature (Figure 5.1b). Compared to the LbL films assembled at 0.5 M NaCl, the PDAC/PSS LbL films assembled at 1.0 M NaCl showed much smaller semicircles even for comparable thicknesses. There was a clear Warburg impedance even at room temperature for LbL films assembled at 1.0 M NaCl. We also observed skewing at high temperatures as before.

In order to analyze the electrochemical properties quantitatively, the impedance spectra were fitted to a modified Randles equivalent circuit (Figure 5.3). This equivalent circuit has been widely used to model electrodes modified with LbL assemblies,[170, 171, 172] polymer films,[173] and polymer brushes.[174, 175] R_s is the solution resistance, and R_f represents the pore resistance of the film.[173] "CPE" stands for constant phase element and represents the non-ideal capacitive behavior of the film. The CPE is frequently used in place of an ideal capacitor to consider depressed semi-circles or non-vertical lines in the low-frequency regions of Nyquist plots.[176] The impedance of a CPE is expressed as $Z = 1/[T(j\omega)^p]$, where j is square root of -1, T is the admittance (CPE-T), and p is an

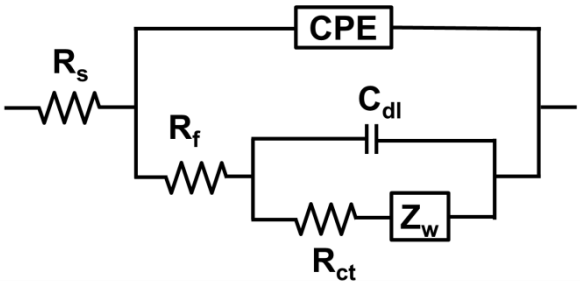

Figure 5.3 Modified Randles equivalent circuit used to model electrochemical impedance spectra. R_s is the solution resistance, R_f is film resistance, CPE is the constant phase element of the film, R_{ct} is charge transfer resistance, C_{dl} is double layer capacitance, and Z_w is Warburg impedance.

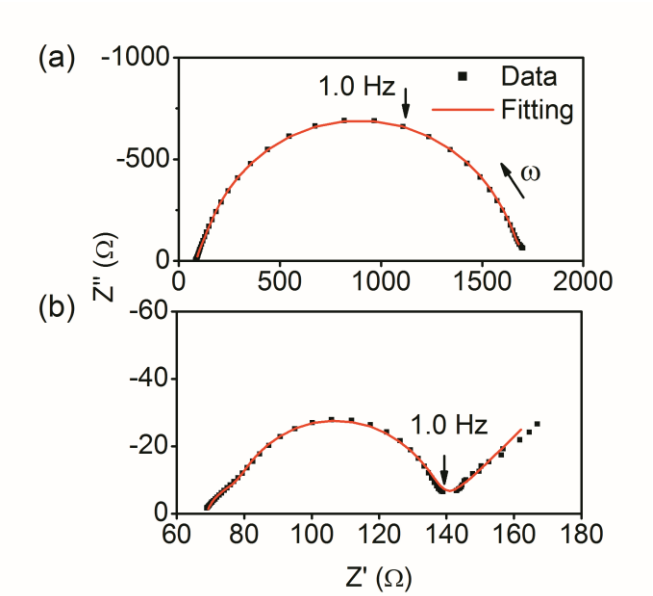

Figure 5.4 Nyquist plots taken at (a) 35 and (b) 75 ℃ for ITO electrodes modified with $(PDAC/PSS)_{11}$ LbL films assembled at 0.5 M NaCl. Black dots represent experimental data, and the red line represents the equivalent circuit model.

adjustable exponent (CPE-P).[176] When p = 1, the CPE becomes an ideal capacitor. For $0.5 < p < 1$, the film is interpreted as being either porous and rough or as having a non-uniform distribution of current. R_{ct} is charge transfer resistance, C_{dl} is double layer capacitance, and Z_w is a Warburg impedance associated with semi-infinite linear diffusion. Figure 5.4 shows typical impedance spectra fitted with the modified Randles equivalent circuit for low and high temperatures. Skewedness in the high frequency region is fit very well by this model, as shown in Figure 5.4b.

5.3.2 Thermal Transition from Circuit Elements

Plots of film resistance (R_f) vs. temperature for LbL films assembled at 0.5 M and 1.0 M NaCl are shown in Figure 5.5. R_f generally decreased in two distinct modes upon heating. In the first mode, R_f decreased rapidly upon heating from room temperature. In the second mode, R_f decreased only slightly above 55 ℃. The transition temperature ($T_{tr,Rf}$) was obtained from the intersection of two lines extrapolated from low and high temperature regions. Both LbL films assembled at 0.5 M and 1.0 M NaCl displayed transition temperatures (52 ± 2 ℃ and 54 ± 1℃, respectively) close to those measured in our previous study using QCM-D and modulated differential scanning calorimetry (51.0 ± 0.2 ℃ and 52 ± 1℃, respectively).[49] We have found that the shape of the R_f-T curve is similar for all cases investigated herein except for one notable exception: PDAC/PSS LbL films assembled at 1.0 M NaCl for thicknesses below 100 nm. In that case, R_f decreased linearly with temperature and no clear transition was observed. This observation is consistent with that of a patchy film in which the electrode is not fully covered.

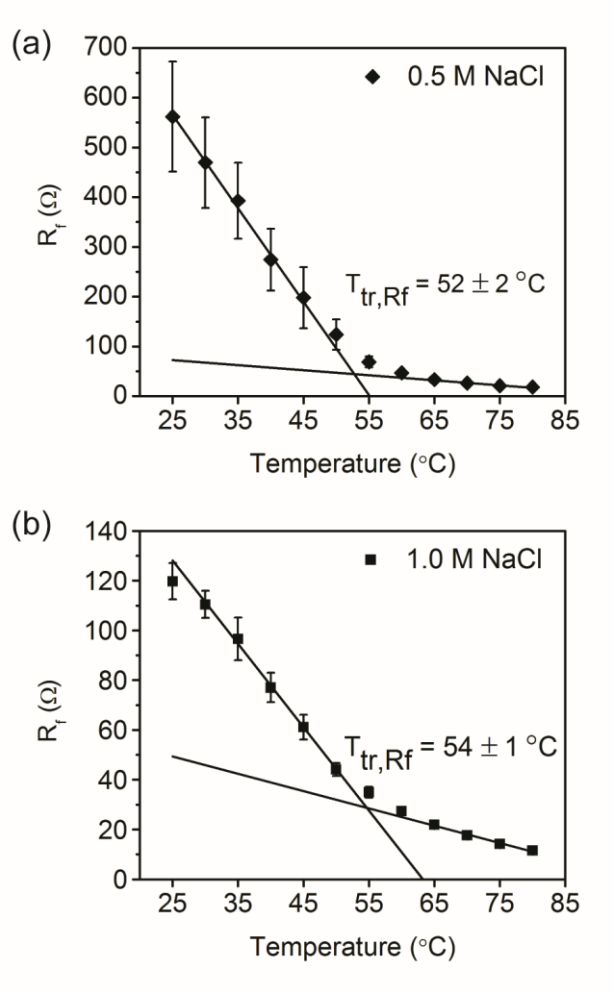

Figure 5.5 Film resistance (R_f) as a function of temperature for (a) $(PDAC/PSS)_{11}$ LbL film assembled at 0.5 M NaCl (~100 nm) and (b) $(PDAC/PSS)_9$ LbL film assembled at 1.0 M NaCl (~225 nm). R_f was obtained from application of the equivalent circuit shown in Figure 5.3 to impedance spectra such as those shown in Figure 5.1. Error bars represent the standard deviation of three separate samples. PSS is the outermost layer.

R_f has been interpreted as the resistance resulting from the penetration of electrolyte through real and virtual pores within the film.[173, 175] R_f is related to the thickness of the film t, the conductivity of the film swollen with electrolyte κ, and the

cross sectional area A_c by Equation 5.1.

$$R_f = \frac{t}{\kappa A_c} \tag{5.1}$$

The steady decrease in R_f with increasing temperature suggests that the film decreases in thickness and/or the conductivity of the film increases. From prior QCM-D measurements, deswelling occurred over a range of 35-50 °C when PSS was the outermost layer, which does not fully explain the decrease in R_f over the full range herein. Therefore, an increase in conductivity of ions through the film must be the major contributing factor for R_f's decrease with increasing temperature. Because transport of monovalent ions is less susceptible to Donnan exclusion compared to multivalent ions or heavily charged electroactive ions such as ferrocyanide/ferricyanide redox couple,[58, 177] it can be concluded that the conductivity mainly arises from ions from the supporting electrolyte and not the redox-active probe.

Considering the inverse relationship between conductivity and R_f, Figure 5.5 can be recast as a steady increase in conductivity from room temperature up to $T_{tr,Rf}$, and then a marginal increase for higher temperatures. Conductivity is closely tied to the structure of the film, such as the shape and occurrence of electrolyte-filled virtual pores through which ions travel as well as the extent of extrinsically compensated sites reserved for ion transport via "hopping". Upon comparison with other investigations, the former likely dominates the temperature-conductivity response. For instance, the stiffness of PDAC/PSS LbL capsules in water decreased fairly linearly until 45 °C and leveled off,[48] in which a transition from a glassy to a viscous fluid state was suggested.

Our forthcoming work shows through simulations that the transition is related to the dehydration of ionic groups along the polyelectrolyte and an increase in polyelectrolyte chain mobility. Such an increase in mobility could be responsible for a restructuring of the film and the virtual pores therein. Also, simulations show no discernable change in the ratio of extrinsic to intrinsic charge compensation above or below the transition.

Given the preceding observations regarding R_f, we next turn to the interpretation of R_{ct}. R_{ct} represents the charge transfer associated with executing the redox reaction, and is, thus, directly related to the redox probe and its state within or just outside the film. Silva *et al.* proposed that in early stages of LbL growth, the surface is patchy and the apparent R_{ct} is strongly tied to the active area of the partially blocked electrode.[60] As the number of layers increases, a homogeneous membrane is eventually achieved for which partitioning of the redox active probe becomes important.[58, 167, 178] Here, we chose to account for both surface coverage and partitioning because our films possess a loose network (which contributes to virtual pores) and because our films are relatively thick (which allows for some partitioning). The partition coefficient K of the redox active probe in the film *vs.* the bulk solution and the surface coverage θ are related to the observed R_{ct} by the following Equation 5.2[60]

$$R_{ct} = \frac{R_{ct,bare}}{K\,(1-\theta)} \tag{5.2}$$

where $R_{ct,bare}$ is the charge transfer resistance of the electrode in the absence of the LbL film. For the ferro/ferricyanide redox couple on bare ITO, R_{ct} = 17.63 Ω cm^2 at 298 K,[179] which would correspond to 37 Ω for our active area of 2.1 cm^2.

Figure 5.6a shows the charge transfer resistance as a function of temperature for the PSS-terminated LbL films assembled at 0.5 M NaCl. At room temperature, R_{ct} is over 50 times higher than $R_{ct,bare}$, which suggests strong partitioning and/or high surface coverage. R_{ct} decreases rapidly as temperature increases and then levels off at high temperatures as similar to the results of R_f vs. temperature. Using a similar procedure as before with R_f, the transition temperature from the R_{ct}-T plots ($T_{tr,Rct}$) was 54.0 ± 0.8 ℃. From Equation 5.2, the decrease in R_{ct} can be interpreted as either an increase in the partition coefficient or a decrease in the surface coverage of the film. The former is less likely because it has been shown that ferricyanide concentration in the film decreases (*i.e.*, K decreases) with increasing temperature.[77] Therefore, we propose that the temperature-dependent behavior of R_{ct} is dominated by the surface coverage of the electrode. Above the $T_{tr,Rct}$, the marginal decrease in R_{ct} suggests that the film is highly permeable to the redox active probe, and perhaps is brought about by an increase in polyelectrolyte mobility and structural rearrangement, leading to a very low surface coverage. In the limiting case of a highly porous or mobile LbL coating, K would approach unity, θ would approach a small finite value, and R_{ct} would approach that of the bare electrode. This situation is perhaps achieved at high temperatures when R_{ct} is fairly low, Figure 5.6a.

On the other hand, for the LbL film assembled at 1.0 M NaCl, a sigmoidal shape is observed (Figure 5.6b). R_{ct} declines rapidly starting at 36 ℃, and then decreases slightly beyond 64 ℃. This sigmoidal shape was observed for both PDAC- and PSS-terminated LbL films assembled at 1.0 M NaCl, and for PSS-terminated LbL films

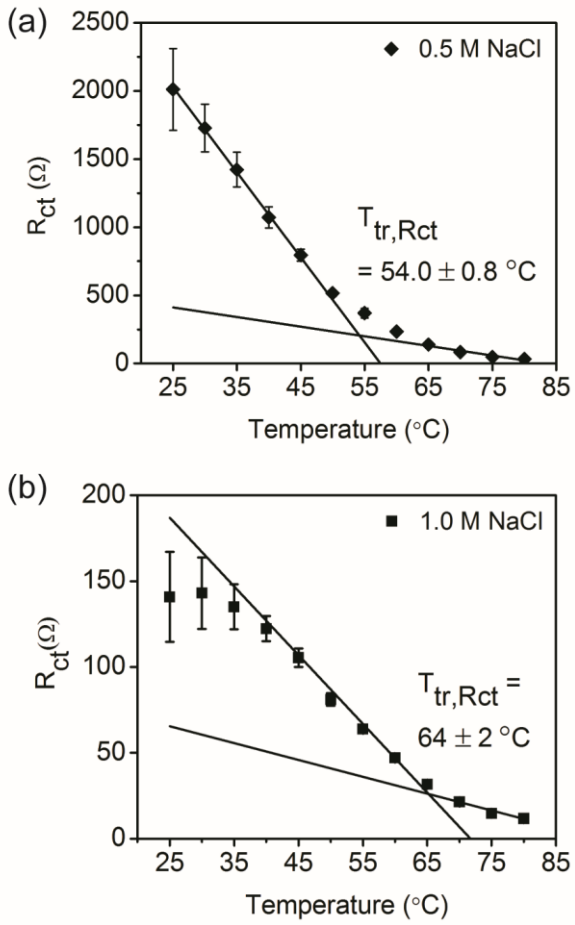

Figure 5.6 Charge transfer resistance (R_{ct}) as a function of temperature for (a) $(PDAC/PSS)_{11}$ LbL films assembled at 0.5 M (~100 nm) and (b) $(PDAC/PSS)_7$ assembled at 1.0 M NaCl (~125 nm). R_{ct} was obtained from application of the equivalent circuit shown in Figure 5.3 to impedance spectra such as those shown in Figure 5.1. PSS is the outermost layer.

assembled at 0.5 M NaCl of just a few layer pairs. It can be inferred that the sigmoidal shape tends to appear for films in which coverage is patchy (0.5 M NaCl of just a few layers) or in which the structure has a high degree of extrinsic charge compensation (1.0 M NaCl). Several competing phenomena are perhaps responsible for this shape. Firstly,

an increase in temperature could lead to a decrease in surface coverage and a decrease in R_{ct} as chains gain more mobility. Secondly (and mentioned previously), the partition coefficient of the redox active label is expected to decrease with increasing temperature, which would lead to an increase in R_{ct}. Thirdly, $R_{ct,bare}$ is expected to decrease with temperature, causing an decrease in the observed R_{ct}; however, inspection of Figure 5.1c shows that any change in $R_{ct,bare}$ is negligible as compared to changes displayed in Figure 5.6.

Upon comparison, R_{ct} was generally much higher for the LbL-coated electrode assembled at 0.5 M NaCl *vs.* 1.0 M NaCl. This result is easily rationalized by considering the structure of the PDAC/PSS LbL film as a function of ionic strength of assembly. Films assembled at higher salt concentrations have more extrinsic charge compensation and form a looser network,[180] which offers decreased surface coverage and lower R_{ct}.

The constant phase element, representing the non-ideal capacitance of the LbL film, was studied as a function of temperature (Figure 5.7). From room temperature to about 55 °C, CPE-P (where CPE-P = p) remained constant at about 0.9, and above 55 °C, CPE-P decreased strongly with temperature. CPE-P is related to surface roughness, water permeation, or the interaction and mobility of polarizable groups. CPE-P generally decreases from 1.0 to 0.5 as the roughness or porosity increases.[176] In corrosion studies of polymer-coated metals, it was shown that CPE-P generally decreases as polymer degradation proceeds due to water permeation into the film.[181, 182] It is also possible that CPE-P decreases as the interaction and mobility of polarizable groups increases.[183] As it

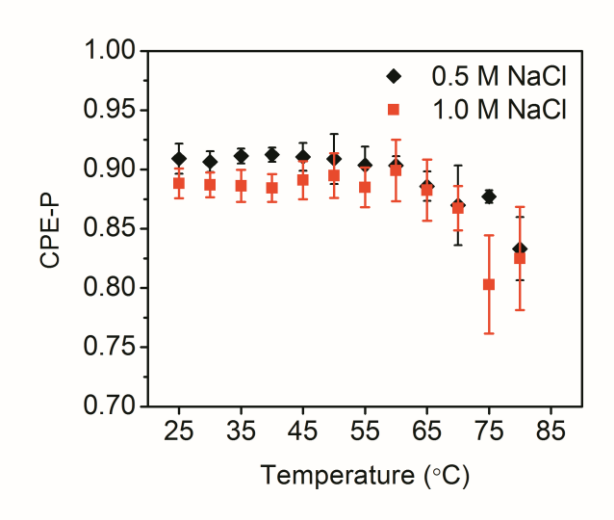

Figure 5.7 CPE-P as a function of temperature for $(PDAC/PSS)_{11}$ LbL film assembled at 0.5 M NaCl and $(PDAC/PSS)_7$ LbL film assembled at 1.0 M NaCl. PSS is the outermost layer.

will be shown later, the roughness of the LbL films actually decreased when the films were annealed in supporting electrolyte at a high temperature. Thus, it is more plausible that the decrease of CPE-P with temperature is linked to an increase in mobility of polyelectrolyte chains. CPE-T was also analyzed, but no clear temperature dependence was observed as compared to CPE-P.

Double layer capacitance (C_{dl}) was also studied as a function of temperature (Figure 5.8). According to the classical double layer model, C_{dl} should decrease with temperature.[176, 184] However, in this study, C_{dl} was fairly constant at low temperatures, and increased slightly above 55 ℃. The slight increase might be related to an increase in internal surface area owing to the formation of new virtual pores.

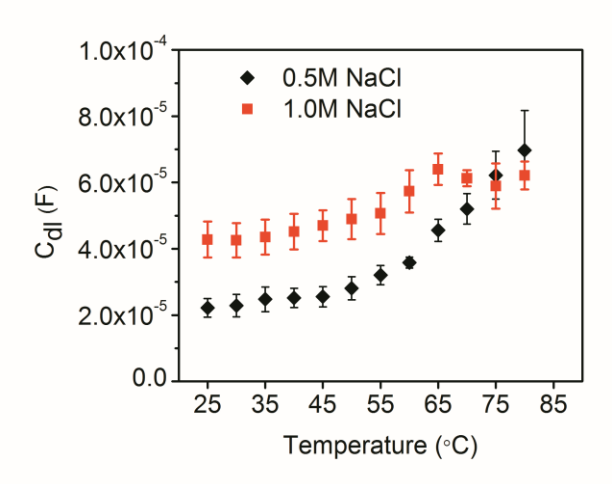

Figure 5.8 C_{dl} as a function of temperature for $(PDAC/PSS)_{11}$ LbL films assembled at 0.5 M NaCl and $(PDAC/PSS)_7$ LbL film assembled at 1.0 M NaCl. PSS is the outermost layer.

The Warburg impedance, which arises from diffusion of redox active probes through the film, was analyzed as a function of temperature. The apparent diffusion coefficient of the redox couple can be calculated from the Warburg impedance according to the following Equation 5.3,[185]

$$D = \left(\frac{\sqrt{2}RT}{n^2F^2A\sigma C_{bulk}}\right)^2 \quad (5.3)$$

where, n is the number of electrons transferred, F is Faraday's constant, A is the electrode area, R is the gas constant, T is absolute temperature, σ is a Warburg parameter, and C_{bulk} is the concentration of the redox probe in bulk solution. The diffusion coefficient for LbL films assembled at 1.0 M NaCl was obtained for all temperatures investigated, but for LbL films assembled at 0.5 M NaCl the diffusion coefficient could

only be obtained above 50 ℃ due to the absence of a Warburg impedance at lower temperatures (Figure 5.9).

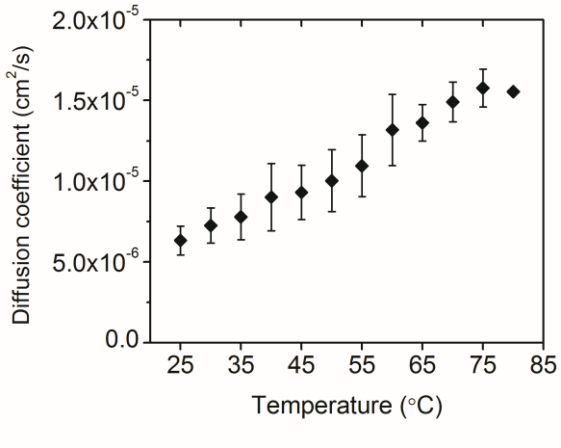

Figure 5.9 Diffusion coefficient of the redox probe as a function of temperature for $(PDAC/PSS)_7$ LbL films assembled at 1.0 M NaCl.

The diffusion coefficient for LbL films assembled at 1.0 M NaCl increased fairly linearly with temperature without any apparent thermal transition and was in the range of 5 x 10^{-6} – 1.5 x 10^{-5} cm^2/s. For bare ITO, we calculated a comparable diffusion coefficient around 10^{-6} – 10^{-5} cm^2/s, consistent with previous literature.[186] This value is much higher than that reported from rotating disc electrode measurements, 10^{-10} – 10^{-9} cm^2/s, in which "reluctant" ion exchange was proposed.[77, 168] Therefore, the diffusion coefficients measured here could represent the diffusion of redox active probes through virtual pores or bulk diffusion from the solution because the values are closer to that of

bulk electrolyte. The former possibility can be eliminated considering that the concentration of the redox active probe decreases as a function of temperature, so one would expect to see a decrease in D according to Equation 5.3. Thus, the diffusion coefficients in Figure 5.9 likely arise from bulk diffusion from the electrolyte to the film.

5.3.3 Factors Influencing the Thermal Transition Temperature

The transition temperatures were investigated as a function of film thickness and salt concentration. Figure 5.10a and b show $T_{tr,Rf}$ and $T_{tr,Rct}$, respectively, for films assembled at 0.5 M and 1.0 M NaCl. It is important to note that $T_{tr,Rf}$ and $T_{tr,Rct}$ are not always identical because they probe separate phenomena. $T_{tr,Rf}$ comes from the resistance of the film, which is swollen with electrolyte, and $T_{tr,Rct}$ comes from the charge transfer resistance associated with redox active probes in the film. In other words, $T_{tr,Rf}$ reports the state of electrolyte in the film, and $T_{tr,Rct}$ probes the state of the redox active probe in the film.

In Figure 5.10a, the $T_{tr,Rf}$ of LbL films assembled at 0.5 M NaCl is around 52.0 ± 0.4 ℃ for all thicknesses, except for ~25 nm film, which shows a slightly lower $T_{tr,Rf}$ of 49.4 ± 0.4℃. For LbL films assembled at 1.0 M NaCl, $T_{tr,Rf}$ remained fairly constant with thickness, having an average value of 54.9 ± 0.4℃. For films assembled at 1.0 M NaCl we did not observe any discernable transitions for thicknesses below 125 nm, perhaps because of patchy growth. There appears to be a lack of strong thickness dependence for $T_{tr,Rf}$, which suggests that the state of the electrolyte in the film does not vary with significantly over the thickness range investigated.

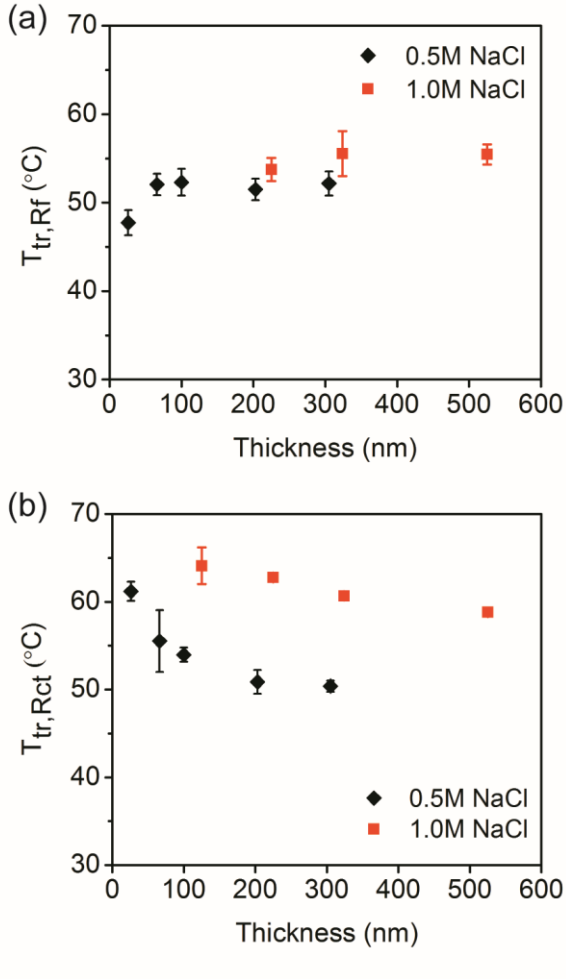

Figure 5.10 The transition temperature ($T_{tr,Rf}$) obtained from plots of R_f vs. temperature, and (b) the transition temperature ($T_{tr,Rct}$) obtained from plots of R_{ct} vs. temperature as a function of film thickness and salt concentration for PSS-terminated LbL films.

The dependence of assembly salt concentration on $T_{tr,Rct}$, on the other hand, is strikingly different (Figure 5.10b). As described earlier, plots of R_{ct} vs. temperature showed one transition for the films assembled at 0.5 M NaCl and a sigmoidal shape with

two transitions for those assembled at 1.0 M NaCl, the higher of which is plotted in Figure 5.10b. For the LbL films assembled at 0.5 M NaCl, $T_{tr,Rct}$ increases from 50.4 ± 0.6 ℃ to 61 ± 1 ℃ as film thickness decreases from 300 nm to 25 nm. For the LbL films assembled at 1.0 M NaCl, $T_{tr,Rct}$ increases from 58.8 ± 0.3 ℃ to 64 ± 2 ℃ as film thickness decreases from 525 nm 125 nm. On average, the $T_{tr,Rct}$ of the LbL film assembled at 1.0 M is about 11 ℃ higher compared to the films assembled at 0.5 M NaCl at the equivalent thickness. The elevated transition temperatures for films assembled at 1.0 M NaCl may be explained in the context of extrinsic charge compensation. Films assembled at 1.0 M NaCl have a higher degree of extrinsic charge compensation, which provides more sites for interaction with (or trapping of) multivalent ferrocyanide and ferricyanide ions. Thus, higher temperatures are needed to undergo the transition.

We next turn to the influence of the outermost layer, which for some LbL systems, strongly affects electrochemical properties via Donnan inclusion and exclusion.[57, 58, 167, 168] For example, an odd-even effect was previously observed via rotating disc electrode experiments, in which Donnan inclusion was shown to increase the local concentration of redox active probes at the film's surface.[168] To understand the effect of the outermost layer, $T_{tr,Rf}$ and $T_{tr,Rct}$ were obtained for LbL films terminated with either PSS or PDAC (Figure 5.11). For comparison, a plot of thickness vs. number of layers is shown in Figure 5.12. For $T_{tr,Rf}$ there is no clear difference between the different terminating layers, which is consistent with the idea that $T_{tr,Rf}$ depends on the

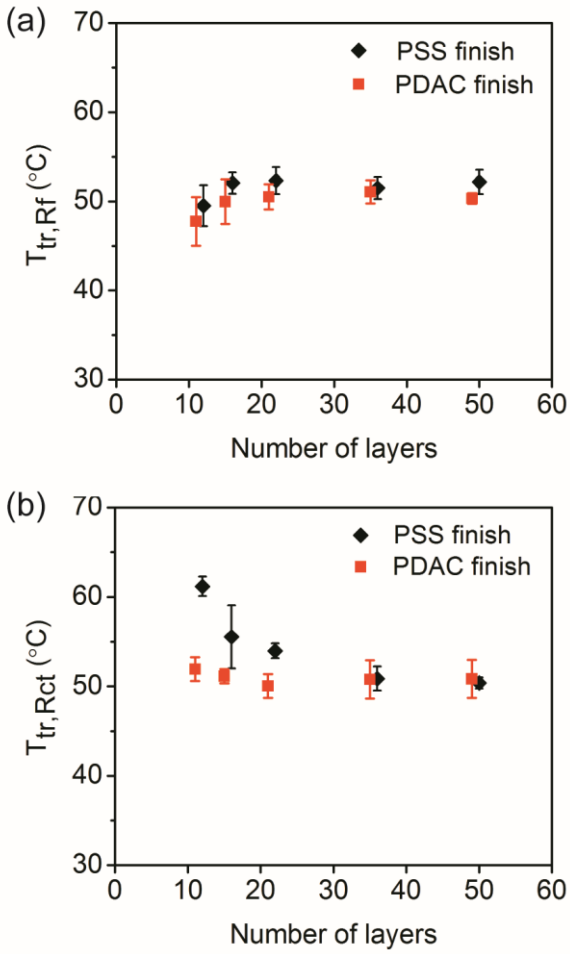

Figure 5.11 (a) The transition temperature (Ttr,Rf) obtained from plots of Rf vs. temperature, and (b) the transition temperature (Ttr,Rct) obtained from the plots of Rct vs. temperature as a function of film thickness and outermost layer for LbL films assembled at 0.5 M NaCl concentration.

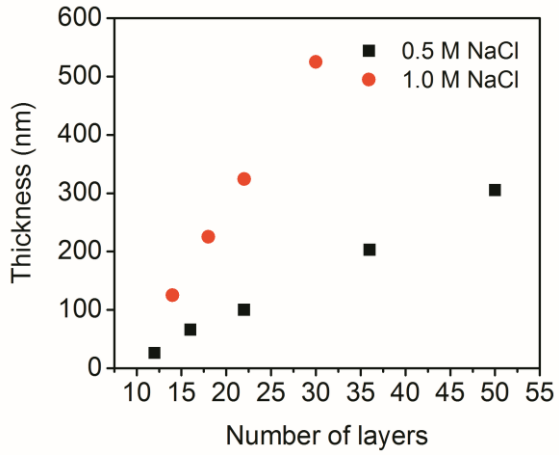

Figure 5.12 Dry PDAC/PSS LbL film thickness vs. number of layers.

conductivity of the film swollen with electrolyte (Figure 5.11a). Had the $T_{tr,Rf}$ been dependent on the multivalent redox probe, a strong odd-even effect would have been apparent. $T_{tr,Rf}$ was fairly constant for 20-50 layers, whereas it decreased slightly below 12 layers, which is about 25 nm in thickness. It has been previously shown that water content in PDAC/PSS LbL films increased from 35% to 65% as the number of layers pairs decreased from 7 to 1,[187] for which water acts as a plasticizer and perhaps lowers the film's $T_{tr.}$ It is also possible that the change in polymer composition or ion-pairing density might have taken place in 25 nm films.

On the other hand, the outermost layer strongly affects $T_{tr,Rct}$, especially for films of 20 layers or less, Figure 5.11b. Above 20 layers, $T_{tr,Rct}$ is around 50 ℃ for both PDAC- and PSS-terminated films. However, the $T_{tr,Rct}$ for PSS-terminated films

increases about 10 ℃ as the number of layers decreases below 20, whereas $T_{tr,Rct}$ remains relatively constant for PDAC-terminated films. One might be tempted to claim that Donnan exclusion of ferro/ferricyanide via PSS is driving the $T_{tr,Rct}$ towards higher temperatures, but a recent study from Ghostine *et al.*[180] indicates that Donnan exclusion can be largely discounted. Beyond a critical number of layer pairs, a reservoir of PDAC builds up within the film, and the net charge is positive regardless of the outermost layer. In this regard, Donnan *inclusion* perhaps becomes the norm for the PDAC/PSS LbL film beyond 20 layers, as evidenced by $T_{tr,Rct}$'s lack of dependence on outermost layer. Below this critical number of layers, the film's net charge flips between positive and neutral,[180] for which the redox active probes alternate between experiencing Donnan inclusion or lack thereof when PDAC or PSS are outermost layers, respectively. It has been suggested[180] that below this critical number of layer pairs the film exists as a glassy stoichiometric complex when PSS is the outermost layer and becomes rubbery when PDAC is outermost. This observation is consistent with the elevated $T_{tr,Rct}$'s for PSS-capped LbL films.

At room temperature, the outermost layer also affects the absolute values of R_{ct} and R_f, which are both higher when PDAC is the outermost (odd) layer are shown in Figure 5.13. R_f is only slightly affected, which supports the supposition that R_f is related to the resistance of the porous electrolyte-swollen film. R_{ct}, on the other hand, is higher in magnitude and strongly sensitive to outermost layer. This might be rationalized by assuming some dependence of partitioning or surface coverage on the outermost layer, in which PDAC-terminated films perhaps might have decreased K and increased θ.

However, the surface coverage is not expected to change strongly based on the outermost layer, so, by elimination, partitioning is likely to dominate. The upwards oscillation of R_{ct} for both PDAC and PSS outermost layers is very similar in trend to the quantity of extrinsic charge, as reported by Ghostine et al.[180] This observation supports the idea that R_{ct} is related to the state of the redox active probe, whose transport is linked to the number of extrinsic sites. It is possible that a large degree of extrinsic compensation slows transport as multiple extrinsic polyelectrolyte sites perhaps trap redox active probes, thus affecting partitioning. This idea is contrary to Donnan inclusion,[57, 188] and has been suggested elsewhere.[167] Had Donnan inclusion dominated,

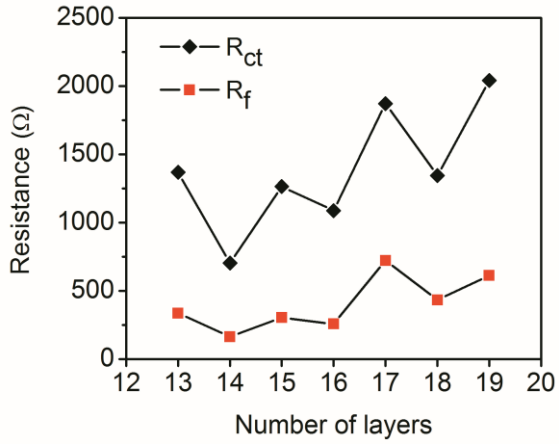

Figure 5.13 R_f and R_{ct} as a function of layers for LbL films assembled at 0.5 M NaCl, evaluated at 25 °C. Odd numbers corresponds to PDAC layers, and even numbers corresponds to PSS layers.

one would have observed consistently lower R_{ct} values for PDAC- capped films, contrary to our findings; therefore we conclude that the extent of extrinsic charge compensation dominates R_{ct}.

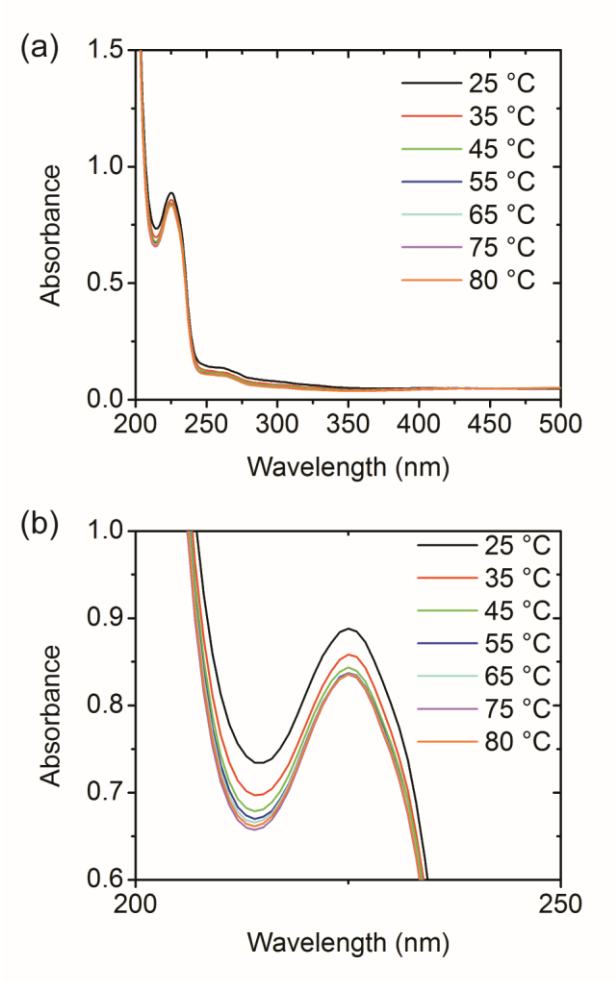

Figure 5.14 UV spectra of PDAC/PSS-coated quartz slides taken after annealing in the supporting electrolyte as a function of temperature. Figure 5.14(b) is magnification of Figure 5.14(a) at the wavelength from 200 nm to 250 nm.

It has been reported that PDAC/PSS LbL films dissolve at high salt concentrations,[189] and there is concern that the LbL film will disassemble in water at high temperatures.[43, 141] To monitor this possibility, an LbL-coated quartz substrate was annealed in the same supporting electrolyte used in EIS measurements at varying temperatures. UV spectra were obtained from the wavelength of 200 nm to 500 nm (Figure 5.14). UV absorbance at a wavelength of 225 nm,[190] which is characteristic of PSS, was measured and scaled against the UV absorbance at room temperature (Figure 5.15). The film retained 94 % of its PSS, even when incubated at 80 °C, and dry film thickness decreased by only about 2 %. Therefore, disassembly during the course of EIS measurements is of minor concern. The dry film thickness also decreased by 2% (Figure 5.16).

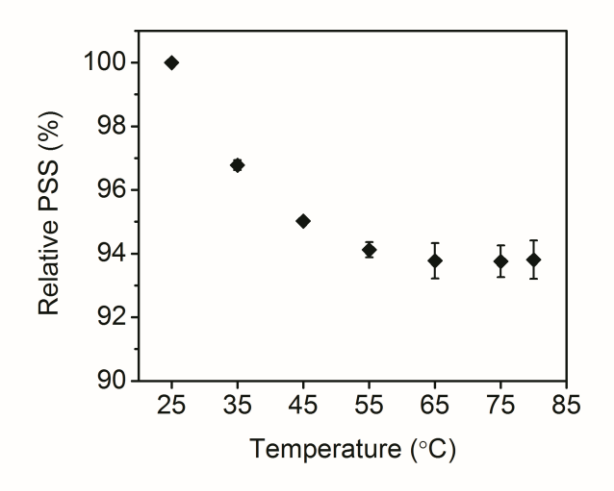

Figure 5.15 The relative amount of PSS in a PDAC/PSS LbL film after annealing in 0.5 M NaCl supporting electrolyte at varying temperatures for 30 min. The relative amount was calculated from the absorbance at 225 nm from UV-vis absorbance spectra, Figure 5.14.

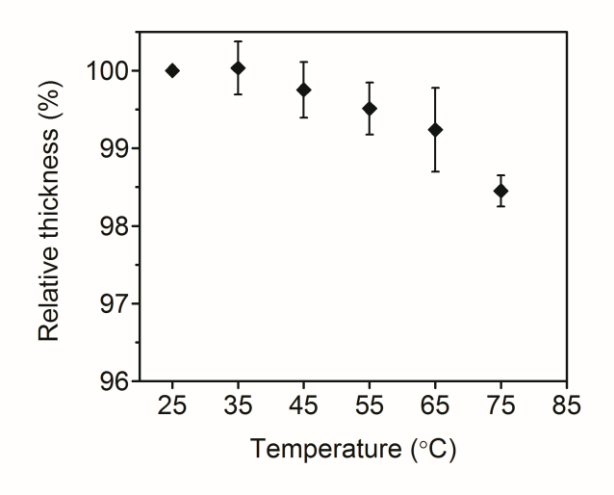

Figure 5.16 The relative dry LbL film thickness after annealing in the 0.5 M NaCl supporting electrolyte at varying temperatures for 30 min. The thickness was measured using ellipsometry.

The surface morphologies of the LbL films were also investigated before and after EIS measurements (Figure 5.17). Prior to EIS measurements, the as-made LbL film exhibited a well-known vermiculate surface morphology[191] with a root mean square (RMS) roughness of 7.5 nm (Figure 5.17a). However, after EIS up to 80 ℃, the vermiculate surface morphology disappeared, and the film became fairly smooth (RMS roughness, 1.3 nm) (Figure 5.17b). Smoothing of LbL films due to salt annealing at room temperature is a well-known phenomenon.[192, 193] However, annealing of LbL films at high temperature has not been reported to our knowledge. To verify whether this is due to the temperature, time, or electrical effects during EIS measurements, we annealed the film in a supporting electrolyte without applying electric field at 25 ℃ for 7 hours, which is the same period LbL films are immersed during EIS measurements, and at

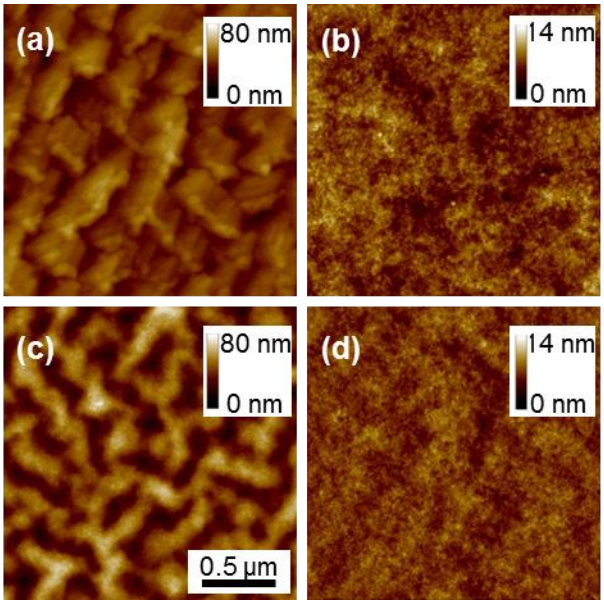

Figure 5.17 AFM topographic images of $(PDAC/PSS)_{11}$ LbL films assembled at 0.5 M NaCl (a) as-made, (b) after EIS measurement, and after annealing in supporting electrolyte (c) at 25 ℃ for 7 hours and (d) at 80 ℃ for 30 min.

80 ℃ for 30 min. After annealing at 25 ℃ for 7 hours, the vermiculate structure is still observed (RMS roughness, 10.5 nm) (Figure 5.17c). On the contrary, the film surface becomes fairly smooth (RMS roughness, 2.5 nm) when annealed at 80 ℃ for 30 min (Figure 5.17d). These results imply that the surface morphology changes are mainly driven by temperature rather than time or electrical effects.

5.4 Conclusion

Thermal transitions for hydrated PDAC/PSS LbL films were studied using electrochemical impedance spectroscopy with ferrocyanide/ferricyanide as a redox active probe for the first time. Thin films (less than 10 layers) behave as patchy coatings,

for which diffusion through the film is similar to bulk electrolyte. Thicker films (greater than 10 layers) exhibit thermal transitions that arise from changes in the film's resistance ($T_{tr,Rf}$) and the charge transfer resistance ($T_{tr,Rct}$). These transitions are not necessarily the same because they arise from different phenomena, as elaborated below.

$T_{tr,Rf}$ is related to the state of the film swollen with electrolyte and the film's network of virtual pores. The $T_{tr,Rf}$ values observed herein coincide with those observed elsewhere via QCM-D and calorimetry,[49] and were largely independent of thickness, outermost layer, and salt concentration. These results indicate that the transition is tied to a structural rearrangement of the LbL film, resulting in increased conductivity through the film.

$T_{tr,Rct}$ is related to the state of the redox active probe near and within the LbL film. Upon going through the transition, the charge transfer decreases and then levels off, suggestive of a net decrease in surface coverage towards a finite value. The $T_{tr,Rf}$ values observed herein are strongly dependent on thickness, outermost layer, and salt concentration. As the number of layers decreased, the identity of the outermost layer began to dominate, for which $T_{tr,Rct}$ was at most 10°C higher for PSS-capped films. Further, as the ionic strength of assembly increased from 0.5 M to 1.0 M NaCl, $T_{tr,Rct}$ was consistently about 10°C higher as well. These results indicate that extrinsic charge compensation plays a large role on the value $T_{tr,Rct}$, for which a higher extent of extrinsic charge compensation drives $T_{tr,Rct}$ towards higher values. This is suggestive of trapping of the negatively charged redox ion probe in pockets of unpaired positively charged

PDAC segments. Donnan inclusion was also considered, but determined not to play a major role as compared to extrinsic charge compensation.

These results highlight the unique information that can be obtained from EIS, in which separate circuit elements report on the state of the film, electrolyte, and redox-active probe as a function of temperature. It allows one to more fully describe the nature of transition, perhaps more so than simple calorimetry.

Our forthcoming work will integrate these results with simulations, which demonstrate that the origin of the polyelectrolyte's mobility upon heating through the transition is tied to rearrangement of water molecules on extrinsically compensated polyelectrolyte segments.

CHAPTER VI

SUMMARY AND FUTURE WORK

6.1 Summary

This thesis investigated thermal transitions in LbL assemblies as a function of film thickness, assembly methods, and assembly condition using various methods. The thermal transitions in the dry state were studied using PEO/PAA and PEO/PMAA hydrogen-bonded LbL assemblies with the film thickness and deposition method as the major parameters. Thermal transitions in the hydrated state were studied using electrostatic LbL assemblies. The shape-transformation of PAH/PAA LbL microtubes in aqueous media, which is associated with the thermal transition of LbL assemblies, was studied at varying temperatures. Temperature-controlled EIS was used to probe the thermal transition of PDAC/PSS LbL assemblies in aqueous media.

Thermal properties of PEO/PAA and PEO/PMAA LbL assemblies were studied as a function of the film thickness using modulated DSC and temperature-controlled ellipsometer (Chapter II). The T_g of freestanding PEO/PAA films increased ~4℃ as the film thickness decreased from 15 μm to 540 nm. For ultrathin PEO/PAA LbL films on silicon substrates, the T_g increased ~ 9℃ as the film thickness decreased from 175 nm to 30 nm. The increase of the T_g for supported ultrathin films was due to the hydrogen-bonding interactions between the film and the substrate. PEO/PMAA LbL assemblies showed a T_g only after thermal crosslinking of acid groups along the PMAA chains. T_g of PEO/PMAA was fairly independent of film thickness. It was attributed to the

hydrophobicity of PMAA arising from methyl groups and the absence of favorable interaction between the film and the substrate. Interestingly, PEO/PMAA LbL films below a thickness of 2.7 μm exhibited PEO melting, indicating PEO phase separation.

Thermal properties of PEO/PAA and PEO/PMAA LbL assemblies prepared by dip- and spray-assisted deposition method were compared (Chapter III). For both LbL assemblies, the T_g's were fairly constant regardless of deposition method. However, the glass transition width was larger for the films prepared by the spray-assisted deposition method. It was attributed to the more heterogeneous structure of spray-assisted LbL films, perhaps arising from the short contact time and convective actionof spraying process. Interestingly, the surface morphologies of PEO/PMAA LbL assemblies depended greatly on deposition method. While the surface morphologies of dip-assisted PEO/PMAA LbL films showed micron-scale surface textures, those of spray-assisted LbL films were very smooth. However, the surface morphologies of PEO/PAA LbL assemblies were smooth regardless of the deposition method. PEO/PMAA LbL assemblies showed phase separation upon thermal crosslinking dependent on assembly pH. The degree of phase separation was larger for the films assembled at a higher assembly pH, but it was not affected by the mode of film deposition.

Temperature-triggered shape-transformations of released and unreleased PAH/PAA LbL assemblies were studied (Chapter IV). The microtubes were fabricated using the porous polycarbonate membranes as sacrificial templates. The microtubes were incubated in aqueous media at temperatures ranging from 25 to 121℃. Released microtubes became spherical and ellipsoidal shape as the incubation temperature

increased. The aspect ratio of microtubes decreased from 5.0 to 1.7, and the outer diameter increased from 1.0 μm to 1.8 μm as the incubation temperature increased. Unreleased microtubes exhibited periodic perforations at fairly regular spacing while maintaining the microtube length. The spacing between the perforations was similar to the values predicted by the theory of Rayleigh instabilities. Above the thermal transition temperature of hydrated PAH/PAA LbL film, the number of perforations increased greatly.

Thermal transitions of PDAC/PSS LbL assemblies in aqueous media were studied using EIS with ferrocyanide/ferricyanide as a redox couple. Two thermal transitions were observed from the plots of film resistance ($T_{tr,Rf}$) and charge transfer resistance ($T_{tr,Rct}$) vs. temperature. $T_{tr,Rf}$ was related to the porous film structure swollen with electrolyte. The $T_{tr,Rf}$ values were fairly close to the values obtained using QCM-D and calorimetry, and were fairly constant regardless of thickness, outermost layer, and salt concentration. $T_{tr,Rct}$ was closely related the state of redox ions in LbL films. As the number of layers decreased below 20, $T_{tr,Rct}$ of PSS-capped films became 10 ℃ higher than that of PDAC-capped film. This is because PSS-capped films that are glassy stoichiometric complex at the early growth become rubbery PDAC-rich complex above critical number of layer pairs. Furthermore, $T_{tr,Rct}$ of PSS-capped films assembled at 1.0 M NaCl was about 11°C higher compared to the PSS-capped films assembled at 0.5M NaCl. This seems to be due to the higher trapping of redox ions in the films assembled at 1.0M NaCl.

In summary, this body of work shows:

- For PEO/PAA LbL films, T_g increased as the film thickness decreased from 175 nm to 30 nm, while, for PEO/PMAA LbL film, T_g was not influenced by the film thickness and small amount of PEO phase separation was found below the thickness of 2.7 μm
- T_g's of PEO/PAA and PEO/PMAA LbL films were not influenced by the deposition method, dip and spray. However, the breadth of the transitions was larger for the spray-assisted films. Interestingly, the surface morphologies of PEO/PMAA were influenced by the deposition method
- While released PAH/PAA LbL microtubes transformed to closed ellipsoids upon heating in pH 5.5 aqueous media, unreleased microtubes exhibited periodic perforations due to Rayleigh instabilities
- Two separate thermal transition temperatures were obtained using temperature-controlled EIS. $T_{tr,Rf}$ was fairly constant regardless of film thickness and salt concentration. In contrast, $T_{tr,Rct}$ was influenced by the film thickness, salt concentration, and outermost layer

6.2 Future Work

Even though thermal transitions in LbL assemblies were studied in many aspects, there are still many interesting areas and challenges to be addressed. For the future work of Chapter II, one of the practical interests might be controlling the T_g of LbL assemblies in dry state. Using the PAA/PMAA mixture as hydrogen donor, it would be possible to

control the T_g of hydrogen-bonded LbL assemblies. Also, it is possible to combine hydrogen-bonded LbL assemblies that have T_g's and electrostatic LbL assemblies, which do not exhibit T_g's. For example, we can alternate the PEO/PAA LbL layers with PAH/PAA LbL layers, controlling the relative film thickness.

Although the thermal transitions in hydrogen-bonded LbL assemblies were studied in Chapter III, there is no study on the thermal transitions of electrostatic LbL assemblies. There have been reports that the structure and properties of electrostatic LbL assemblies are different for those prepared by dipping and spraying. Since electrostatic LbL assemblies do not show a T_g in dry state, thermal transitions must be studied in a hydrated state. Studies on thermal transitions using modulated DSC and EIS may provide us with useful information in comparing dip- vs. spray-assisted LbL assemblies.

Next, controlling the perforation size and distribution on the LbL microtubes is a very interesting topic as an extension of the study in Chapter IV. In this thesis, the periodic perforations were formed on the microtube surface when the unreleased microtubes were incubated in pH 5.5 water at high temperatures. The interfacial energy and the mobility of the polymer chains seem to be important factors. It is well-known that the micro- or nanopores are formed in the film when the LbL films are immersed in an acidic solution.[194, 195] Thus, if we treat the unreleased LbL microtubes in acidic solutions of various pH at varying incubation temperatures, interesting structures might arise in LbL microtubes. Furthermore, it may be possible to make the pores in the released microtubes. Future work might use a mixture of organic solvent and water. If the organic solvent is a nonsolvent for the LbL microtubes, it will help maintain the

microtube structure. The presence of water might facilitate the polymer-chain rearrangement at high temperatures, and interesting porous structures may emerge. If we control the pH of the water in the solvent mixture, it may be possible to obtain a variety of porous structures.

Finally, more studies are needed regarding the nature of thermal transitions of LbL assemblies in the hydrated states although we studied thermal transitions using EIS in Chapter V. It is unclear why electrostatic LbL assemblies exhibit a T_g in the hydrated state, whereas the dry LbL assemblies do not. It would be interesting to study the thermal transitions in LbL films using temperature-controlled ellipsometry in aqueous media. In-situ measurements of film thickness as a function of temperature would provide useful information. We can examine whether LbL films swell or shrink with the temperature. Also, we can see what happens at the thermal transition. We can verify whether the transition is similar to the first- or second-order transition, or something else.

According to recent QCM-D studies, the thermal transition was characterized as a dissipation increase coupled with the influx of water with polymer. Furthermore, a forthcoming paper from our group and the Sammalkorpi's group shows simulations that the thermal transition is related to the rearrangement of water molecules around ionic groups on the polyelectrolytes, leading to enhanced polyelectrolyte mobility. More research on the thermal transition in the aspect of interactions between water molecules and polymer chains is needed.

REFERENCES

1. Iler, R. K. Multilayers of colloidal particles. *Journal of Colloid and Interface Science* **1966,** *21* (6), 569-594.

2. Decher, G. Fuzzy nanoassemblies: Toward layered polymeric multicomposites. *Science* **1997,** *277* (5330), 1232-1237.

3. Bucur, C. B.; Sui, Z.; Schlenoff, J. B. Ideal mixing in polyelectrolyte complexes and multilayers: Entropy driven assembly. *J. Am. Chem. Soc.* **2006,** *128* (42), 13690-13691.

4. Bieker, P.; Schönhoff, M. Linear and exponential growth regimes of multilayers of weak polyelectrolytes in dependence on pH. *Macromolecules* **2010,** *43* (11), 5052-5059.

5. Schoeler, B.; Kumaraswamy, G.; Caruso, F. Investigation of the influence of polyelectrolyte charge density on the growth of multilayer thin films prepared by the layer-by-layer technique. *Macromolecules* **2002,** *35* (3), 889-897.

6. Dubas, S. T.; Schlenoff, J. B. Polyelectrolyte multilayers containing a weak polyacid: construction and deconstruction. *Macromolecules* **2001,** *34* (11), 3736-3740.

7. Stockton, W. B.; Rubner, M. F. Molecular-level processing of conjugated polymers .4. Layer-by-layer manipulation of polyaniline via hydrogen-bonding interactions. *Macromolecules* **1997,** *30* (9), 2717-2725.

8. Sukhishvili, S. A.; Granick, S. Layered, erasable polymer multilayers formed by hydrogen-bonded sequential self-assembly. *Macromolecules* **2002,** *35* (1), 301-310.

9. Erel-Unal, I.; Sukhishvili, S. A. Hydrogen-bonded multilayers of a neutral polymer and a polyphenol. *Macromolecules* **2008,** *41* (11), 3962-3970.

10. Castelnovo, M.; Joanny, J. F. Formation of polyelectrolyte multilayers. *Langmuir* **2000,** *16* (19), 7524-7532.

11. Shafir, A.; Andelman, D. Polyelectrolyte multilayer formation: Electrostatics and short-range interactions. *Eur. Phys. J. E* **2006,** *19* (2), 155-162.

12. Elbert, D. L.; Herbert, C. B.; Hubbell, J. A. Thin polymer layers formed by polyelectrolyte multilayer techniques on biological surfaces. *Langmuir* **1999,** *15* (16), 5355-5362.

13. Picart, C.; Mutterer, J.; Richert, L.; Luo, Y.; Prestwich, G. D.; Schaaf, P.; Voegel, J. C.; Lavalle, P. Molecular basis for the explanation of the exponential growth of polyelectrolyte multilayers. *Proceedings of the National Academy of Sciences of the United States of America* **2002,** *99* (20), 12531-12535.

14. Lavalle, P.; Picart, C.; Mutterer, J.; Gergely, C.; Reiss, H.; Voegel, J. C.; Senger, B.; Schaaf, P. Modeling the buildup of polyelectrolyte multilayer films having exponential growth. *J. Phys. Chem. B* **2004,** *108* (2), 635-648.

15. Michel, A.; Izquierdo, A.; Decher, G.; Voegel, J. C.; Schaaf, P.; Ball, V. Layer by layer self-assembled polyelectrolyte multilayers with embedded phospholipid vesicles obtained by spraying: Integrity of the vesicles. *Langmuir* **2005,** *21* (17), 7854-7859.

16. Porcel, C.; Lavalle, P.; Ball, V.; Decher, G.; Senger, B.; Voegel, J. C.; Schaaf, P. From exponential to linear growth in polyelectrolyte multilayers. *Langmuir* **2006,** *22* (9), 4376-4383.

17. Hoda, N.; Larson, R. G. Modeling the buildup of exponentially growing polyelectrolyte multilayer films. *J. Phys. Chem. B* **2009,** *113* (13), 4232-4241.

18. Porcel, C.; Lavalle, P.; Decher, G.; Senger, B.; Voegel, J. C.; Schaaf, P. Influence of the polyelectrolyte molecular weight on exponentially growing multilayer films in the linear regime. *Langmuir* **2007,** *23* (4), 1898-1904.

19. Xu, L.; Pristinski, D.; Zhuk, A.; Stoddart, C.; Ankner, J. F.; Sukhishvili, S. A. Linear versus exponential growth of weak polyelectrolyte multilayers: Correlation with polyelectrolyte complexes. *Macromolecules* **2012,** *45* (9), 3892-3901.

20. Kharlampieva, E.; Kozlovskaya, V.; Ankner, J. F.; Sukhishvili, S. A. Hydrogen-bonded polymer multilayers probed by neutron reflectivity. *Langmuir* **2008,** *24* (20), 11346-11349.

21. Lösche, M.; Schmitt, J.; Decher, G.; Bouwman, W. G.; Kjaer, K. Detailed structure of molecularly thin polyelectrolyte multilayer films on solid substrates as revealed by neutron reflectometry. *Macromolecules* **1998,** *31* (25), 8893-8906.

22. Gopinadhan, M.; Ahrens, H.; Gunther, J. U.; Steitz, R.; Helm, C. A. Approaching the precipitation temperature of the deposition solution and the effects on the

internal order of polyelectrolyte multilayers. *Macromolecules* **2005,** *38* (12), 5228-5235.

23. Cho, J.; Char, K.; Hong, J. D.; Lee, K. B. Fabrication of highly ordered multilayer films using a spin self-assembly method. *Adv. Mater.* **2001,** *13* (14), 1076-1078.

24. Cho, J. H.; Lee, S. H.; Kang, H. M.; Char, K.; Koo, J.; Seung, B. H.; Lee, K. B. Quantitative analysis on the adsorbed amount and structural characteristics of spin self-assembled multilayer films. *Polymer* **2003,** *44* (18), 5455-5459.

25. Choi, I.; Suntivich, R.; Pamper, F. A.; Synatschke, C. V.; Muller, A. H. E.; Tsukruk, V. V. pH-controlled exponential and linear growing modes of layer-by-layer assemblies of star polyelectrolytes. *J. Am. Chem. Soc.* **2011,** *133* (24), 9592-9606.

26. Seo, J.; Lutkenhaus, J. L.; Kim, J.; Hammond, P. T.; Char, K. Effect of the layer-by-layer (LbL) deposition method on the surface morphology and wetting behavior of hydrophobically modified PEO and PAA LbL films. *Langmuir* **2008,** *24* (15), 7995-8000.

27. Jiang, C. Y.; Markutsya, S.; Tsukruk, V. V. Compliant, robust, and truly nanoscale free-standing multilayer films fabricated using spin-assisted layer-by-layer assembly. *Adv. Mater.* **2004,** *16* (2), 157-161.

28. Izquierdo, A.; Ono, S. S.; Voegel, J. C.; Schaaf, P.; Decher, G. Dipping versus spraying: exploring the deposition conditions for speeding up layer-by-layer assembly. *Langmuir* **2005,** *21* (16), 7558-7567.

29. Schlenoff, J. B.; Dubas, S. T.; Farhat, T. Sprayed polyelectrolyte multilayers. *Langmuir* **2000,** *16* (26), 9968-9969.

30. Fendler, J. H. *Nanoparticles and nanostructured films: Preparation, characterization and applications*. Wiley-VCH: Weinhein, Germany, 1998.

31. Azzaroni, O.; Lau, K. H. A. Layer-by-layer assemblies in nanoporous templates: Nano-organized design and applications of soft nanotechnology. *Soft Matter* **2011,** *7* (19), 8709-8724.

32. Zhang, L.; Vidyasagar, A.; Lutkenhaus, J. L. Fabrication and thermal analysis of layer-by-layer micro- and nanotubes. *Curr. Opin. Colloid Interface Sci.* **2012,** *17* (2), 114-121.

33. Liang, Z. J.; Susha, A. S.; Yu, A. M.; Caruso, F. Nanotubes prepared by layer-by-layer coating of porous membrane templates. *Adv. Mater.* **2003,** *15* (21), 1849-1853.

34. Ai, S. F.; Lu, G.; He, Q.; Li, J. B. Highly flexible polyelectrolyte nanotubes. *J. Am. Chem. Soc.* **2003,** *125* (37), 11140-11141.

35. Sullivan, D. M.; Bruening, M. L. Ultrathin, gas-selective polyimide membranes prepared from multilayer polyelectrolyte films. *Chem. Mat.* **2003,** *15* (1), 281-287.

36. Chia, K. K.; Rubner, M. F.; Cohen, R. E. pH-responsive reversibly swellable nanotube arrays. *Langmuir* **2009,** *25* (24), 14044-14052.

37. Lazzara, T. D.; Lau, K. H. A.; Abou-Kandil, A. I.; Caminade, A. M.; Majoral, J. P.; Knoll, W. Polyelectrolyte layer-by-layer deposition in cylindrical nanopores. *ACS Nano* **2010,** *4* (7), 3909-3920.

38. Roy, C. J.; Dupont-Gillain, C.; Demoustier-Champagne, S.; Jonas, A. M.; Landoulsi, J. Growth mechanism of confined polyelectrolyte multilayers in nanoporous templates. *Langmuir* **2010,** *26* (5), 3350-3355.

39. Lutkenhaus, J. L.; Hrabak, K. D.; McEnnis, K.; Hammond, P. T. Elastomeric flexible free-standing hydrogen-bonded nanoscale assemblies. *J. Am. Chem. Soc.* **2005,** *127* (49), 17228-17234.

40. Lutkenhaus, J. L.; McEnnis, K.; Hammond, P. T. Tuning the glass transition of and ion transport within hydrogen-bonded layer-by-layer assemblies. *Macromolecules* **2007,** *40* (23), 8367-8373.

41. Shao, L.; Lutkenhaus, J. L. Thermochemical properties of free-standing electrostatic layer-by-layer assemblies containing poly(allylamine hydrochloride) and poly(acrylic acid). *Soft Matter* **2010,** *6* (14), 3363-3369.

42. Jang, W. S.; Jensen, A. T.; Lutkenhaus, J. L. Confinement effects on cross-Linking within electrostatic layer-by-layer assemblies containing poly(allylamine hydrochloride) and poly(acrylic acid). *Macromolecules* **2010,** *43* (22), 9473-9479.

43. Köhler, K.; Shchukin, D. G.; Möhwald, H.; Sukhorukov, G. B. Thermal behavior of polyelectrolyte multilayer microcapsules. 1. The effect of odd and even layer number. *J. Phys. Chem. B* **2005,** *109* (39), 18250-18259.

44. Köhler, K.; Möhwald, H.; Sukhorukov, G. B. Thermal behavior of polyelectrolyte multilayer microcapsules: 2. Insight into molecular mechanisms for the PDADMAC/PSS system. *J. Phys. Chem. B* **2006,** *110* (47), 24002-24010.

45. Leporatti, S.; Gao, C.; Voigt, A.; Donath, E.; Mohwald, H. Shrinking of ultrathin polyelectrolyte multilayer capsules upon annealing: A confocal laser scanning microscopy and scanning force microscopy study. *Eur. Phys. J. E* **2001,** *5* (1), 13-20.

46. Köhler, K.; Shchukin, D. G.; Sukhorukov, G. B.; Möhwald, H. Drastic morphological modification of polyelectrolyte microcapsules induced by high temperature. *Macromolecules* **2004,** *37* (25), 9546-9550.

47. He, Q.; Song, W.; Möhwald, H.; Li, J. Hydrothermal-induced structure transformation of polyelectrolyte multilayers: From nanotubes to capsules. *Langmuir* **2008,** *24* (10), 5508-5513.

48. Mueller, R.; Köhler, K.; Weinkamer, R.; Sukhorukov, G.; Fery, A. Melting of PDADMAC/PSS capsules investigated with AFM force spectroscopy. *Macromolecules* **2005,** *38* (23), 9766-9771.

49. Vidyasagar, A.; Sung, C.; Gamble, R.; Lutkenhaus, J. L. Thermal transitions in dry and hydrated layer-by-layer assemblies exhibiting linear and exponential growth. *ACS Nano* **2012,** *6* (7), 6174-6184.

50. Vidyasagar, A.; Sung, C.; Losensky, K.; Lutkenhaus, J. L. pH-dependent thermal transitions in hydrated layer-by-layer assemblies containing weak polyelectrolytes. *Macromolecules* **2012,** *45* (22), 9169-9176.

51. Fortier-McGill, B.; Reven, L. ^{2}H NMR studies of polymer multilayer capsules, films, and complexes. *Macromolecules* **2009,** *42* (1), 247-254.

52. Forrest, J. A.; Dalnoki-Veress, K. The glass transition in thin polymer films. *Advances in Colloid and Interface Science* **2001,** *94* (1-3), 167-196.

53. Schönhoff, M. Layered polyelectrolyte complexes: physics of formation and molecular properties. *J. Phys.-Condes. Matter* **2003,** *15* (49), R1781-R1808.

54. Ariga, K.; Hill, J. P.; Ji, Q. M. Layer-by-layer assembly as a versatile bottom-up nanofabrication technique for exploratory research and realistic application. *Phys. Chem. Chem. Phys.* **2007,** *9* (19), 2319-2340.

55. Krogman, K. C.; Lyon, K. F.; Hammond, P. T. Metal ion reactive thin films using spray electrostatic LbL assembly. *J. Phys. Chem. B* **2008,** *112* (46), 14453-14460.

56. Kolasinska, M.; Krastev, R.; Gutberlet, T.; Warszynski, P. Layer-by-layer deposition of polyelectrolytes. Dipping versus spraying. *Langmuir* **2009,** *25* (2), 1224-1232.

57. Pardo-Yissar, V.; Katz, E.; Lioubashevski, O.; Willner, I. Layered polyelectrolyte films on Au electrodes: Characterization of electron-transfer features at the charged polymer interface and application for selective redox reactions. *Langmuir* **2001,** *17* (4), 1110-1118.

58. Harris, J. J.; Stair, J. L.; Bruening, M. L. Layered polyelectrolyte films as selective, ultrathin barriers for anion transport. *Chem. Mat.* **2000,** *12* (7), 1941-1946.

59. Alonso-Garcia, T.; Rodriguez-Presa, M. J.; Gervasi, C.; Moya, S.; Azzaroni, O. Electrochemical determination of the glass transition temperature of thin polyelectrolyte brushes at solid-liquid Interfaces by impedance spectroscopy. *Anal. Chem.* **2013,** *85* (14), 6561-6565.

60. Silva, T. H.; Garcia-Morales, V.; Moura, C.; Manzanares, J. A.; Silva, F. Electrochemical impedance spectroscopy of polyelectrolyte multilayer modified gold electrodes: Influence of supporting electrolyte and temperature. *Langmuir* **2005,** *21* (16), 7461-7467.

61. Tang, Z. Y.; Wang, Y.; Podsiadlo, P.; Kotov, N. A. Biomedical applications of layer-by-layer assembly: From biomimetics to tissue engineering. *Adv. Mater.* **2006,** *18* (24), 3203-3224.

62. Farhat, T. R.; Hammond, P. T. Designing a new generation of proton-exchange membranes using layer-by-layer deposition of polyelectrolytes. *Adv. Funct. Mater.* **2005,** *15* (6), 945-954.

63. Hyder, M. N.; Lee, S. W.; Cebeci, F. Ç.; Schmidt, D. J.; Shao-Horn, Y.; Hammond, P. T. Layer-by-layer assembled pyaniline nanofiber/multiwall carbon nanotube thin film electrodes for high-power and high-energy storage applications. *ACS Nano* **2011,** *5* (11), 8552-8561.

64. Lee, D.; Rubner, M. F.; Cohen, R. E. All-nanoparticle thin-film coatings. *Nano Lett.* **2006,** *6* (10), 2305-2312.

65. Podsiadlo, P.; Paternel, S.; Rouillard, J. M.; Zhang, Z. F.; Lee, J.; Lee, J. W.; Gulari, L.; Kotov, N. A. Layer-by-layer assembly of nacre-like nanostructured composites with antimicrobial properties. *Langmuir* **2005,** *21* (25), 11915-11921.

66. Decher, G.; Hong, J. D.; Schmitt, J. Buildup of ultrathin multilayer films by a self-assembly process: III. Consecutively alternating adsorption of anionic and cationic polyelectrolytes on charged surfaces. *Thin Solid Films* **1992,** *210-211* (2), 831-835.

67. Kleinfeld, E. R.; Ferguson, G. S. Stepwise formation of multilayered nanostructural films from macromolecular precursors. *Science* **1994,** *265* (5170), 370-373.

68. Decher, G.; Lehr, B.; Lowack, K.; Lvov, Y.; Schmitt, J. New nanocomposite films for biosensors - layer-by-layer adsorbed films of polyelectrolytes, proteins or DNA. *Biosens. Bioelectron.* **1994,** *9* (9-10), 677-684.

69. Bertrand, P.; Jonas, A.; Laschewsky, A.; Legras, R. Ultrathin polymer coatings by complexation of polyelectrolytes at interfaces: suitable materials, structure and properties. *Macromol. Rapid Commun.* **2000,** *21* (7), 319-348.

70. Shiratori, S. S.; Rubner, M. F. pH-dependent thickness behavior of sequentially adsorbed layers of weak polyelectrolytes. *Macromolecules* **2000,** *33* (11), 4213-4219.

71. Lutkenhaus, J. L.; McEnnis, K.; Hammond, P. T. Nano- and microporous layer-by-layer assemblies containing linear poly(ethylenimine) and poly(acrylic acid). *Macromolecules* **2008,** *41* (16), 6047-6054.

72. Quinn, J. F.; Caruso, F. Facile tailoring of film morphology and release properties using layer-by-layer assembly of thermoresponsive materials. *Langmuir* **2004,** *20* (1), 20-22.

73. Salomäki, M.; Vinokurov, I. A.; Kankare, J. Effect of temperature on the buildup of polyelectrolyte multilayers. *Langmuir* **2005,** *21* (24), 11232-11240.

74. Dubas, S. T.; Schlenoff, J. B. Factors controlling the growth of polyelectrolyte multilayers. *Macromolecules* **1999,** *32* (24), 8153-8160.

75. Poptoshev, E.; Schoeler, B.; Caruso, F. Influence of solvent quality on the growth of polyelectrolyte multilayers. *Langmuir* **2004,** *20* (3), 829-834.

76. Schmitt, J.; Grunewald, T.; Decher, G.; Pershan, P. S.; Kjaer, K.; Losche, M. Internal structure of layer-by-layer adsorbed polyelectrolyte films-a neutron and x-ray reflectivity study. *Macromolecules* **1993,** *26* (25), 7058-7063.

77. Ghostine, R. A.; Schlenoff, J. B. Ion diffusion coefficients through polyelectrolyte multilayers: Temperature and charge dependence. *Langmuir* **2011,** *27* (13), 8241-8247.

78. Gu, X. K.; Knorr, D. B.; Wang, G. J.; Overney, R. M. Local thermal-mechanical analysis of ultrathin interfacially mixed poly(ethylene oxide)/poly(acrylic acid) layer-by-layer electrolyte assemblies. *Thin Solid Films* **2011,** *519* (18), 5955-5961.

79. DeLongchamp, D. M.; Hammond, P. T. Highly ion conductive poly(ethylene oxide)-based solid polymer electrolytes from hydrogen bonding layer-by-layer assembly. *Langmuir* **2004,** *20* (13), 5403-5411.

80. Kozlovskaya, V.; Ok, S.; Sousa, A.; Libera, M.; Sukhishvili, S. A. Hydrogen-bonded polymer capsules formed by layer-by-layer self-assembly. *Macromolecules* **2003,** *36* (23), 8590-8592.

81. Kharlampieva, E.; Sukhishvili, S. A. Release of a dye from hydrogen-bonded and electrostatically assembled polymer films triggered by adsorption of a polyelectrolyte. *Langmuir* **2004,** *20* (22), 9677-9685.

82. Overney, R. M.; Buenviaje, C.; Luginbuhl, R.; Dinelli, F. Glass and structural transitions measured at polymer surfaces on the nanoscale. *Journal of Thermal Analysis and Calorimetry* **2000,** *59* (1-2), 205-225.

83. Alcoutlabi, M.; McKenna, G. B. Effects of confinement on material behaviour at the nanometre size scale. *J. Phys.-Condes. Matter* **2005,** *17* (15), R461-R524.

84. Roth, C. B.; Dutcher, J. R. Glass transition and chain mobility in thin polymer films. *Journal of Electroanalytical Chemistry* **2005,** *584* (1), 13-22.

85. Keddie, J. L.; Jones, R. A. L.; Cory, R. A. Size-dependent depression of the glass-transition temperature in polymer films. *Europhysics Letters* **1994,** *27* (1), 59-64.

86. Ellison, C. J.; Torkelson, J. M. The distribution of glass-transition temperatures in nanoscopically confined glass formers. *Nat. Mater.* **2003,** *2* (10), 695-700.

87. Ellison, C. J.; Torkelson, J. M. Sensing the glass transition in thin and ultrathin polymer films via fluorescence probes and labels. *J. Polym. Sci. Pt. B-Polym. Phys.* **2002,** *40* (24), 2745-2758.

88. Keddie, J. L.; Jones, R. A. L.; Cory, R. A. Interface and surface effects on the glass-transition temperature in thin polymer films. *Faraday Discussions* **1994,** *98*, 219-230.

89. Fryer, D. S.; Nealey, P. F.; de Pablo, J. J. Thermal probe measurements of the glass transition temperature for ultrathin polymer films as a function of thickness. *Macromolecules* **2000,** *33* (17), 6439-6447.

90. Ge, S.; Pu, Y.; Zhang, W.; Rafailovich, M.; Sokolov, J.; Buenviaje, C.; Buckmaster, R.; Overney, R. M. Shear modulation force microscopy study of near surface glass transition temperatures. *Phys. Rev. Lett.* **2000,** *85* (11), 2340-2343.

91. Beaucage, G.; Composto, R.; Stein, R. S. Ellipsometric study of the glass transition and thermal expansion coefficients of thin polymer films. *Journal of Polymer Science Part B: Polymer Physics* **1993,** *31* (3), 319-326.

92. Rodahl, M.; Kasemo, B. A simple setup to simultaneously measure the resonant frequency and the absolute dissipation factor of a quartz crystal microbalance. *Rev. Sci. Instrum.* **1996,** *67* (9), 3238-3241.

93. Marx, K. A. Quartz crystal microbalance: A useful tool for studying thin polymer films and complex biomolecular systems at the solution-surface interface. *Biomacromolecules* **2003,** *4* (5), 1099-1120.

94. Voinova, M. V.; Rodahl, M.; Jonson, M.; Kasemo, B. Viscoelastic acoustic response of layered polymer films at fluid-solid interfaces: Continuum mechanics approach. *Physica Scripta* **1999,** *59* (5), 391-396.

95. Liu, G. M.; Zhao, J. P.; Sun, Q. Y.; Zhang, G. Z. Role of chain interpenetration in layer-by-layer deposition of polyelectrolytes. *J. Phys. Chem. B* **2008,** *112* (11), 3333-3338.

96. Gill, P.; Sauerbrunn, S.; Reading, M. Modulated differential scanning calorimetry. *Journal of Thermal Analysis and Calorimetry* **1993,** *40* (3), 931-939.

97. Ho, B. C.; Lee, Y. D.; Chin, W. K. Thermal-degradation of polymethacrylic acid. *Journal of Polymer Science Part a-Polymer Chemistry* **1992,** *30* (11), 2389-2397.

98. Lazzari, M.; Kitayama, T.; Hatada, K.; Chiantore, O. Effect of stereoregularity on the thermal behavior of poly(methacrylic acid)s. 2. Decomposition at low temperatures. *Macromolecules* **1998,** *31* (23), 8075-8082.

99. Mark, J. E. *Physical properties of polymers handbook*; 2nd ed.; Springer: New York, NY, 2007.

100. Wunderlich, B. *Thermal analysis of polymeric materials*; Springer: New York, NY, 2005.

101. Young, R. J.; Lovell, P. A. *Introduction to polymers*; 3rd ed.; Chapman and Hall: London, United Kingdom, 2011.

102. Tate, R. S.; Fryer, D. S.; Pasqualini, S.; Montague, M. F.; Pablo, J. J. d.; Nealey, P. F. Extraordinary elevation of the glass transition temperature of thin polymer films grafted to silicon oxide substrates. *The Journal of Chemical Physics* **2001,** *115* (21), 9982-9990.

103. Dubin, P.; Bock, J.; Davis, R.; Schulz, D. N.; Thies, C. *Macromolecular complexes in chemistry and biology*; Springer-Verlag: New York, NY, 1994.

104. Ikawa, T.; Abe, K.; Honda, K.; Tsuchida, E. Interpolymer complex between poly(ethylene oxide) and poly(carboxylic acid). *Journal of Polymer Science Part a-Polymer Chemistry* **1975,** *13* (7), 1505-1514.

105. Cimmino, S.; Dipace, E.; Martuscelli, E.; Silvestre, C. Evaulation of the equilibrium melting temperature and structure-analysis of poly(ethylene oxide) poly(methyl methacrylate) blends. *Makromolekulare Chemie-Macromolecular Chemistry and Physics* **1990,** *191* (10), 2447-2454.

106. DeMaggio, G. B.; Frieze, W. E.; Gidley, D. W.; Zhu, M.; Hristov, H. A.; Yee, A. F. Interface and surface effects on the glass transition in thin polystyrene films. *Phys. Rev. Lett.* **1997,** *78* (8), 1524-1527.

107. Ellis, T. S.; Karasz, F. E.; Brinke, G. T. The influence of thermal properties on the glass transition temperature in styrene/divinylbenzene network–diluent systems. *Journal of Applied Polymer Science* **1983,** *28* (1), 23-32.

108. Tsuchida, E.; Osada, Y.; Ohno, H. Formation of interpolymer complexes. *J. Macromol. Sci.-Phys.* **1980,** *B17* (4), 683-714.

109. Frank, C. W.; Hemker, D. J.; Oyama, H. T. Hydrophobic effects on complexation and aggregation in water-soluble polymers - Fluorescence, pH, and dynamic light-scattering measurements. *Acs Symposium Series* **1991,** *467*, 303-319.

110. Miyoshi, T.; Takegoshi, K.; Hikichi, K. High-resolution solid-state C-13 nuclear magnetic resonance study of a polymer complex: Poly(methacrylic acid) poly(ethylene oxide). *Polymer* **1996,** *37* (1), 11-18.

111. van Zanten, J. H.; Wallace, W. E.; Wu, W.-l. Effect of strongly favorable substrate interactions on the thermal properties of ultrathin polymer films. *Physical Review E* **1996,** *53* (3), R2053-R2056.

112. Schaaf, P.; Voegel, J. C.; Jierry, L.; Boulmedais, F. Spray-assisted polyelectrolyte multilayer buildup: From step-by-step to single-step polyelectrolyte film constructions. *Adv. Mater.* **2012,** *24* (8), 1001-1016.

113. Nogueira, G. M.; Banerjee, D.; Cohen, R. E.; Rubner, M. F. Spray-layer-by-layer assembly can more rapidly produce optical-quality multistack heterostructures. *Langmuir* **2011,** *27* (12), 7860-7867.

114. Popa, G.; Boulmedais, F.; Zhao, P.; Hemmerle, J.; Vidal, L.; Mathieu, E.; Felix, O.; Schaaf, P.; Decher, G.; Voegel, J. C. Nanoscale precipitation coating: The deposition of Inorganic films through step-by-step spray-assembly. *ACS Nano* **2010,** *4* (8), 4792-4798.

115. Cado, G.; Kerdjoudj, H.; Chassepot, A.; Lefort, M.; Benmlih, K.; Hemmerle, J.; Voegel, J. C.; Jierry, L.; Schaaf, P.; Frere, Y.; Boulmedais, F. Polysaccharide flms built by simultaneous or alternate spray: A rapid way to engineer biomaterial surfaces. *Langmuir* **2012,** *28* (22), 8470-8478.

116. Krogman, K. C.; Zacharia, N. S.; Schroeder, S.; Hammond, P. T. Automated process for improved uniformity and versatility of layer-by-layer deposition. *Langmuir* **2007,** *23* (6), 3137-3141.

117. Félix, O.; Zheng, Z. Q.; Cousin, F.; Decher, G. Are sprayed LbL-films stratified? A first assessment of the nanostructure of spray-assembled multilayers by neutron reflectometry. *C. R. Chim.* **2009,** *12* (1-2), 225-234.

118. Sung, C.; Vidyasagar, A.; Hearn, K.; Lutkenhaus, J. L. Effect of thickness on the thermal properties of hydrogen-bonded LbL assemblies. *Langmuir* **2012,** *28* (21), 8100-8109.

119. Lee, H.; Mensire, R.; Cohen, R. E.; Rubner, M. F. Strategies for hydrogen bonding based layer-by-layer assembly of poly(vinyl alcohol) with weak polyacids. *Macromolecules* **2012,** *45* (1), 347-355.

120. Zhuk, A.; Pavlukhina, S.; Sukhishvili, S. A. Hydrogen-bonded layer-by-layer temperature-triggered release films. *Langmuir* **2009,** *25* (24), 14025-14029.

121. Tong, W. J.; Gao, C. Y.; Mohwald, H. Single polyelectrolyte microcapsules fabricated by glutaraldehyde-mediated covalent layer-by-layer assembly. *Macromol. Rapid Commun.* **2006,** *27* (24), 2078-2083.

122. Kharlampieva, E.; Sukhishvili, S. A. Polyelectrolyte multilayers of weak polyacid and cationic copolymer: Competition of hydrogen-bonding and electrostatic interactions. *Macromolecules* **2003,** *36* (26), 9950-9956.

123. Choi, J.; Rubner, M. F. Influence of the degree of ionization on weak polyelectrolyte multilayer assembly. *Macromolecules* **2005,** *38* (1), 116-124.

124. Jiang, M.; Li, M.; Xiang, M. L.; Zhou, H. Interpolymer complexation and miscibility enhancement by hydrogen bonding. In *Polymer Synthesis Polymer-Polymer Complexation*, Abe, A.; Albertsson, A. C.; Cantow, H. J.; Dusek, K.; Edwards, S.; Hocker, H.; Joanny, J. F.; Kausch, H. H.; Kobayashi, T.; Lee, K. S.;

McGarth, J. E.; Monnerie, L.; Stupp, S. I.; Suter, U. W.; Thomas, E. L.; Wegner, G.; Young, R. J., Eds.; Springer-Verlag Berlin: Berlin, Germany, 1999; Vol. 146, pp 121-196.

125. Seo, J.; Lutkenhaus, J. L.; Kim, J.; Hammond, P. T.; Char, K. Development of surface morphology in multilayered films prepared by layer-by-layer deposition using poly(acrylic acid) and hydrophobically modified poly(ethylene oxide). *Macromolecules* **2007,** *40* (11), 4028-4036.

126. Zimnitsky, D.; Shevchenko, V. V.; Tsukruk, V. V. Perforated, freely suspended layer-by-layer nanoscale membranes. *Langmuir* **2008,** *24* (12), 5996-6006.

127. Zhang, J.; Fredin, N. J.; Lynn, D. M. Apparent dewetting of ultrathin multilayered polyelectrolyte films incubated in aqueous environments. *Langmuir* **2007,** *23* (23), 11603-11610.

128. Qin, S.; Wei, D. S.; Liao, Q.; Jin, X. G. Dewetting process of polyelectrolyte multilayer films in hot water. *Macromol. Rapid Commun.* **2006,** *27* (1), 11-14.

129. Lin, W.; Guan, Y.; Zhang, Y.; Xu, J.; Zhu, X. X. Salt-induced erosion of hydrogen-bonded layer-by-layer assembled films. *Soft Matter* **2009,** *5* (4), 860-867.

130. Reiter, G. Dewetting of highly elastic thin polymer films. *Phys. Rev. Lett.* **2001,** *87* (18).

131. Painter, P. C.; Shenoy, S. L.; Bhagwagar, D. E.; Fishburn, J.; Coleman, M. M. Effect of hydrogen-bonding on the melting-point depression in polymer blends where one-component crystallizes. *Macromolecules* **1991,** *24* (20), 5623-5629.

132. Johnston, A. P. R.; Cortez, C.; Angelatos, A. S.; Caruso, F. Layer-by-layer engineered capsules and their applications. *Curr. Opin. Colloid Interface Sci.* **2006,** *11* (4), 203-209.

133. von Klitzing, R. Internal structure of polyelectrolyte multilayer assemblies. *Phys. Chem. Chem. Phys.* **2006,** *8* (43), 5012-5033.

134. Lavalle, P.; Voegel, J. C.; Vautier, D.; Senger, B.; Schaaf, P.; Ball, V. Dynamic aspects of films prepared by a sequential deposition of species: perspectives for smart and responsive materials. *Adv. Mater.* **2011,** *23* (10), 1191-1221.

135. del Mercato, L. L.; Rivera-Gil, P.; Abbasi, A. Z.; Ochs, M.; Ganas, C.; Zins, I.; Sonnichsen, C.; Parak, W. J. LbL multilayer capsules: recent progress and future outlook for their use in life sciences. *Nanoscale* **2010,** *2* (4), 458-467.

136. Köhler, K.; Sukhorukov, G. B. Heat treatment of polyelectrolyte multilayer capsules: A versatile method for encapsulation. *Adv. Funct. Mater.* **2007,** *17* (13), 2053-2061.

137. Tong, W. J.; She, S. P.; Xie, L. L.; Gao, C. Y. High efficient loading and controlled release of low-molecular-weight drugs by combination of spontaneous deposition and heat-induced shrinkage of multilayer capsules. *Soft Matter* **2011,** *7* (18), 8258-8265.

138. Becker, A. L.; Johnston, A. P. R.; Caruso, F. Layer-by-layer-assembled capsules and films for therapeutic delivery. *Small* **2010,** *6* (17), 1836-1852.

139. Komatsu, T. Protein-based nanotubes for biomedical applications. *Nanoscale* **2012,** *4* (6), 1910-1918.

140. Wang, Y.; Angelatos, A. S.; Caruso, F. Template synthesis of nanostructured materials via layer-by-layer assembly. *Chem. Mat.* **2008,** *20* (3), 848-858.

141. Gao, C. Y.; Leporatti, S.; Moya, S.; Donath, E.; Mohwald, H. Swelling and shrinking of polyelectrolyte microcapsules in response to changes in temperature and ionic strength. *Chemistry-a European Journal* **2003,** *9* (4), 915-920.

142. Dejugnat, C.; Köhler, K.; Dubois, M.; Sukhorukov, G. B.; Mohwald, H.; Zemb, T.; Guttmann, P. Membrane densification of heated polyelectrolyte multilayer capsules characterized by soft X-ray microscopy. *Adv. Mater.* **2007,** *19* (10), 1331-1336.

143. Dubrovskii, A. V.; Shabarchina, L. I.; Kim, Y. A.; Sukhorukov, B. I. Influence of the temperature on polyelectrolyte microcapsules: Light scattering and confocal microscopy data. *Russian Journal of Physical Chemistry* **2006,** *80* (10), 1703-1707.

144. Ibarz, G.; Dahne, L.; Donath, E.; Mohwald, H. Controlled permeability of polyelectrolyte capsules via defined annealing. *Chem. Mat.* **2002,** *14* (10), 4059-4062.

145. Kato, N.; Caruso, F. Homogeneous, competitive fluorescence quenching immunoassay based on gold nanoparticle/polyelectrolyte coated latex particles. *J. Phys. Chem. B* **2005,** *109* (42), 19604-19612.

146. Schnackel, A.; Hiller, S.; Reibetanz, U.; Donath, E. Fluorescent bead arrays by means of layer-by-layer polyelectrolyte adsorption. *Soft Matter* **2007,** *3* (2), 200-206.

147. Rayleigh, L. On te instability of jets. *Proceedings of the London Mathematical Society* **1878,** *s1-10* (1), 4-13.

148. Nichols, F. A.; Mullins, W. W. Surface - (interface-) and volume-diffusion contributions to morphological changes driven by capillarity. *Transactions of the Metallurgical Society of Aime* **1965,** *233* (10), 1840-1848.

149. Chen, J. T.; Zhang, M. F.; Russell, T. P. Instabilities in nanoporous media. *Nano Lett.* **2007,** *7* (1), 183-187.

150. Schlitt, S.; Greiner, A.; Wendorff, J. H. Cylindrical polymer nanostructures by solution template wetting. *Macromolecules* **2008,** *41* (9), 3228-3234.

151. Feng, X. D.; Jin, Z. X. Spontaneous formation of nanoscale polymer spheres, capsules, or rods by evaporation of polymer solutions in cylindrical alumina nanopores. *Macromolecules* **2009,** *42* (3), 569-572.

152. Chen, D.; Chen, J. T.; Glogowski, E.; Emrick, T.; Russell, T. P. Thin film instabilities in blends under cylindrical confinement. *Macromol. Rapid Commun.* **2009,** *30* (4-5), 377-383.

153. Feng, X. D.; Mei, S. L.; Jin, Z. X. Wettability transition induced transformation and entrapment of polymer nanostructures in cylindrical nanopores. *Langmuir* **2011,** *27* (23), 14240-14247.

154. Fan, P.-W.; Chen, W.-L.; Lee, T.-H.; Chen, J.-T. Annealing effect on electrospun polymer fibers and their transformation into polymer microspheres. *Macromol. Rapid Commun.* **2012,** *33* (4), 343-349.

155. Fox, T. G.; Flory, P. J. Viscosity-molecular weight and viscosity-temperature relationships for polystyrene and polyisobutylene. *J. Am. Chem. Soc.* **1948,** *70* (7), 2384-2395.

156. Wu, S. Surface and interfacial tensions of polymer melts 2. Poly(methyl methacrylate), poly(n-butyl methacrylate), and polystyrene. *J. Phys. Chem.* **1970,** *74* (3), 632-638.

157. Nichols, F. A. Spheroidization of rod-shaped particles of finite length. *J. Mater. Sci.* **1976,** *11* (6), 1077-1082.

158. Boudou, T.; Crouzier, T.; Ren, K. F.; Blin, G.; Picart, C. Multiple functionalities of polyelectrolyte multilayer films: New biomedical applications. *Adv. Mater.* **2010,** *22* (4), 441-467.

159. Xiang, Y.; Lu, S. F.; Jiang, S. P. Layer-by-layer self-assembly in the development of electrochemical energy conversion and storage devices from fuel cells to supercapacitors. *Chem. Soc. Rev.* **2012,** *41* (21), 7291-7321.

160. Malikova, N.; Pastoriza-Santos, I.; Schierhorn, M.; Kotov, N. A.; Liz-Marzan, L. M. Layer-by-layer assembled mixed spherical and planar gold nanoparticles: Control of interparticle interactions. *Langmuir* **2002,** *18* (9), 3694-3697.

161. Lee, D.; Omolade, D.; Cohen, R. E.; Rubner, M. F. pH-dependent structure and properties of TiO2/SiO2 nanoparticle multilayer thin films. *Chem. Mat.* **2007,** *19* (6), 1427-1433.

162. Sung, C.; Vidyasagar, A.; Hearn, K.; Lutkenhaus, J. L. Temperature-triggered shape-transformations in layer-by-layer microtubes. *Journal of Materials Chemistry B* **2014,** *2* (15), 2088-2092.

163. Shamoun, R. F.; Hariri, H. H.; Ghostine, R. A.; Schlenoff, J. B. Thermal transformations in extruded saloplastic polyelectrolyte complexes. *Macromolecules* **2012,** *45* (24), 9759-9767.

164. Gabai, R.; Sallacan, N.; Chegel, V.; Bourenko, T.; Katz, E.; Willner, I. Characterization of the swelling of acrylamidophenylboronic acid-acrylamide hydrogels upon interaction with glucose by faradaic impedance spectroscopy, chronopotentiometry, quartz-crystal microbalance (QCM), and surface plasmon resonance (SPR) experiments. *J. Phys. Chem. B* **2001,** *105* (34), 8196-8202.

165. Zhou, J. H.; Wang, G.; Hu, J. Q.; Lu, X. B.; Li, J. H. Temperature, ionic strength and pH induced electrochemical switching of smart polymer interfaces. *Chem. Commun.* **2006,** (46), 4820-4822.

166. Lu, H. Y.; Hu, N. F. Salt-induced swelling and electrochemical property change of hyaluronic acid/myoglobin multilayer films. *J. Phys. Chem. B* **2007,** *111* (8), 1984-1993.

167. Barreira, S. V. P.; Garcia-Morales, V.; Pereira, C. M.; Manzanares, J. A.; Silva, F. Electrochemical impedance spectroscopy of polyelectrolyte multilayer modified electrodes. *J. Phys. Chem. B* **2004,** *108* (46), 17973-17982.

168. Farhat, T. R.; Schlenoff, J. B. Ion transport and equilibria in polyelectrolyte multilayers. *Langmuir* **2001,** *17* (4), 1184-1192.

169. Farhat, T. R.; Schlenoff, J. B. Doping-controlled ion diffusion in polyelectrolyte multilayers: Mass transport in reluctant exchangers. *J. Am. Chem. Soc.* **2003,** *125* (15), 4627-4636.

170. Harris, J. J.; DeRose, P. M.; Bruening, M. L. Synthesis of passivating, nylon-like coatings through cross-linking of ultrathin polyelectrolyte films. *J. Am. Chem. Soc.* **1999,** *121* (9), 1978-1979.

171. Gu, N.; Wei, D.; Niu, L.; Ivaska, A. Study on charge transfer reactions at multilayers of polyoxometalates clusters and poly(allylamine hydrochloride) (Grotthuss-018). *Electrochimica Acta* **2006,** *51* (27), 6038-6044.

172. Ruan, Q. C.; Zhu, Y. C.; Li, F.; Xiao, J. W.; Zeng, Y.; Xu, F. F. Investigation of layer-by-layer assembled heparin and chitosan multilayer films via electrochemical spectroscopy. *Journal of Colloid and Interface Science* **2009,** *333* (2), 725-733.

173. Amirudin, A.; Thierry, D. Application of electrochemical impedance spectroscopy to study the degradation of polymer-coated metals. *Progress in Organic Coatings* **1995,** *26* (1), 1-28.

174. Zhou, F.; Hu, H. Y.; Yu, B.; Osborne, V. L.; Huck, W. T. S.; Liu, W. M. Probing the responsive behavior of polyelectrolyte brushes using electrochemical impedance spectroscopy. *Anal. Chem.* **2007,** *79* (1), 176-182.

175. Garcia, T. A.; Gervasi, C. A.; Presa, M. J. R.; Otamendi, J. I.; Moya, S. E.; Azzaroni, O. Molecular transport in thin thermoresponsive poly(N-isopropylacrylamide) brushes with varying grafting density. *Journal of Physical Chemistry C* **2012,** *116* (26), 13944-13953.

176. Lvovich, V. F. *Impedance spectroscopy: Applications to electrochemical and dielectric phenomena*; John Wiley & Sons, Inc.: Hoboken, NJ, 2012.

177. Krasemann, L.; Tieke, B. Selective ion transport across self-assembled alternating multilayers of cationic and anionic polyelectrolytes. *Langmuir* **2000,** *16* (2), 287-290.

178. Cheng, Z. L.; Cheng, L.; Dong, S. J.; Yang, X. R. Formation and characterization of heteropolyacid/polycation multilayer films on gold electrode. *J. Electrochem. Soc.* **2001,** *148* (5), E227-E232.

179. Umadevi, S.; Ganesh, V.; Berchmans, S. Liquid crystal (LC) monolayer on Indium Tin Oxide (ITO): structural and electrochemical characterization. *RSC Advances* **2014,** *4* (32), 16409-16417.

180. Ghostine, R. A.; Markarian, M. Z.; Schlenoff, J. B. Asymmetric growth in polyelectrolyte multilayers. *J. Am. Chem. Soc.* **2013,** *135* (20), 7636-7646.

181. Vanwesting, E. P. M.; Ferrari, G. M.; Dewit, J. H. W. The determination of coating performance with impedance measurements-3. In-situ determination of loss of adhesion. *Corrosion Sci.* **1994,** *36* (6), 979-994.

182. Frechette, E.; Compere, C.; Ghali, E. Evaluation of the corrosion-resistance of painted steels by impedance measurements. *Corrosion Sci.* **1992,** *33* (7), 1067-1081.

183. Vanwesting, E. P. M.; Ferrari, G. M.; Dewit, J. H. W. The determination of coating performance with impedance measurements. 1. Coating polymer properties. *Corrosion Sci.* **1993,** *34* (9), 1511-1530.

184. Inzelt, G.; Lang, G. Impedance analysis of poly(tetracyanoquinodimethane) electrodes - effect of electrolyte concentration and temperature. *Electrochimica Acta* **1991,** *36* (8), 1355-1361.

185. Vyas, R. N.; Li, K. Y.; Wang, B. Modifying Randles circuit for analysis of polyoxometalate layer-by-layer Films. *J. Phys. Chem. B* **2010,** *114* (48), 15818-15824.

186. Sabatani, E.; Cohenboulakia, J.; Bruening, M.; Rubinstein, I. Thioaromatic monolayers on gold - A new family of self-assembling monolayers. *Langmuir* **1993,** *9* (11), 2974-2981.

187. Ramos, J. J. I.; Stahl, S.; Richter, R. P.; Moya, S. E. Water content and buildup of poly(diallyldimethylammonium chloride)/poly(sodium 4-styrenesulfonate) and poly(allylamine hydrochloride)/poly(sodium 4-styrenesulfonate) polyelectrolyte multilayers studied by an in situ combination of a quartz crystal microbalance with dissipation monitoring and spectroscopic ellipsometry. *Macromolecules* **2010,** *43* (21), 9063-9070.

188. Han, S.; Lindholm-Sethson, B. Electrochemistry at ultrathin polyelectrolyte films self-assembled at planar gold electrodes. *Electrochimica Acta* **1999,** *45* (6), 845-853.

189. Han, L. L.; Mao, Z. W.; Wuliyasu, H.; Wu, J. D.; Gong, X.; Yang, Y. G.; Gao, C. Y. Modulating the structure and properties of poly(sodium 4-styrenesulfonate)/poly(diallyldimethylammonium chloride) multilayers with concentrated salt solutions. *Langmuir* **2012,** *28* (1), 193-199.

190. Ladhari, N.; Hemmerle, J.; Ringwald, C.; Haikel, Y.; Voegel, J. C.; Schaaf, P.; Ball, V. Stratified PEI-(PSS-PDADMAC)(20)-PSS-(PDADMAC-TiO2)(n) multilayer films produced by spray deposition. *Colloid Surf. A-Physicochem. Eng. Asp.* **2008,** *322* (1-3), 142-147.

191. McAloney, R. A.; Sinyor, M.; Dudnik, V.; Goh, M. C. Atomic force microscopy studies of salt effects on polyelectrolyte multilayer film morphology. *Langmuir* **2001,** *17* (21), 6655-6663.

192. Dubas, S. T.; Schlenoff, J. B. Swelling and smoothing of polyelectrolyte multilayers by salt. *Langmuir* **2001,** *17* (25), 7725-7727.

193. McAloney, R. A.; Dudnik, V.; Goh, M. C. Kinetics of salt-induced annealing of a polyelectrolyte multilayer film morphology. *Langmuir* **2003,** *19* (9), 3947-3952.

194. Hiller, J.; Mendelsohn, J. D.; Rubner, M. F. Reversibly erasable nanoporous anti-reflection coatings from polyelectrolyte multilayers. *Nat. Mater.* **2002,** *1* (1), 59-63.

195. Mendelsohn, J. D.; Barrett, C. J.; Chan, V. V.; Pal, A. J.; Mayes, A. M.; Rubner, M. F. Fabrication of microporous thin films from polyelectrolyte multilayers. *Langmuir* **2000,** *16* (11), 5017-5023.